THE APPLICATION OF RATE THEORY TO THE FAILURE OF SOILD PROPELLANTS

Gordon C. Smith, et al

California Institute of Technology

Prepared for:

Air Force Rocket Propulsion Laboratory

July 1973

AFRPL-TR-73-54

THE APPLICATION OF RATE THEORY TO THE FAILURE OF SOLID PROPELLANTS

GRADUATE AERONAUTICAL LABORATORIES
CALIFORNIA INSTITUTE OF TECHNOLOGY

G. C. Smith
K. Palaniswamy
W. G. Knauss

July 1973

AFRPL-TR-73-54

Approved For Public Release
Distribution Unlimited

AIR FORCE ROCKET PROPULSION LABORATORY
DIRECTOR OF SCIENCE AND TECHNOLOGY
AIR FORCE SYSTEMS COMMAND
EDWARDS, CALIFORNIA

195

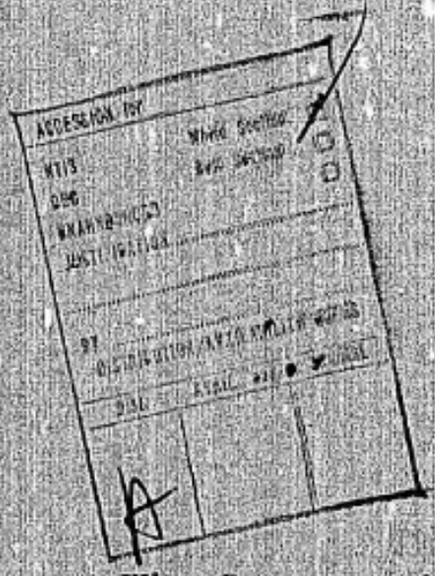

NOTICE

When Government drawings, specifications, or other data are used for any purpose other than in connection with a definitely related Government procurement operation, the United States Government thereby incurs no responsibility nor any obligation whatsoever; and the fact that the Government may have formulated, furnished, or in any way supplied the said drawings, specifications, or other data, is not to be regarded by implication or otherwise as in any manner licensing the holder or any other person or corporation, or conveying any rights or permission to manufacture, use, or sell any patented invention that may in any way be related thereto.

UNCLASSIFIED
Security Classification

DOCUMENT CONTROL DATA - R & D

(Security classification of title, body of abstract and indexing annotation must be entered when the overall report is classified)

1. ORIGINATING ACTIVITY *(Corporate author)*
CALIFORNIA INSTITUTE OF TECHNOLOGY
1201 EAST CALIFORNIA BLVD.
PASADENA, CALIFORNIA

2a. REPORT SECURITY CLASSIFICATION
UNCLASSIFIED

2b. GROUP

3. REPORT TITLE
THE APPLICATION OF RATE THEORY TO THE FAILURE OF SOLID PROPELLANTS

4. DESCRIPTIVE NOTES *(Type of report and inclusive dates)*
FINAL REPORT

5. AUTHOR(S) *(First name, middle initial, last name)*
GORDON C SMITH
KARUPPAGOUNDER PALANISWAMY
WOLFGANG G KNAUSS

6. REPORT DATE	7a. TOTAL NO. OF PAGES	7b. NO. OF REFS
JUNE 30, 1973	~~190~~ 195	93

8a. CONTRACT OR GRANT NO	9a. ORIGINATOR'S REPORT NUMBER(S)
Fo4611-71-C-0027	SM 73-3
b. PROJECT NO. 63630013059600	
c.	9b. OTHER REPORT NO(S) *(Any other numbers that may be assigned this report)*
d.	

10. DISTRIBUTION STATEMENT
Approved for Public Release
Distribution Unlimited

11. SUPPLEMENTARY NOTES Details of illustrations in this document may be better studied on microfiche.

12. SPONSORING MILITARY ACTIVITY
Air Force Rocket Propulsion Laboratory
Director of Laboratories
Edwards, CA 93523
Air Force Systems Command,
United States Air Force

13. ABSTRACT

The process of failure accumulation in composite propellants is studied. One part of the study is concerned with the experimental tracing of void and microcrack formation. A second part deals with the development of a physical model of microcrack growth in which cracks grow as a function of time and load history. The law for crack growth rate is based on the fracture mechanics of fracture in viscoelastic solids. Correlation of calculations and experiments on uniaxially strained tensile specimens in single loading-unloading cycles as well as repetitive load cycling (fatigue) shows that the model, though relatively simple when compared with the actual physical situation, is surprisingly accurate in representing the damage accumulated under strain. Damage is directly coupled with the constitutive behavior because the growth of flaws modified the propellant rigidity. Tests on cylinders under simultaneous tension and torque indicate that the failure process in this biaxial strain state loading is nearly the same as in the uniaxial strain state.

DD FORM 1 NOV 1473

UNCLASSIFIED
Security Classification

14. KEY WORDS	LINK A		LINK B		LINK C	
	ROLE	WT	ROLE	WT	ROLE	WT
SOLID PROPELLANTS						
FRACTURE						
FAILURE						
RATE THEORY						
CRACK PROPAGATION						

FOREWORD

This report was prepared by the Graduate Aeronautical Laboratories, California Institute of Technology (GALCIT), Pasadena, California under Contract FO4611-71-C-0027, Project 3059 for the Air Force Rocket Propulsion Laboratory (MKPB), Edwards Air Force Base, California. Dr. R. L. Peeters was the Air Force Project Engineer and Dr. W. G. Knauss was the GALCIT principal investigator. The work described in this report was performed during the period from 7 December 1971 to 30 April 1973.

During the final stages of this effort while the senior author was on sabbatical leave, Dr. C. D. Babcock willingly and effectively served as the principal investigator. The authors, in particular the senior author, are very grateful for this assistance. The authors further wish to acknowledge Messrs. E. Duran and V. Culler of the Jet Propulsion Laboratory and the Air Force Rocket Propulsion Laboratory for their support in machining the test specimens.

This technical report has been reviewed and is approved.

Dr. Randall L. Peeters, Materials Engineer
Surveillance and Mechanical Behavior Section
Air Force Rocket Propulsion Laboratory

ABSTRACT

The process of failure accumulation in composite propellants is studied. One part of the study is concerned with the experimental tracing of void and microcrack formation. A second part deals with the development of a physical model of microcrack growth in which cracks grow as a function of time and load history. The law for crack growth rate is based on the fracture mechanics of fracture in viscoelastic solids. Correlation of calculations and experiments on uniaxially strained tensile specimens in single loading-unloading cycles as well as repetitive load cycling (fatigue) shows that the model, though relatively simple when compared with the actual physical situation, is surprisingly accurate in representing the damage accumulated under strain. Damage is directly coupled with the constitutive behavior because the growth of flaws modified the propellant rigidity. Tests on cylinders under simultaneous tension and torque indicate that the failure process in this biaxial strain state loading is nearly the same as in the uniaxial strain state.

TABLE OF CONTENTS

TABLE OF CONTENTS (Cont'd)

LIST OF FIGURES

LIST OF FIGURES (Cont'd)

LIST OF FIGURES (Cont'd)

LIST OF FIGURES (Cont'd)

LIST OF FIGURES (Cont'd)

LIST OF SYMBOLS

a	experimentally determined parameter
A	area
A_o	activation energy
$A\epsilon_{max}$	shift factor
b	experimentally determined parameter
B	$\frac{a}{7C_o}[\pi C_o E_o \dot{\epsilon}_o]$
C	half crack length
C_1	experimentally determined constant
C_2	experimentally determined constant
C_i	crack length of the i^{th} crack
C_o	initial half crack length
C_{t1}	constant
d	outer diameter of a hollow sphere
D	damage function
D^*	spring stiffness
$E(t)$	instantaneous modulus; $\frac{\sigma}{\ell_o(t)[\lambda(t)-1]}$
E_{eff}	effective Young's modulus
E_i	tensile modulus measured normal to a crack
E_o	Young's modulus
E_{rel}	relaxation modulus
$F(\sigma)$	function of applied stress
G	amplitude
k	Boltzmann's constant
K	stress intensity factor

LIST OF SYMBOLS (Cont'd)

K_i	bulk modulus of the i^{th} element
K_o	critical stress intensity factor
K^*	bulk modulus for the composite
$\ell(t)$	length of tear element leg
$\ell_o(t)$	length of tear element leg in undeformed state
L	length of wave generating device
m	power of crack rate law
m_t	power of crack rate law
M	mass
N	number of cracks in a region
N^*	number of unbroken bonds
p	rate of sucrose conversion
P	proportionality factor
r_i	volume fraction of the i^{th} type elements
R	$\frac{2\pi C_o^2}{A}$
R_1	$1-1/9\{(1-\alpha^*)\,S+U\,(1-\beta^*)U\}$
R_2	$1/3(K_i-\frac{2}{3}\mu_i)\,[1-(1-\alpha^*)S]$
S	$\frac{K_i-K^*}{\alpha^*(K^*-K_i)-K^*}$
t	time
T	temperature ^oC
T_{ab}	absolute temperature ^oK

LIST OF SYMBOLS (Cont'd)

U	$\frac{\mu_i-\mu^*}{\beta^*(\mu^*-\mu_i)-\mu^*}$
V	volume
W	strain energy density
$\overline{W}$	strain energy
x	experimental constants (Arrhenius)
y	experimental constants (Arrhenius)
z	experimental constants (Arrhenius)
α^*	$\frac{1+\nu^*}{3(1-\nu^*)}$
β^*	$\frac{2(4-5\nu^*)}{15(1-\nu^*)}$
δ	$\tan^{-1} \epsilon_{22}/\epsilon_{11}$
ϵ	strain
ϵ_{CH}	strain calculated from test machine displacement
ϵ_{max}	maximum strain (arbitrarily defined)
ϵ_o	constant strain
$\dot{\epsilon}_o$	constant strain rate
$\overline{\epsilon}$	average strain
ϵ^*	macroscopic averaged strain
ϵ_{11}	principal strain
ϵ_{22}	principal strain
λ_1	constant
$\lambda(t)$	$\ell(t)/\ell_o(t)$
λ_2	constant
μ	shear modulus of the i^{th} element

LIST OF SYMBOLS (Cont'd)

μ^*	shear modulus of the composite
ν	Poisson's ratio
ν^*	Poisson's ratio for the composite
ξ	C/C_o
σ	stress
σ^*	macroscopic averaged stress
τ	$\frac{a}{C_o}\left[\sqrt{\pi} C_o E_o \epsilon_o\right]^n t$
τ_o	constant
τ^*	time to rupture
ω	frequency

1. Introduction

Since the beginning of solid propellant rocket technology the design of solid rockets has labored under the need to predict the failure of a rocket motor. This need has oscillated between a definition of failure and, if a definition was agreed upon, an appropriate way to describe or analytically characterize the failure. From a mechanical viewpoint there has been relatively little argument about the observation that the appearance of cracks in a solid rocket motor is not a desirable occurrence, though the presence of cracks need not necessarily imply a malfunction of an ignited rocket motor. Consequently, mechanical failure has usually been associated with fracture or the generation of new surface in the solid propellant. However, it has been a major quest of solid propellant mechanical behavior research to describe the conditions that lead to the appearance of cracks, and it must be recognized that even the way in which this description was to be accomplished was, and is not clear.

Yet the problem is not purely scientific. Although we believe we know how fractures are generated in motors we do not generally possess the analytical tools to exploit this knowledge. Consider, for example, a motor which is stored for a long time under thermally and cure-induced stresses. At points or small (diffuse) domains of elevated tensile stresses the composite propellant will exhibit binder-particle separation and thereby reduce its rigidity (or increase its compliance). As a consequence the deformation in that small domain increases and adjacent material can unload somewhat. There occurs a redistribution of the stresses and of strain energy. With time

additional binder-particle separation and void formation occurs, partially as the result of the redistribution of stress, partially because the binder-particle separation process is a time-dependent phenomenon; ruptures in the binder phase add to the lowering of the rigidity and to the spatial redistribution of the strain energy. If the redistribution of energy can continue at the expense of void formation and binder ligament rupture, the strain in the region under consideration will become so large that it can be accommodated and alleviated only by rupture of the binder; as a consequence a crack is formed within this region. It is entirely conceivable, however, that an equilibrium can be achieved in the distribution of the stresses (and of energy density*) around the mechanically highly worked region. In that event a crack would not appear in any time.

We have just described a phenomenon in which a) the failure process is coupled inseparably with the non-linear constitutive response of the composite propellant and b) which is possibly restricted to a small domain, at least initially, and in which c) the failure process involves the redistribution of an inhomogeneous stress and strain field.

For the purposes of design and mechanical performance analysis one has usually taken a different viewpoint. One performs first a stress and deformation analysis (in most if not all cases linearly elastic or linearly viscoelastic) and examines subsequently

---

*This may be considered also as the energy stored elastically in the binder ligaments.

whether the stresses or the deformations exceed certain permissible values. These values are termed colloquially "allowables" and are recognized to depend on the history of deformation (or on stress state history). The allowables are determined in laboratory tests involving homogeneous stress and deformation states. No uniform agreement exists as to how the allowables are to be defined. With reference to the uniaxial stress state they are taken variously as the maximum stress achievable in a constant strain rate uniaxial extension test, the strain at which this maximum occurs, or other suitable descriptions as delineated in the ICRPG Handbook on Mechanical Behavior of Solid Propellants. As a practical matter one tends, for example, toward a maximum or critical strain criterion when fracture at the surface of the bore or grain perforation is concerned and towards a criterion based on stress if failure is anticipated in a corner or near the case of the motor.

Thus an uncertainty is associated with the assignment of the allowables and is a consequence of considering the failure analysis separately from the stress analysis. In other words, if one were able to conduct a stress and deformation analysis of a rocket motor employing the (realistically) non-linear material characteristics, then the occurrence of failure (fracture) should be a natural outcome of that analysis. Instead one performs stress analyses in the absence of the failure process and tries to predict from the calculated stresses whether the material will sooner or later become locally unstable to admit the appearance of a crack.

In his thesis which is concerned with non-linear constitutive behavior of propellants Farris states [Farris 70] e.g. that if "...the degree of damage and the constitutive equation are uncoupled (it) can lead only to erroneous results...".

If these comments imply a criticism of the currently practiced methods of stress and failure analysis, it must be recognized, however, that this situation is conditioned by the lack of knowiedge concerning the non-linear constitutive behavior of propellants as well as by the absence of methods to conduct non-linear stress analyses with time-dependent properties. Moreover, the division into a stress analysis separate from a (subsequent) failure analysis has followed the tradition in design with metals where the onset of yield has often been taken as the failure limit. It must be clear, however - and this point has not always been understood in the propellant industry - that failure - not necessarily fracture - defined only as the onset of plastic deformation, i.e., termination of linearly elastic behavior, is justified when one uses only linearly elastic stress analysis; but to define fracture in a constitutively non-linear solid it is necessary to provide a stress analysis which incorporates the constitutive behavior realistically up to the point of fracture.

Biased by these habits of failure analysis with yielding metals as well as by the lack of knowledge regarding the non-linear constitutive behavior of solid propellants, efforts have continued to establish failure criteria (failure surfaces) with the aid of laboratory tests. These (small scale) examinations are conducted on homogeneously stressed (strained) specimens. To what extent these criteria

are then applicable to the prediction of failures in motors - where they are occasioned in strong interaction with non-linear constitutive response - has not been made clear. But we can infer from the relatively poor experience with attempted motor failure (fracture) prediction that the state of failure prediction is none too good. It is our opinion that part of this regrettable situation is founded on the neglect of the strong interaction between the failure process and the non-linear constitutive response of the material.

One might argue that in spite of this unresolved matter there are engineering approximations which allow one to proceed with practical designs. This is certainly true if one is willing to live with the relatively wide bounds provided by such estimates. Other branches of engineering face similar problems. For many years foundation engineers have designed safe (and unsafe) footings for structures. Their methods and tools of analysis have been nearly the same as those available to the rocket designer. However, because of the significantly greater latitude in margins of safety accorded to the foundation engineer, he tends to have a higher degree of success; he would be in dire straits also if the final or systems safety margin were to drop significantly below unity.

Therefore we contend that to achieve the high degree of reliability in motor failure prediction we must begin to detach ourselves from the conventional analysis methods and adopt those which are more commensurate with the physical processes that give rise to failure. Although the application of rate theory to the fracture of polymers constitutes a step in that direction, it was only a small step, for it still implied the separability of the stress and failure analysis.

2. Synopsis of Program Scope

The fact that failure of solid propellants is a process which depends (more or less) continuously on the load or deformation history has been recognized in the propellant industry under the term cumulative damage. The evidence of this damage has been described variously as dewetting, vacuole formation, filler binder separation, binder rupture, etc. However, the description of how the physical phenomena underlying these damage appearances has not been clarified beyond a qualitative state. It seemed therefore enticing to apply the equations of chemical rate theory to the pseudo-description of the failure development in these filled polymers. We shall review the concepts of chemical rate theory in some detail later. For the present it suffices to remark that for complex time-dependent processes, the chemical rate theory provides only a mathematical framework which is, in its soundest form, based on atomistic and molecular processes. In solid propellants the dominant phenomena seem to be occurring at the microscopic to macroscopic rather than at the atomistic level. While it is true that ultimately all microscopic and macroscopic phenomena can be described in terms of atomistic mechanics - provided an infinity of time and patience is available - it seems hazardous at best to ignore the macroscopic processes of the failure process and to try to characterize fracture in terms of mathematics appropriate to molecular processes under ideal situations (not necessarily in the solid state).

One can therefore suggest that the equations of the chemical rate theory be used to describe the microscopic phenomena of failure development in propellants or other materials for that matter. However, then one must ask whether such a mathematical description is in accord with physical observations. It is therefore necessary to either make direct or indirect observation of the process of failure in order to evaluate the applicability of the equations of rate theory to this observed process. We have not explored the direct observations because of lack of necessary equipment. *

In the past dilatation measurements have been used to indicate internal damage [Farris, 1968a, b]. However the relation of vacuole formation to damage had been argued without taking into account that the voiding was a time-dependent process. Furthermore, at small strains, where irreversible damage occurs also [Farris, 1970], volume dilatation was not measurable. Hence volume dilatation seemed to be a rather questionable indicator of propellant damage; the reason appears to be that internal fractures can occur in the microstructure of the propellant which are not necessarily associated with a net volume increase under stress.

---

*We have considered, for example, the photographic observation of the damage near the surface of a propellant sample. If recorded through a TV camera attached to an optical microscope, the output could be analyzed electrically into signals resulting from light and dark areas. If the sample is illuminated under a low angle with respect to the surface, then holes should record as shadows while the solid would record lighter. After suitable calibration and normalization with respect to the initial and undeformed state the ratio of dark and light area per frame could have been evaluated for the increase in holes (number and sine) in the deformed state as a function of a continuously increasing strain.

We therefore turned to an attempt at a less direct observation of damage produced under continuous straining. Details of this attempt are presented later.

The intent was to measure the change in attenuation of high frequency sound waves as a function of the number of internal cavities formed and/or enlarged in the stressed material. We believe that the method failed because other phenomena which could not be removed through calibration dominated a part of the deformation cycle. We thus found that the application of a uniaxial stress (probably) increased the packing of the composite structure and induced an increase in the rigidity transverse to the tension, which packing was counteracted by the numerous growth of voids as sizable strains ($\sim 10\%$) were produced. Thus the hope of detecting damage at small strains which is also not accessible by volumetric measurements and which is important for failure under small strains sustained for long times, did not materialize.

We made a detailed and careful experimental study with the high frequency device described later. For it seemed to us that the direct verification of the applicability of rate theory to solid propellants stood or fell with an experimental method to follow the development of the damage. We considered using the dielectric properties of the strained propellant; but in view of the findings at the Lockheed Propulsion Company [Cantey] that the propellant dielectric properties were not related easily to the microstructure of the propellant, a dielectric characterization of the microfracture process seemed to be an ill-advised attempt, unless considerable

effort was expended in making such a method into a truly meaningful tool. It was our feeling that such was not possible under the scope of the program. In this appraisal we were mindful of the need for relatively simple characterization techniques; for if experimental methods for mechanical failure characterization become significantly more complex than those accommodated by equipment currently available in most propellant laboratories, then such characterization would not be likely to be carried out. This fact must be understood as an implicit part of the program.

We therefore decided to exploit the less direct information contained in the propellant deformation characteristics, since these are intimately linked with the microstructural degradation. In making this decision we have done the following: While we attempted first to find an experimental technique which would allow the relatively simple correlation with the proposed reaction rate theory we now resorted to the application of very simple experimental techniques (measuring the constitutive response) at the expense of developing the theoretical framework. One might ask whether it is easier to develop an experimental technique than a theoretical frame with the aid of which one extracts information from the simpler experiments. Although we leaned towards an experimental rather than theoretical effort we felt nevertheless that it would be easier to convey to the solid propellant designer the <u>results</u> of a theoretical study than to transfer the execution of what was certainly to be a rather elaborate experimental method of damage measurement. It should also be stated that by this course of development

the "modelling" of the fracture process has shifted from the (proposed) manipulation of a set of rate equations to the developing of a consistent mathematical and physical model of the progressive fracture of a composite propellant. Furthermore, in order to introduce the element of time into the analysis one need not be tied necessarily to the equations of chemical reaction rate theory but it is possible and potentially advantageous to use alternate descriptors for the time dependence of the fracture process. For this reason we do not insist on using the names "Chemical Reaction Rate Theory" or "Theory of Absolute Reaction Rates" since these imply the description of rate processes in a very special way. Rather we shall generally speak only of a rate theory, as indicated in the title of this report.

The idea that we pursue then is the modelling of the development of microscopic fractures, either by particle binder separation or by binder fracture. These fractures grow with time as a function of the applied loads. They are assumed to grow through several stages: First cracks appear which are small compared to the dominant dimensions of the microstructure; as they grow larger so that their stress fields influence each other strongly their growth is controlled more appropriately by a tearing process [Thomas], [Greensmith, 1960]. The solid is divided into many subregions each of which contains a flaw, the initial flaw size distribution being arbitrary. The stresses in each of the subregions are related to the macroscopically applied stresses through a model of particulate composites proposed by Budiansky [Budiansky]. The damage at

any time t is then defined as the ratio of total surface area generated by fracture up to that point, to the maximum possible surface area that can be generated under any circumstances. The calculations are demonstrated for several load histories in the uniaxial stress state.

For the investigation of failure in biaxial stress states, an accessory was constructed for the Instron Tester which permitted the simultaneous application of tension and torsion to cylindrical specimens. The machining of these specimens turned out to be an expensive proposition.

3. Review of Reaction Rate Theory as Commonly Applied to the Fracture of Solids

In 1889 S. Arrhenius suggested that the rate of sucrose conversion in solution was governed by the rate p as given by the equation

$$\ell n\, p = \ell n\, x - \frac{y}{zT_{ab}} \qquad (1)$$

which we recognize as a form of the more familiar expression

$$p = x\, e^{-y/zT_{ab}} \qquad (2)$$

where x, y, and z are constants and T_{ab} the absolute temperature. Subsequently many simple reactions which were slow enough to be followed quantitatively were found to follow the same law.

The advent of statistical mechanics and its application to the probability of atomistic or molecular interaction leads to a theoretical foundation for the experimental knowledge. This foundation is related to two thoughts, namely to

a) the probability of finding an atom (or ion) in a sufficiently high energy state to interact with another atom (or ion) and to

b) the probability of two atoms (or ions) being close enough to interact, such as a result of Brownian random motion in liquids and gases.

If we allow ourselves to be somewhat non-specific for the moment we observe that there are also many processes in solids which can be correlated by an exponential relation similar to equations (1) and (2). If such processes involve association or dissociation of atoms or ions the temptation is close to assign to this

association or dissociation a dominant role in the whole process. We feel that such an assignment has been and is being made in the fracture of polymers, and that this assignment may not be justifiable in principle, though experiments over limited ranges of test conditions do not contradict it. Molecular phenomena connected with creep and relaxation can also be described in similar ways [Tobolsky and Eyring] and thus a distinction between processes dominated by molecular dissociation or molecular reorientation is rather tenuous. The measurement of radical formation in a deformation process may be merely an accompaniment of the deformation process. One cannot say unequivocally that the observed time dependence is the result of the time it takes radicals to dissociate. In Appendix A we have reviewed most of the currently available literature on the application of reaction rate theory to unfilled polymers.

The view that is expressed in these papers is essentially the following: When molecules are subjected to forces which tend to break them (e.g., tension along the backbone chain) the time it takes to effect the break is an exponential function of the applied stress. More specifically, it is believed that the time dependence of the macroscopic fracture process derives from the time it takes the molecular bond to break while it is being stressed as if it were isolated from the rest of the molecules.

A view that is not expressed, but which is equally plausible - depending on one's viewpoint, more plausible - is this: Let us assume that a molecule chain can rupture whenever it is subjected to a critical (tensile) load, and that the time necessary for this

to occur is very short compared to the time scale of the experiments which are normally conducted in the laboratory. Upon load application the microstructure of the polymer deforms and in this process polymer chains strain as a consequence of the deformation process. The deformation and rearrangement of the microstructure is a time-dependent process. One could argue - and we think safely so - that the time dependence in polymer fracture can derive from the molecular rearrangement which loads the polymer chains more or less gradually. After some chains have broken further rearrangement is possible which then may lead to further chain ruptures. These deformation processes may be described approximately by the same rate equations as the molecular dissociation process [Tobolsky and Eyring]; consequently, if measurements of the number of broken polymer chain radicals as a function of the macroscopic stress history can be described approximately by reaction rate equations, this fact does not per se prove that the time or load history effect is the result of the molecular dissociation process.

In fact the two processes occur simultaneously, side by side and not entirely independent of each other. Measurement of the radicals formed yields only the end result without differentiation of the processes that produced it.

Thus it is quite possible that the rate theory of polymer fracture is not in fact a Reaction Rate Theory (rate of chemical bond dissociation) but a Deformation Rate Theory.

One might ask why it is important to examine the fracture of homogeneous polymers so critically in connection with the failure

of composite propellants. It seems to us that if one wishes to apply a concept of molecular fracture to the failure of composite propellants one should be convinced first that the concept is applicable to homogeneous polymers. Otherwise one runs the danger of developing a curve fitting procedure, the limitations of which are not clear.

We do not wish to imply that curve fitting is bad per se; the first progress in ordering and understanding physical processes is aided greatly by correlating physical observations. But it may be dangerous to associate false concepts with the failure process, even though these concepts can produce a certain degree of success in correlating available experimental data.

In solid propellants the failure process is accompanied by phenomena which involve domains large compared to atomistic or molecular dimensions. To ignore this fact would seem a serious mistake and a description by continuum rather than atomistic mechanics appears called for.

It is of course possible that the macroscopic processes leading to the failure of composite propellants (dewetting, binder rupture and tearing) could be described on the average by the equations of chemical reaction rate theory. But it seems dubious that such a description can be successful if it neglects the details of the mechanical processes leading to failure (initial and continuous dewetting, binder fracture, ligament formation and ligament rupture).

4. Failure Detection Study

Failure of propellants in laboratory tests has not always been defined consistently. One variously takes a) the ultimate maximum principal tensile strain at rupture, b) the maximum principal stress (occurring at a principal strain of less than the maximum strain), c) the principal strain sustained under b), or d) a smaller strain defined in the ICRPG Test Procedures Handbook. Excepting the definitions a) and b) none of the definitions are objective, and the usefulness of definitions a) and b) has often been questioned, since they lead to rather non-conservative designs. It must be remembered, however, that this shortcoming may be due to the inadequate methods of stress analysis rather than a poor definition of failure.

Nevertheless it seemed imperative from the outset of this study that a consistent definition of damage and failure must be available which is virtually free of subjective measurement interpretation. To give an example of particularly subjective interpretation of failure data we cite the determination of the failure strain at the maximum principal stress; since the stress maximum is usually a very flat one, the assignment of a strain at the maximum stress is open to a considerable range of interpretation.

We shall see later that in strain cycling experiments on TPH 1011 propellant multiple cracks (1-2 mm long) appear in specimens long before one can consider the specimen failed by any of the above mentioned criteria. The appearance of several cracks was not accompanied by any marked change in the stress-strain response of the material. This phenomenon was observed only during uniaxial

tensile tests in our later studies; it has not been considered as a laboratory failure mode to our knowledge except in sheets of propellant. For the initial part of our studies we therefore proceeded with the generally held notion that propellants (in the uniaxial stress state) fail by a global deterioration from which cracks develop at a rather late stage of the deformation history. This notion appears to derive from failure observation in monotonic load histories when, in our experience, crack formation was often indeed observed rather late in the deformation history.

In contrast, the JP 500 propellant seldom exhibited cracks prior to the final rupture even and therefore a homogeneous failure process under the monotonic and cyclic load histories examined appeared appropriate, but not necessarily for the TPH 1011 propellant. Nevertheless, since this recognition came somewhat late in this study we record our investigation of an (assumed) homogeneous fracture process.*

In pursuing the measurement of the macroscopically homogeneous failure process by voiding and binder rupture we were dissuaded early in our study by colleagues in the propellant industry from using the volume dilatation as an indicator of the damage accrued in the material. The dissuasion was based on the observation that damage could be detected by examining the stress-strain

---

*We should note, however, that if the mode of failure, i.e., the localized (cracking) versus the homogeneous (dewetting and blanching) form is a function of the deformation history, then a reaction rate theory which draws on homogeneous processes seems a poor candidate theory for failure prediction.

behavior of propellant before a volume dilatation could be observed. While this fact is true at strains below a few per cent, dilatation is observable - if the first stress-invariant is positive - at larger strains and corroborates at least qualitatively how one would expect the homogeneously accumulated damage to behave. As the final fracture point is approached, say in a constant strain rate test, the volume dilatation increases rapidly just as one would expect from the generation and enlargement of damage voids in the composite.

In searching for an alternate method of damage detection which was manageable under the available budget and which was simple enough to be acceptable by the propellant industry we explored an electro-mechanical device. The question that motivated us originally was whether the modification of the high frequency wave transmission characteristics by the appearance of voids or cracks could be used to trace the mechanical degradation of the material. We thus constructed an electromechanical oscillator composed of two Vernitron piezo-electric ceramic discs 3/8" in diameter and each 1/8" thick stacked in series (called the driver) and a transducer (called the receiver) dimensioned identically to convert mechanical pulses into voltage signals (figure 1). The driver discs executed axial deformation upon voltage application and the receiver produced a voltage output proportional to the axial compression or expansion.

Operation with the device across thin propellant slabs (about 1/8" thick) turned out to produce a great number of closely spaced resonances above 30 kcps; moreover, these resonances

shifted in a not too predictable manner when a strain was applied to the propellant. We spent a reasonable time trying to separate out the resonance response from any underlying systematic variation of the signal with strain but convinced ourselves that flaw detection in this way (at frequencies above 30 kcps) would always remain a dubious effort. We therefore attempted a different approach which might function at lower frequencies.

In figure 2 we depict the driver and receiver mounted on opposite sides of a tensile specimen. If the clamp is sufficiently weak only the propellant provides a (visco)elastic coupling between the driver and the receiver. If the propellant weakens due to the formation of voids in the failure process, the coupling should become weaker with increasing strain (provided one does not operate near a natural frequency of the system) and the change in the receiver output would then be related approximately to the deterioration of the material.

In considering this method of damage detection one assumes that the damage changes the material properties isotropically, or at least nearly so. In fact one knows that such is not the case if one considers the analogous case of an isotropic solid which generates penny-shaped thin cracks normal to the direction of maximum tension. If one were to characterize the tension or compression properties parallel to the cracks, i.e., normal to the maximum tension one would find, ideally speaking, no effect of the cracks as long as the tension is so small that the cracks are virtually undeformed or unopened. However, as the tension increases and deforms the cracks

into cavities elongated in the direction of maximum tension these "transverse" properties would change. It seemed to us that this effect could have been calibrated out of the measurements in order to deduce the rate of generation of new fractures at strain levels that are of interest in propellant fracture studies.

Material characterization of propellants in multiaxial stress-states is in a very poor state. There existed, to our knowledge, no quantitative measurement that would have given us a clue of how the deformation characteristics transverse to the tension change with the tensile strain (stress). We therefore proceeded on the assumption that measurable damage was at least approximately isotropic.

The construction of the electromechanical device (EMD) involved essentially only two minor problems. The careful formation of the solder joints so that the piezoelectric ceramic discs, the shim-stock conductors and the brass base would not fail by fatigue (fatigue failures occurred several times in the beginning of the investigations); second the proper shielding of the receiver from the electric field of the close-by driver.

Initial measurements gave erratic results. We therefore examined the effect of using silicone grease (stop cock grease) as a coupling agent between the EMD and the propellant. Observation under an 80-power microscope did not reveal any visual influence of the grease on the propellant over a period of three days and repeating measurements with the EMD after three days produced the same results if the EMD-propellant assembly was not disturbed.

We thus concluded that the use of the silicone grease would not influence the mechanical behavior of the propellant during the tests which we contemplated. It was found, however, that the EMD response was a function of the pressure with which the device was held against the propellant, and also a function of time. In figure 3 we show the EMD signal as a function of time for various compressive loads across the EMD-propellant assembly; the propellant was not strained during these tests. We believe that the observed time effect is associated with the flow of the silicone grease under the EMD "stamp." To obtain nearly reproducible, or at least consistent, measurements it was necessary to apply the grease liberally. Figures 4 and 5 show a plot of the EMD response at 16000 cps under increasing compressive load on the EMD (no load on the propellant perpendicular to the EMD-axis) in connection with different materials. The data correspond to times after load application ($\sim$ 60 sec) when according to figure 3 a nearly steady state signal was achieved. For the relatively soft materials, TPH 1011 propellant and the polyurethane elastomer Solithane, the response is similar. The flow of the silicone grease is affected by the low rigidity of the material. For the rather stiff materials, PMMA and aluminium the change in output with load is significantly less than for propellant or Solithane. For loads exceeding about 200 gms we could not guarantee that the pressure distribution over the greased surfaces of the EMD was uniform; the reason for this uncertainty was that due to the larger size of the weights used to apply the pressure, the fixture through which the device was loaded did not permit an accurate

We thus concluded that the use of the silicone grease would not influence the mechanical behavior of the propellant during the tests which we contemplated. It was found, however, that the EMD response was a function of the pressure with which the device was held against the propellant, and also a function of time. In figure 3 we show the EMD signal as a function of time for various compressive loads across the EMD-propellant assembly; the propellant was not strained during these tests. We believe that the observed time effect is associated with the flow of the silicone grease under the EMD "stamp." To obtain nearly reproducible, or at least consistent, measurements it was necessary to apply the grease liberally. Figures 4 and 5 show a plot of the EMD response at 16000 cps under increasing compressive load on the EMD (no load on the propellant perpendicular to the EMD-axis) in connection with different materials. The data correspond to times after load application ($\sim$60 sec) when according to figure 3 a nearly steady state signal was achieved. For the relatively soft materials, TPH 1011 propellant and the polyurethane elastomer Solithane, the response is similar. The flow of the silicone grease is affected by the low rigidity of the material. For the rather stiff materials, PMMA and aluminium the change in output with load is significantly less than for propellant or Solithane. For loads exceeding about 200 gms we could not guarantee that the pressure distribution over the greased surfaces of the EMD was uniform; the reason for this uncertainty was that due to the larger size of the weights used to apply the pressure, the fixture through which the device was loaded did not permit an accurate

We thus concluded that the use of the silicone grease would not influence the mechanical behavior of the propellant during the tests which we contemplated. It was found, however, that the EMD response was a function of the pressure with which the device was held against the propellant, and also a function of time. In figure 3 we show the EMD signal as a function of time for various compressive loads across the EMD-propellant assembly; the propellant was not strained during these tests. We believe that the observed time effect is associated with the flow of the silicone grease under the EMD "stamp." To obtain nearly reproducible, or at least consistent, measurements it was necessary to apply the grease liberally. Figures 4 and 5 show a plot of the EMD response at 16000 cps under increasing compressive load on the EMD (no load on the propellant perpendicular to the EMD-axis) in connection with different materials. The data correspond to times after load application ($\sim$60 sec) when according to figure 3 a nearly steady state signal was achieved. For the relatively soft materials, TPH 1011 propellant and the polyurethane elastomer Solithane, the response is similar. The flow of the silicone grease is affected by the low rigidity of the material. For the rather stiff materials, PMMA and aluminium the change in output with load is significantly less than for propellant or Solithane. For loads exceeding about 200 gms we could not guarantee that the pressure distribution over the greased surfaces of the EMD was uniform; the reason for this uncertainty was that due to the larger size of the weights used to apply the pressure, the fixture through which the device was loaded did not permit an accurate

We thus concluded that the use of the silicone grease would not influence the mechanical behavior of the propellant during the tests which we contemplated. It was found, however, that the EMD response was a function of the pressure with which the device was held against the propellant, and also a function of time. In figure 3 we show the EMD signal as a function of time for various compressive loads across the EMD-propellant assembly; the propellant was not strained during these tests. We believe that the observed time effect is associated with the flow of the silicone grease under the EMD "stamp." To obtain nearly reproducible, or at least consistent, measurements it was necessary to apply the grease liberally. Figures 4 and 5 show a plot of the EMD response at 16000 cps under increasing compressive load on the EMD (no load on the propellant perpendicular to the EMD-axis) in connection with different materials. The data correspond to times after load application ($\sim$60 sec) when according to figure 3 a nearly steady state signal was achieved. For the relatively soft materials, TPH 1011 propellant and the polyurethane elastomer Solithane, the response is similar. The flow of the silicone grease is affected by the low rigidity of the material. For the rather stiff materials, PMMA and aluminium the change in output with load is significantly less than for propellant or Solithane. For loads exceeding about 200 gms we could not guarantee that the pressure distribution over the greased surfaces of the EMD was uniform; the reason for this uncertainty was that due to the larger size of the weights used to apply the pressure, the fixture through which the device was loaded did not permit an accurate

We thus concluded that the use of the silicone grease would not influence the mechanical behavior of the propellant during the tests which we contemplated. It was found, however, that the EMD response was a function of the pressure with which the device was held against the propellant, and also a function of time. In figure 3 we show the EMD signal as a function of time for various compressive loads across the EMD-propellant assembly; the propellant was not strained during these tests. We believe that the observed time effect is associated with the flow of the silicone grease under the EMD "stamp." To obtain nearly reproducible, or at least consistent, measurements it was necessary to apply the grease liberally. Figures 4 and 5 show a plot of the EMD response at 16000 cps under increasing compressive load on the EMD (no load on the propellant perpendicular to the EMD-axis) in connection with different materials. The data correspond to times after load application ($\sim$60 sec) when according to figure 3 a nearly steady state signal was achieved. For the relatively soft materials, TPH 1011 propellant and the polyurethane elastomer Solithane, the response is similar. The flow of the silicone grease is affected by the low rigidity of the material. For the rather stiff materials, PMMA and aluminium the change in output with load is significantly less than for propellant or Solithane. For loads exceeding about 200 gms we could not guarantee that the pressure distribution over the greased surfaces of the EMD was uniform; the reason for this uncertainty was that due to the larger size of the weights used to apply the pressure, the fixture through which the device was loaded did not permit an accurate

We thus concluded that the use of the silicone grease would not influence the mechanical behavior of the propellant during the tests which we contemplated. It was found, however, that the EMD response was a function of the pressure with which the device was held against the propellant, and also a function of time. In figure 3 we show the EMD signal as a function of time for various compressive loads across the EMD-propellant assembly; the propellant was not strained during these tests. We believe that the observed time effect is associated with the flow of the silicone grease under the EMD "stamp." To obtain nearly reproducible, or at least consistent, measurements it was necessary to apply the grease liberally. Figures 4 and 5 show a plot of the EMD response at 16000 cps under increasing compressive load on the EMD (no load on the propellant perpendicular to the EMD-axis) in connection with different materials. The data correspond to times after load application ($\sim$60 sec) when according to figure 3 a nearly steady state signal was achieved. For the relatively soft materials, TPH 1011 propellant and the polyurethane elastomer Solithane, the response is similar. The flow of the silicone grease is affected by the low rigidity of the material. For the rather stiff materials, PMMA and aluminium the change in output with load is significantly less than for propellant or Solithane. For loads exceeding about 200 gms we could not guarantee that the pressure distribution over the greased surfaces of the EMD was uniform; the reason for this uncertainty was that due to the larger size of the weights used to apply the pressure, the fixture through which the device was loaded did not permit an accurate

We thus concluded that the use of the silicone grease would not influence the mechanical behavior of the propellant during the tests which we contemplated. It was found, however, that the EMD response was a function of the pressure with which the device was held against the propellant, and also a function of time. In figure 3 we show the EMD signal as a function of time for various compressive loads across the EMD-propellant assembly; the propellant was not strained during these tests. We believe that the observed time effect is associated with the flow of the silicone grease under the EMD "stamp." To obtain nearly reproducible, or at least consistent, measurements it was necessary to apply the grease liberally. Figures 4 and 5 show a plot of the EMD response at 16000 cps under increasing compressive load on the EMD (no load on the propellant perpendicular to the EMD-axis) in connection with different materials. The data correspond to times after load application (~60 sec) when according to figure 3 a nearly steady state signal was achieved. For the relatively soft materials, TPH 1011 propellant and the polyurethane elastomer Solithane, the response is similar. The flow of the silicone grease is affected by the low rigidity of the material. For the rather stiff materials, PMMA and aluminium the change in output with load is significantly less than for propellant or Solithane. For loads exceeding about 200 gms we could not guarantee that the pressure distribution over the greased surfaces of the EMD was uniform; the reason for this uncertainty was that due to the larger size of the weights used to apply the pressure, the fixture through which the device was loaded did not permit an accurate

We thus concluded that the use of the silicone grease would not influence the mechanical behavior of the propellant during the tests which we contemplated. It was found, however, that the EMD response was a function of the pressure with which the device was held against the propellant, and also a function of time. In figure 3 we show the EMD signal as a function of time for various compressive loads across the EMD-propellant assembly; the propellant was not strained during these tests. We believe that the observed time effect is associated with the flow of the silicone grease under the EMD "stamp." To obtain nearly reproducible, or at least consistent, measurements it was necessary to apply the grease liberally. Figures 4 and 5 show a plot of the EMD response at 16000 cps under increasing compressive load on the EMD (no load on the propellant perpendicular to the EMD-axis) in connection with different materials. The data correspond to times after load application ($\sim$60 sec) when according to figure 3 a nearly steady state signal was achieved. For the relatively soft materials, TPH 1011 propellant and the polyurethane elastomer Solithane, the response is similar. The flow of the silicone grease is affected by the low rigidity of the material. For the rather stiff materials, PMMA and aluminium the change in output with load is significantly less than for propellant or Solithane. For loads exceeding about 200 gms we could not guarantee that the pressure distribution over the greased surfaces of the EMD was uniform; the reason for this uncertainty was that due to the larger size of the weights used to apply the pressure, the fixture through which the device was loaded did not permit an accurate

We thus concluded that the use of the silicone grease would not influence the mechanical behavior of the propellant during the tests which we contemplated. It was found, however, that the EMD response was a function of the pressure with which the device was held against the propellant, and also a function of time. In figure 3 we show the EMD signal as a function of time for various compressive loads across the EMD-propellant assembly; the propellant was not strained during these tests. We believe that the observed time effect is associated with the flow of the silicone grease under the EMD "stamp." To obtain nearly reproducible, or at least consistent, measurements it was necessary to apply the grease liberally. Figures 4 and 5 show a plot of the EMD response at 16000 cps under increasing compressive load on the EMD (no load on the propellant perpendicular to the EMD-axis) in connection with different materials. The data correspond to times after load application (~60 sec) when according to figure 3 a nearly steady state signal was achieved. For the relatively soft materials, TPH 1011 propellant and the polyurethane elastomer Solithane, the response is similar. The flow of the silicone grease is affected by the low rigidity of the material. For the rather stiff materials, PMMA and aluminium the change in output with load is significantly less than for propellant or Solithane. For loads exceeding about 200 gms we could not guarantee that the pressure distribution over the greased surfaces of the EMD was uniform; the reason for this uncertainty was that due to the larger size of the weights used to apply the pressure, the fixture through which the device was loaded did not permit an accurate

placement of the weights. We therefore do not attribute much significance to the data at the 275 gm load for the rigid materials in figure 5. For later measurements the compression force was provided by a clamp as shown in figure 2; it exerted a force of approximately 50 gms across a propellant sample 1/8" thick.

We examined the frequency response of the EMD when coupled with a slice of propellant; both TPH 1011 and JP 500 series propellant were examined. Because of the similarity of the resultant data only the TPH 1011 data are recorded. In figure 6 we show the response of the EMD as a function of frequency and propellant temperature. We note that for the two samples used two sets of systematically ordered response curves resulted. This indicates an observation we made repeatedly: that the same measurements on different samples of the same propellant and of the same dimensions produced measurements that differed by factors of up to two.

We can understand the response depicted in figure 6 by alluding to a simple analog. If we consider the receiver as a rigid mass m which is being driven by the driver through a spring of (variable) stiffness D* (here actually a viscoelastic spring) the force acting on the mass should be proportional to the output of the EMD. The amplitude of the force for an undamped spring-mass system is

$$G = \frac{D^*\omega^2}{\left|\frac{D^*}{M} - \omega^2\right|} \cdot \text{Const} \qquad (1)$$

For small frequencies this amplitude is thus independent of D* and proportional to ω^2, while for $\omega >> D^*/M$ the amplitude is proportional to D*; rigid body resonance occurs at $D^* = M\omega^2$. In figure 6 the maxima

around 10 kcps correspond to the resonance which is strongly damped because of the viscoelastic properties of the propellant. However, instead of a plateau for $\omega >> D^*/M$ we observe a rise in the transducer output amplitude which we identify with higher resonance modes of the EMD. For a brass bar of the same length as the EMD without propellant the frequency of 60 kcp excites the fundamental mode of axial vibration (half wave length equal to the length of the EMD) and we therefore attribute the rise in the EMD output around 50 kcp to such a resonance. For higher frequencies there occur many resonances which we have not recorded here, but which we associate with higher modes and the fact that the EMD is not a simple bar but a composite of different pieces soldered together.

It should be mentioned that if the device had fulfilled the objective of our pursuit we could have extended its useful range - namely the plateau region. Decreasing the mass of both driver and receiver through shortening their lengths would have moved the resonance points to higher frequencies but the standing wave mode would have moved further than the rigid body resonance since the former is proportional to L^{-1} while the latter is proportional to $L^{-1/2}$. This change was not attempted. In figure 7 we have summarized measurements at 1600 cps for different specimens at different temperatures. It seems clear from the wide data scatter that an absolute measurement of any damage would have been a difficult undertaking at best. On the other hand, the consistent response as a function of frequency in figure 6 seems to indicate that measurements of <u>changes</u> relative to some initial state would be quite possible. This variation

of measurement results is only in part due to the method of affixing the EMD to the propellant and to the previous (mechanical) history of the propellant sample; it is also evidence of property variations. Since the EMD samples a mechanical property over a relatively small region the data scatter should be larger than for a measurement averaged over a larger volume.

For the following measurements we therefore cut all the test specimens from a relatively small block of propellant with the intent to obtain samples of nearly uniform properties.

Since during the straining of a tensile specimen its thickness changes one must observe whether the mere change in thickness is responsible for any possibly observed signals during straining. We thus measured the response of the EMD in conjunction with propellant slices of different thickness, taking great care to attach the EMD to the propellant in a consistent way. The result is shown in figure 8. Suppose we start with a specimen 0.15" thick and strain it by 20% (at best); then its lateral contraction would be at most ($\nu = \frac{1}{2}$) on the order of 0.015" (10%). This thickness change could then produce a change in the EMD output of about 15 per cent. We shall see shortly that a change of this size is not important at some temperatures while it is significant at others.

We turn next to measurements with the EMD on propellant during uniaxial straining. For this purpose we employed specimens as shown in figure 9; they were die-stamped from a sheet which had been milled with a fly cutter of $\frac{1}{2}$" radius at the Jet Propulsion Laboratory. For handling the sheet and the specimens were supported

by heavy cardboard in order to reduce as much as possible any internal damage before the specimens were tested.

In order to measure the strain in the dog bone specimen simply we determined the strain photographically in the central specimen section and compared it with the strain calculated from the separation of the tabs (= Instron crosshead separation) and a constant gage length of 3 3/8". The result shown in figure 10 allows the calculation of the strain in the central portion of the specimen from the Instron crosshead separation.

In figure 11 we show the load exerted on a dog bone specimen of TPH 1011 propellant at 10° C against time together with the EMD output (rms) during a constant rate of extension test. At temperatures above 0° C it was always found that the transducer output increased first with rising uniaxial stress before falling off some time before the maximal load was achieved. Figures 12 and 13 show results of tests conducted on TPH 1011 and JPL 500 series propellant under comparable test conditions.* In contrast, at temperatures below -10° C the response of the EMD did not initially follow the applied stress as indicated, for example at -20° C for TPH 1011 in figure 14. A summary of EMD responses for $0° C \leq T \leq 40° C$ is shown in figure 15, all of which show maxima around strains in the range 8 - 15%. A series of tests for various straining rates and at temperatures of zero degrees C and higher are recorded in figures 16 through 22 with bars on the load-vs-time curves denoting the load

---

*Only deviation from EMD output from initial value shown.

and time at which the maximum of the EMD output occurred. At 10° C and 0° C, identifiable points of maximum EMD response were observed.

We believe that the following process gives rise to the observed response measured by the EMD: Although a contraction of the material could cause a signal increase in accordance with figure 8 a quick estimate will show that the rise of the EMD signal with applied tensile load exceeds the effect expected from a Poisson contraction. During the tensile deformation the particulate matter in the propellant becomes more tightly packed transverse to the tension axis; this packing is probably also associated with touching of the particles and the creation of fractures might facilitate this rearrangement process under load. As a consequence, the rigidity of the specimen transverse to the tension increases (at least under the small deformations and stresses produced by the EMD). As long as the binder is soft enough (at the higher temperatures) this particle-particle approachment is possible relatively quickly, but it becomes more difficult as the binder becomes more viscous at the lower temperatures. At increasing strains the particle packing is disturbed increasingly by the development of fractures and voids which tend to loosen the particle-binder structures.

Since we cannot describe these two competitive processes quantitatively it is impossible to interpret the maximum in the EMD response conclusively. However, it should be clear if our simple picture of the micro-deformations is approximately correct that by the time the EMD output has reached its maximum the internal destruction of the material has progressed so far that its effect is being distinctly felt transversely to the tension axis. While we

cannot argue conclusively that the material has "failed" at that point it seems plausible that it cannot sustain a stress very long which is nearly equal to that at which the EMD displays its maximal response.

Let us thus accept, tentatively, that the point of maximal EMD response indicates that the microscopic destruction of the propellant structure is overcoming the lateral granular compaction occasioned primarily by the deformation process. Then the occurrence of the maximal EMD response can be interpreted as the onset of massive internal damage. How much strength or deformability the propellant has after that point has been reached is a matter to be discussed later. It is interesting now to observe that the strain, at which this event occurs in figures 11-13 and 16-22, is significantly smaller than the strain at maximum stress (maximum load); on the basis of this failure criterion based on an internal state of propellant damage, the designs of motors would turn out to be more conservative than those constructed on the basis of current techniques.

Let us summarize the results of this section. We have searched for a method of detecting the development of internal damage, which we attempted to accomplish with an electromechanical device (EMD). We spent a considerable time in investigating the characteristics of this device and the parameters that influence its consistent operation. Although the EMD was not found suitable for absolute measurements of propellant damage it is believed suitable to define a "failure" condition in an objective way which is connected with the micromechanical breakdown of the propellant in monotonic load histories.

In addition the device has yielded new information on the

small deformation characteristics of uniaxially stressed propellant. Damage is apparently associated with the tension direction at small strains and becomes evident normal to the tension axis at higher strains as a result of massive void generation* and their coalescence to larger voids. Sizable damage occurs below stresses and strains designated usually as allowable stresses and strains.

---

*In the unloaded state these voids may shrink to cracks.

5. Failure Model

a. Some Preliminary Observations

As we have indicated in the introduction, the lack of a method for the direct monitoring of propellant damage requires the development of a failure model which explains the evidence of damage in terms of the mechanical properties under deformation.

We shall first give a qualitative account of the failure process as we view it and how it is related to the constitutive response of the damaged material. The damage sustained by composite propellants under deformation is primarily a consequence of the fact that these materials are, as their name implies, composite solids, in which the hard particles outrank the soft binder-phase both by weight and by volume. The particle packing is usually so dense that particles are in direct contact or separated from others only by layers which are thin compared to the average diameter of the particles. When the composite is subjected to deformations, experienced macroscopically as homogeneous, the micro-structure of the propellant experiences inhomogeneous deformations; moreover, because of the great difference in the rigidity of the filler particles and the polymeric binder, the greatest contribution by far to the macroscopic deformation arises from that of the soft binder. If one considers that the binder contribution is only 20-25 per cent of the propellant volume and furthermore the fact that the inhomogeneous deformation of the binder around the particles induces locally large strains, it is easy to realize that particle-binder separation and/or binder rupture must occur. This observation is most obvious when one thinks of tensile

strains on the order of a few per cent. However, even for shear deformations it should be clear that the motion of the granular, hard component, with a good fraction of the grains in (frictional) contact, engenders particle motion (translation and rotation) which strains the thinly interspersed binder to the failure point.

This suggestion can be gaged qualitatively from figure 23. A unit cell from a regular and two dimensionally periodic system containing a (relatively) rigid cylinder is deformed in shear. If the cylinder has a diameter nearly equal to the cell dimension then the shear that is possible before the cylinders would touch the cell wall and each other is small; of course, if the cell material adheres to the cylinder and remains intact, i.e., does not fracture, then the cylinders will not touch but merely deform the cell material very highly near "contact points" A and B. A fracture thus generated may temporarily generate a void which can close again under further macroscopic strain increments. Macroscopically there may therefore not be any readily detectable volume change until such large macroscopic strains have been achieved. The interconnection of many of such small fractures produces a macroscopically evident discontinuity along which sliding can take place.

In tensile deformation the generation of fractures is even more readily obvious. Particles held together by only a thinly distributed binder, which is solid but soft, can accommodate strains on the order of a few per cent only if they detach from the binder. We need not necessarily consider these fractures to be located neatly on the surface of particles where the tension-parallel diameter touches the particle surface as shown in figures 24a and b idealized

as nearly spherical. Such fractures can take many orientations as shown for the undeformed state in figure 24c by a few examples. Fractures will occur as the result of microstructural deformations which are induced by previous fractures. These "secondary" fractures or "fractures induced by fractures and subsequent deformations" are of course not aligned in a simple way with respect to the direction of maximal tension. Suppose a piece of propellant has been strained to some maximum strain ϵ_{max} and is then unloaded to zero stress and zero deformation, and that sufficient time has been allowed for this purpose. If we now examine the "solid" internally and microscopically we would find it riddled with fractures which are oriented, if not completely at random, at least not uniformly with respect to the tension. A possible two-dimensional analog is shown in figure 25. When the material is stressed the forces are transmitted by a circuitous path passing between the fractures. In the undeformed state the orientation of this path is piecewise as random as the orientation of the fractures. But as the macroscopic sample is stressed (extended) these paths tend to straighten and induce increasing resistance to further deformation. We may liken this situation somewhat to the orientation of a (Gaussian) rubber network which produces the characteristically strong upswing in the uniaxial stress-strain curve due to molecule orientation. In figure 26 we have sketched a loading (path 1) and unloading (path 2) sequence of the stress-strain behavior.

If one then reloads the material along path two, one produces few, if any, new fractures until the previous maximum strain has been achieved; further straining produces new fractures which

then determine the subsequent unloading and reloading paths as for example path 4 in figure 26.

So far we have not included rate or time effects in our consideration. If the binder is viscoelastic then unloading and loading may not occur along the same path. Upon unloading the fracture surfaces may not close perfectly and immediately but may take time to find their matching partners (if they find them at all); upon reloading the fracture surface will tend to stick because of binder tackiness and thus weak re-fracturing occurs. The result is a loading and unloading loop as shown in figure 27. Furthermore, upon straining the propellant by the same cyclic history (say a saw-tooth strain history as is easily accomplished on an Instron tester) old fractures will tend to grow during each new strain application, and new ones may start but the rate of growth of these fractures decreases with each subsequent cycle since the stress is relieved by the crack growth.

Since the investigation of the deformation characteristics was not the primary aspect of this program we did not study the loading and unloading characteristics thoroughly. But in the course of trying to clarify mechanics of the mechanical degradation we performed a series of tests of which we will describe representative excerpts.

All tests were carried out on the Instron tester; although not all tests were conducted at different temperatures in the range from -40° C to +40° C, about 20 tests in this range were performed which parallel those we record here for room temperature. In figure 28 we illustrate the strain histories which are characterized by a

sequence of groups each possessing n loadings and unloadings at constant strain rates; in each group the maximum strain remained the same. In most tests we let n = 5 so as not to prolong the tests inordinately. The appearance of the stress strain cycle was generally as shown in figure 29. As long as the maximum strain encountered in the past deformation history was not exceeded or approached closely for a long time the loading stress-strain characteristics were identical as shown in figure 30; the loading sequence for this test was slightly different than indicated in figure 28 and is shown inset in figure 30. This observation indicates that essentially no new fractures were generated as long as one stayed away from the previously encountered maximum strain. When this strain was exceeded new fractures were generated as indicated in figure 30 by extension beyond ten per cent.

It is interesting to note that the new fractures occur in such a way that the deformation characteristics remain essentially the same in the following sense: Suppose we plot the unloading (or, presumably, the loading) stress-strain curves which are obtained after five cycles (n = 5 in figure 28). As we unload from successively higher values of ε_{max}, then these unloading curves can be obtained with good approximation from a single curve by multiplying the strain by a function of the maximum strain from which unloading occurs. In figures 31 and 32 we present the unloading curves obtained by unloading from the values of ε_{max} shown inset in the figures. Using the lowest value of ε_{max} as an arbitrary reference all the remaining curves can be collapsed onto one if the strain for each curve is divided by the factor $A\varepsilon_{max}$ which is shown as a function of ε_{max} in figure 33.

The same is repeated for the JPL 500 Series propellant in figures 34-36. Figures 31 and 32 show an identical series of tests on two specimens of TPH 1011 propellant produced identical results with uncharacteristically small data scatter. The same is true for the results on JPL 500 Series propellant shown in figures 34 and 35. Tests conducted at lower temperatures indicate the same phenomenon although the detailed appearance of the unloading characteristic is affected by the more viscous response of the binder.

From these observations we should like to draw conclusions regarding the way in which damage is accumulated in the form of fractures. Since the interaction of the non-linear properties of the propellant constituents with the fracture process generates a rather complicated picture as reflected in the constitutive behavior, it is virtually impossible to make unequivocal statements in this respect. Nevertheless, it appears at least reasonable and plausible that the similarity in the unloading stress-strain behavior is the result of a geometric similarity of the way in which the fractures arrange themselves in the propellant. In other words, if one examines the internal pattern of fractures and fissures in a propellant strained only a small amount (say 5%), one should probably find, on a statistical basis, roughly the same distribution of fracture sizes and orientation with respect to the micro-structure and with respect to the orientation of the applied load. The generation of new fracture surface with increasing strain is due to both initiation of new fractures and growth of old ones; how much of the new surface is generated by starting a new fracture or by extending an existing one, cannot be discerned. Yet it would

be quite important for a fracture model to distinguish between the two contributions in order to represent the physics of the problem properly. In our later modelling we shall assume that small fractures exist already according to some distribution and that they will grow to produce larger fractures where growth is evidenced in the deformation characteristics.

We have mentioned already that the characteristic upturn in the unloading-reloading stress-strain curve may be a result of the way in which fractures are arranged in the propellant; some material may not transmit much of the load at small deformations while at larger deformations they contribute to the force transmission. We have likened this response to the molecular mechanisms that occur in the large extension of elastomers.

One can argue, of course, that the highly non-linear stress-strain behavior is the consequence of the non-linear stress-strain behavior of the elastomer's binder and has little to do with how the fractures influence the transmission of forces through the propellant.

In our later account we shall see that we have taken the viewpoint that the non-linear characteristics of the propellant stress-strain behavior is due to the non-linear rubber elasticity. This seemed to us initially the simpler way of approaching the failure problem.

So far, we have dealt with the binder as if it were an elastic solid rather than a viscoelastic one. Since the glass temperature of many binders is on the order of -70 to -90° C most operations above -30° C do not invoke the glass-to-rubber transition and one operates in the near-rubbery domain of the elastomer. However, when the

rates of deformation become large as at the tip of a crack whose tip moves only relatively slowly, viscoelastic response does become important. One should distinguish therefore on the one hand a nearly elastic response of the binder if it experiences the moderate deformation rates associated with its deformation in between the granular solids, and on the other hand, a viscoelastic or time-dependent response when crack propagation is concerned. In a propellant where the binder obeys such a behavior one would observe neither stress relaxation nor creep if no microscopic fractures were initiated or grown; but if relaxation or creep does occur it would be attributed - primarily at least - to the growth of fractures and voids, which growth occurs as a function of time. We believe that such a representation of the binder is adequate for our later purpose.

In figure 37 we have plotted unloading stress-strain curves from tests conducted at different temperatures. All specimens were strained with the same constant strain rate history (1 in./min. cross head speed) but unloaded with constant strain rate histories for which the unloading rate varied between 0.02 in./min and 1 in./min. Although one observes a difference in the data derived from the 23° C tests and those conducted at +5° C, there is no systematic difference between the +5° C, -15° C and -25° C data. At any one temperature there was no systematic change in the unloading curves with rate of unloading.

During unloading, the generation of new cracks or growth of old ones should be inhibited or prevented since the stress drops off very rapidly. The fact that the change in the rate of unloading does

not produce a noticeably systematic difference may be taken as evidence that the viscoelastic response of the binder can be well approximated by elastic response as long as we are not concerned with the propagation of fractures in the binder or at interfaces between the filler particles and the binder.

b. A Simple Example of the Influence of Time Dependent Fracture on Macroscopic Constitutive Response

Let us consider as a simple analog of a fracturing propellant a two-dimensional solid exhibiting essentially elastic properties under normal loading conditions; but if cracks propagate in the material their growth is governed by the (residual) viscoelastic properties. We picture the two-dimensional solid as being riddled by cracks of such size but with such spacing that the stress fields of the cracks do not interact. We can then characterize the solid approximately by an element of area A containing a single crack as shown in figure 38. The number density of cracks is thus $1/A$. The stress acting on the element is σ which is approximately equal to the far field stress acting on the solid which contains many of the cracks. The initial size of the cracks is $2c_o$. We next calculate the elastic strain energy (approximately) contained in the element of figure 38; it is given for a crack of arbitrary size c which is small compared to the edge length of the area A (figure 38).

$$\overline{W}(\sigma, c) = \frac{\sigma^2}{2E_o}\left[A + 2\pi c^2\right] \qquad (1)$$

with E_o = Young's modulus. Upon using the relation for the strain commensurate with the applied stress σ

$$\varepsilon = \frac{\partial \overline{W}(\sigma, c)/A}{\partial \sigma} \tag{2}$$

one obtains

$$\varepsilon = \frac{\sigma}{E_o}\left[1 + \frac{2\pi c^2}{A}\right] \tag{3}$$

and therefore

$$\sigma = \left\{\frac{E_o}{1 + \frac{2\pi c^2}{A}}\right\}\varepsilon \tag{4}$$

The term in brackets is an "equivalent average modulus" which accounts for the presence of the crack(s). If one now imagines that the cracks can grow as a function of time, then this "equivalent average modulus" (EAM) decreases with time. Thus the ongoing internal, and possibly macroscopically invisible, damage manifests itself in a softening of the material.

In order to determine how the EAM varies we must know how the cracks grow with time. Let us characterize the stresses at the tip of a crack by a stress intensity factor K, which we shall assume for demonstrative purposes to be equal to

$$K = \sigma\sqrt{\pi c} \tag{5}$$

Both σ and c may be functions of time. We approximate the dependence of the rate of crack propagation on K by the relation*

---

*This relation is valid over a considerable range of crack tip velocities as shown in W. G. Knauss, "Stable and Unstable Crack Propagation in Viscoelastic Materials"; Proc. Soc. Rheology 13:3, 291-313 (1969) for a polyurethane elastomer. Recent and unpublished measurements on a propellant binder have shown the same behavior.

$$\frac{dc}{dt} = \dot{c} = a(K-K_o)^m \tag{6}$$

where a, m and K_o are experimentally determined parameters. Equation (6) is not valid at very high values of K.* Below $K = K_o$ crack propagation does not occur. Now let $c/c_o = \xi$ and express $\dot{c} = \dot{\xi} c_o$ through (5) and (6) to obtain

$$\dot{\xi} = \frac{a}{c_o} [\sqrt{\pi c_o}\ \sigma\ \xi^{1/2} - K_o]^m \tag{7}$$

For the present calculations we simplify matters by letting $K_o = 0$ (no lower fracture limit).** From (4) we have for the stress, in terms of ξ

$$\sigma(t) = \frac{E_o}{1 + \frac{2\pi c_o^2}{A} \xi^2(t)}\ \epsilon(t) \tag{8}$$

which yields with (7) and the assumption that $K_o = 0$

$$\dot{\xi} = \frac{a}{c_o} \left[\sqrt{\pi c_o}\ E_o \epsilon\ \frac{\xi^{1/2}}{1+\frac{2\pi c_o^2}{A} \xi^2} \right]^m \tag{9}$$

or, with $R \equiv \frac{2\pi c_o^2}{A}$,

$$\left[\frac{1+R\xi^2}{\sqrt{\xi}}\right]^m d\xi = \frac{a}{c_o} [\sqrt{\pi c_o}\ E_o \epsilon\ ]^m dt \tag{10}$$

Let $\epsilon(t) = \epsilon_o$, a constant. Then the deformation history corresponds to a relaxation experiment. For arbitrary m, (10) must be integrated

---

*K must be somewhat less than a value that would invoke glassy material response at the crack tip.

**This will mean that cracks can grow at very small stresses as long as the latter are different from zero.

numerically. But if we let m be an integer the left-hand side can be expanded by the binomial theorem to yield, with

$$\tau = \frac{a}{c_o}\left[\sqrt{\pi c_o}\, E_o \varepsilon_o\right]^m t \tag{11}$$

$$\left\{\xi^{-m/2} \sum_{n=0}^{m} \binom{m}{n} R^n \xi^{2n}\right\} d\xi = d\tau \tag{12}$$

For a reasonable value of m = 6* one obtains then by integration from the time t = 0 to t

$$\tau = \frac{1}{2}\left[1-\xi^{-2}\right] + 6R\,\ell n\xi + \sum_{n=2}^{6} \binom{6}{n} R^n \frac{\xi^{2(n-1)}-1}{2(n-1)} \tag{13}$$

Equation 13 gives the size of the cracks $c = c_o \xi$ implicitly as a function of the time t by virtue of (11). If we now substitute the crack size so determined into the "stress-strain relation" (4) or (8)

$$\frac{\sigma(t)}{\varepsilon_o} = \frac{E_o}{1+R\xi^2} = E_{rel}(t) \tag{14}$$

we obtain a "relaxation modulus" $E_{rel}(t)$ which is the result of time-dependent fracture. In figure 39 we show this "relaxation modulus" for several values of R; at long times when the stress has reached sufficiently low values the stress intensity factor should drop to a value for which crack propagation is no longer possible; further relaxation would then stop. We have indicated this physical behavior by the dashed extensions of the solid curve.

We note furthermore, from figure 39, that the slope of the

---

*The measured value for the aforementioned polyurethane material was about 5.8.

fracture-relaxation modulus is considerably different from that of the pure polymer. Furthermore, the relaxation times for the pure polymer would be much shorter than those encountered in the fracture-controlled relaxation. This follows from the fact that the elastomer can behave essentially in an elastic manner yet permit very slow crack propagation under appropriately small stresses at the crack tip. This behavior coincides with observations on propellants which have characteristically small log-log slopes of relaxation behavior, and their relaxation behavior continues often longer than one would expect from the relaxation behavior of the binder alone.

We conclude this introductory example of how the fracture process is reflected in the constitutive response by pointing out that the calculations given here for constant strain (relaxation) can be performed for arbitrary strain histories. If we let $\varepsilon(t) = \dot{\varepsilon}_o t$ (constant strain rate) in (8) then (10) would read

$$\left[\frac{1+R\xi^2}{\sqrt{\xi}}\right]^m d\xi = \left[\frac{a}{c_o}\sqrt{\pi c_o}\, E_o \dot{\varepsilon}_o\right]^m t^m\, dt \qquad (15)$$

and instead of (13) we would have

$$Bt^7 = \frac{1}{2}\left[1-\xi^{-2}\right] + 6R\ell n\xi + \sum_{n=2}^{6} \binom{6}{n} R^n \frac{\xi^{2(n-1)}-1}{2(n-1)} \qquad (16)$$

with

$$B = \frac{a}{7c_o}\left[\pi c_o E_o \dot{\varepsilon}_o\right]^6$$

Substitution of ξ from (16) into (8) with $\varepsilon = \dot{\varepsilon}_o t$ would give the stress response in a constant strain rate experiment.

6. The Effective Modulus of a Solid Containing Cracks

The idea of a solid containing many cracks is central to our later development, and in particular the effect which the presence of many flaws or cracks has on the rigidity of the fracturing solid. We therefore conducted a simple experimental investigation with SBR* sheets to check whether results obtained with the linearly elastic theory was or was not without merit, when applied to an elastomer undergoing large deformation.

Consider a finite (rectangular) sheet of thickness t and lateral (not cross-sectional) area A which contains a through crack whose length 2c is small compared to the lateral dimensions. Let the Young's modulus of the continuum be E_o and apply a stress σ to the sheet such that a tensile force acts normal to the crack. Assuming that the crack is sufficiently small compared to the sheet dimensions so that the stresses around the crack are approximated by the solution for the infinite sheet we can calculate the energy $\overline{W}$ contained in the sheet per unit thickness as (plane stress)

$$\overline{W} \doteq \frac{\sigma^2}{2E_o} [A + 2\pi c^2] \tag{17}$$

and the average strain energy density (per unit thickness) in the sheet as

$$W \doteq \frac{\sigma^2}{2E_o} [1 + \frac{2\pi c^2}{A}] \tag{18}$$

If several cracks (N) exist in the sheet such that their stress fields do not influence each other markedly, nor are influenced by the proximity of the free boundary the average strain energy density is

$$W \doteq \frac{\sigma^2}{2E_o} [1 + \frac{2\pi}{A} \sum_{i=1}^{N} c_i^2] \tag{19}$$

---

*Styrene-Butadiene Rubber

If we now treat the sheet (which is under uniaxial tension) as a solid, i.e., forget that it contains cracks, then it would possess an effective Young's modulus E_{eff} such that

$$\sigma = E_{eff}\bar{\varepsilon} \tag{20}$$

where $\bar{\varepsilon}$ is the average strain measured, say, by the average separation displacement which those edges of the sheet experience to which the stress σ is applied; in reality those edges do not undergo a uniform displacement because the presence of the cracks influences the displacement field there. Writing the strain energy density for a uniaxially strained sheet having the property (20) as

$$W = \frac{\sigma^2}{2E_{eff}} \tag{21}$$

we find by comparing (19) and (21) that

$$\frac{E_o}{E_{eff}} = 1 + \frac{2\pi}{A}\sum_{i=1}^{N} c_i^2 \tag{22}$$

To provide an experimental check on relation (22) when the material is a rubber we conducted two experiments. In figure 40 we show a sheet of SBR rubber into which a sequence of cracks ($c = \frac{1}{4}$") was cut according to the numbers displayed. The average modulus of the sheet was then measured, under strains of the order of five percent, as a function of the number of cracks. In figure 41 the ratio of E_{eff}/E_o is shown as curve I. Since the cracks were all of the same length ($2c = \frac{1}{2}$") one obtains from (22)

$$\frac{E_o}{E_{eff}} - 1 = N\frac{2\pi c^2}{A} \tag{23}$$

Thus plotting $\frac{E_o}{E_{eff}} - 1$ vs N should yield a linear relationship with the slope $2\pi c^2/A$.

In figure 42 the plot for equation (23) is shown to yield a slope of $2\pi c^2/A = 0.017$, while the calculated value is 0.0162, a discrepancy of five percent.

From figure 40 one might question whether the cracks were not spaced too closely in order not to interact. Some time after the measurements were completed, crack interaction calculations became available [Pucik] which indicate that for an arrangement of cracks as shown in figure 40 the interaction of cracks happens to be rather weak. For a less regular arrangement of cracks the same would not necessarily be true. In general we expect no drastic changes in the results if the separation of the cracks is on the order of their length or more.

A second set of measurements was conducted wherein cracks were enlarged successively at 17 locations, 1/8" at a time. Thus after every 17th cut there existed a set of 17 cracks of equal size, (2c = 1/8, 1/4, 3/8, 1/2, 5/8").

All data for this set of measurements are shown as curve II in figure 41. If we isolate those points for which all cracks were of equal length (according to the solid line drawn through the data) we can calculate again $E_o/E_{ff} - 1$ with N = const and c varying. According to equation (23) this value should vary with the square of the crack length; this dependence is shown in figure 42 as curve II which has the relation

$$\frac{E_o}{E_{eff}} - 1 = 6.08\, c^2 \qquad (24)$$

While we cannot claim on the basis of these limited measurements that the simple relation (22) for the effective modulus is valid for all the situations which we may encounter later, we could nevertheless be encouraged to use it since it describes the functional dependence of the effective elastic modulus on the size and number of cracks surprisingly well.

We must add that for the solid containing three-dimensional cracks the term Nc^2/A should be replaced by Nc^3/V where V is the volume of the solid; in addition the factor 2π would change. However, since we planned to work in our later development with a two-dimensional model we would retain the two-dimensional result (22); this choice was not necessarily the best one, and, given the need for decision again, we would probably choose to work with the three-dimensional formulation that is analogous to equation (23).

7. Macroscopic Failure

We discuss first the process by which we think the filled polymer failed and then attempt a modelling of this physical process. To begin with we remind ourselves that the propellants we consider are composite solids. In the process of production, the cure shrinkage and the thermal differential contraction of the various phases introduce microscopic self-stresses in the macroscopically unstressed solid. Depending on the adhesive strength between the filler particles and the binder, voids and cracks or binder-particle separation may exist already at this stage in the "solid."* Upon application of a macroscopically uniform stress the composite experiences, microscopically speaking, inhomogeneous stress fields in and around the filler particles. Because of this inhomogeneity at the microscale, stress elevations are bound to interact with flaws of which there must be an abundance because of the very large number of particles in a unit volume of composite. Stressing the composite propellant will therefore cause flaws that already exist to enlarge and will also generate new ones, as for example, at spots where the binder-particle interface exhibits a poor bond or a particularly high stress. In figure 43 we show a sequence of a two-dimensional composite arrangement (or a section through a three-dimensional one) under increasing strain.** The flaws will grow in a complicated way because the

---

*Incomplete wetting of the particles by the binder may also induce interface flaws; here the viscosity of the uncured binder probably plays a significant role, since it controls the spreading uncured binder over the solid particles.

**The number of flaws per unit area shown is larger than is probably physically reasonable; this is done only for illustration purposes.

generation or enlargement of flaws will allow the motion (translation and rotation) of particles which affect the stress field in which neighboring flaws grow. Some flaws will grow faster as a result of increased stresses; others will grow slower or come to a stop. The large deformations accompanying this process will often drastically change the loading which the "crack" periphery experiences during the fracture process, and we cannot, therefore, speak of a clear crack propagation problem as we are used to from standard fracture mechanics practice.

One would expect that the larger flaws begin to propagate at relatively low stress levels; furthermore, they are likely to come to a halt again when the stress field along their periphery is lowered because of adjacent particles. It is thus plausible that at low stress levels many flaws will be generated because many of them come to a stop after which others still have a chance to grow and propagate. At higher stress levels it is reasonable that cracks which start early may be temporarily retarded but continue to grow so that others, initially smaller cracks, do not have a chance to grow to large dimensions before total failure occurs. This notion is at least consistent with the following observation: propellant broken at low extension rates and low stress level tend to undergo a relatively homogeneous dewetting process throughout the test specimen, while at high extension rates (low temperatures) a relatively <u>local</u> rather than homogeneously distributed crack growth phenomenon occurs.

The final failure in the form of generation of new (macroscopic) propellant surface is the result of the coalescence of the

many cracks which have been generated and enlarged continuously in the deformation process.

We see thus the failure of composite propellants as a more or less continuous process of crack generation and growth and the final rupture process as the coalescence of numerous such microcracks into a macrocrack.

This final rupture can be effected by a relatively small number of large cracks or by a great number of small cracks. The process of coalescence, like the whole crack growth process, depends on the stresses at the crack periphery (crack tip in two dimensions) where stresses are strongly affected when cracks approach each other in the coalescence process. Coalescence of cracks is very difficult to treat even approximately in analytical form and thus even an approximate treatment of the final stages of macroscopic fracture surface generation is difficult to establish.

However, it seems reasonable that such a final failure is not far away if the total area generated by the microcracks is close to or equal to some critical value. Thus either a large number of small cracks or a few large ones may induce rupture.

a. A Two-dimensional Model

Consider the (rectangular) two-dimensional assembly of squares in figure 44 and allow each square, subsequently called an element, to contain at most one crack; not every element has to contain a crack or a flaw. We consider the properties of each element to conform to that of an isotropic and homogeneous solid. If we now allow cracks to appear and grow in some of these elements,

the stiffness of these elements will decrease, which effect is detected macroscopically, i.e., averaged over many elements, as a loss in the rigidity of the solid, which is composed of these elements. If the deformation of this composite solid, or assemblage of elements, is prescribed in the form of a macroscopically averaged strain ε^* (in figure 44) then the loss in overall rigidity will also affect the stress in each one of the elements and therefore influences the further rate of crack propagation in the elements.

In order to account for this interaction of the individual elements - which exhibit different average properties depending on the size of the flaw contained in them - with the overall properties of the composite we have several avenues available.

First we assign to each element elastic average properties which account for the size of a crack contained in it; we shall further attempt to distinguish later whether the flaw contained in an element has the character of a crack or a tear, but this distinction is not important now. We could next assume that either a parallel or a series arrangement of all the elements would give an estimate of the modulus or compliance of the whole composite. Under a reconsideration of this work we might attempt to work with such a simple concept just to see how adequate an approach it would present. However, upon scanning the literature on composites we felt that the series and parallel arrangement had produced some rather wide bounds on the average mechanical properties of composites and that a more refined estimate was in order. This refinement was bought, however, at the expense of computational involvement.

We therefore use the results obtained by Budiansky for the elastic moduli of heterogeneous materials composed of linearly elastic phases. The material properties of the binder are, of course, not linearly elastic and are indeed at best non-linearly elastic. We found after some attempts that it was too ambitious an undertaking considering the scope of this program to develop a comparable composite model allowing for non-linear material properties. We thus accepted the approximation inherent in the application of Budiansky's work to our problem.

Let μ^* and K^* be, respectively, the shear and bulk modulus of the composite and let μ_i and K_i be the corresponding properties for the i^{th} element (yet to be defined) and let ν^* be Poisson's ratio for the composite, and r_i the total volume fraction of elements of type i.† Then μ^* and K^* are determined by [Budiansky]

$$1 = \sum_{i=1}^{N} \frac{r_i}{1+\beta^*\left(\frac{\mu_i}{\mu^*}\right)-1)} \tag{25}$$

$$1 = \sum_{i=1}^{N} \frac{r_i}{1+\alpha^*\left(\frac{K_i}{K^*}-1\right)} \tag{26}$$

$$\left.\begin{aligned} \text{where } \alpha^* &= \frac{1+\nu^*}{3(1-\nu^*)} \\ \beta^* &= \frac{2(4-5\nu^*)}{15(1-\nu^*)} \end{aligned}\right\} \tag{27}$$

Since the composite Poisson's ratio ν^* is a non-trivial function of μ^* and K^* equations (25-27) constitute highly non-linear equations for the composite material properties μ^* and K^*. We therefore allowed

---

†For our case all elements have cracks of length 2c.

the approximation $\nu^* = 1/3$ in equations (27) only so that α^* and β^* were constants. Since α^* and β^* do not vary greatly in the interval $0 \leq \nu^* \leq 1/2$ ($1/3 \leq \alpha^* \leq 1$, $2/5 \leq \beta^* \leq 8/15$) this inconsistency may not be of any great consequence. We can then solve (25) and (26) using Newton's method for the properties μ^* and K^* provided we know the properties of the i^{th} element. The properties of the i^{th} element depend, however, on the size (and geometry) of the flaw imbedded in it. The size of the flaw is a function of the stresses that have acted on the element in the past. We thus have to relate the instantaneous stresses and strains on the macroscopic composite, i.e., σ^*, and ε^* in figure 44, to the stresses and strains acting on the individual elements. Once we know these latter stresses on the elements we can calculate how fast the flaw grows in that element.

The relation between the macroscopic stress σ^* and strain ε^* on the one hand, and the stress σ_i acting on the i^{th} element may be estimated by Eshelby's analysis [Eshelby] of a spherical inclusion in an infinite medium under stress. For uniaxial tension we have

$$\sigma^* = \frac{1}{9}(3K^* + 16\mu^*)\,\varepsilon^* \tag{28}$$

and from Eshelby's work approximately† for the stress in the i^{th} element

$$\sigma_i = (2R_1\mu_i + R_2)\,\varepsilon^* \tag{29}$$

where $R_1 = 1 - \frac{1}{9}\{(1-\alpha^*)\,S + U\,(1-\beta^*)U\}$

$R_2 = \frac{1}{3}(K_i - \frac{2}{3}\mu_i)\,[1-(1-\alpha^*)S]$

---

†The approximation involves the substitution of a spherical inclusion for a two-dimensional square element as indicated in figure 44.

$$S = \frac{K_i - K^*}{\alpha^*(K^* - K_i) - K^*}$$

$$U = \frac{\mu_i - \mu^*}{\beta^*(\mu^* - \mu_i) - \mu^*}$$

$$\alpha^*(\nu^* = \frac{1}{3}) = \frac{2}{3}$$

$$b^*(\nu^* = \frac{1}{3}) = \frac{7}{15}$$

In figure 45 we show the flow chart of the computations which calculate the properties of the composite solid as a function of the crack size in the i^{th} element, which crack size(s) are in turn governed by the rate law for crack growth in terms of the stress history applied to the i^{th} element.

We have yet to determine the properties of the i^{th} element in terms of the flaw size c_i, and discuss the rate law by which the flaws are to grow in dependence on the stress σ_i applied to the i^{th} element.

At this point one might ask the question: In view of the experiments with the multiply cracked sheets why did we choose Budiansky's analysis to determine the macroscopic properties by which the applied stress σ^* or strain ε^* is related to the stress acting to propagate an individual crack? In answer to this question we felt:

1) The fact that cracks need not always grow but can come to a halt called for an approach wherein a crack could only grow to a given size (size of an element)
2) We were not certain that the interaction of the cracks as arranged regularly in the experiments was not significantly different if they were arranged more randomly.

In other words, our experiment might correspond accidentally well to the equation derived from linear elasticity theory.

3) It was not clear how tearing could be accommodated by the simple multiply cracked sheet model (see later development of tearing element).

In retrospect it does not appear, however, that the various assumptions underlying our present course of simulating the effects of cracks and flaws on the macroscopic properties of the composite are any more refined than those that would have to be made if a crack-perforated sheet had been used as investigated in section 5. A more comprehensive study would probably have to explore these various possibilities further.

b. Crack and Tear Elements

We consider that a flaw can grow normal to the direction of maximum tension; as long as the flaw is small compared to any other (micro)structural size we may speak of a crack and assume that the stresses at its tips (periphery) are a function of its size and increase monotonically with an increase in the load acting far from the crack. If such a crack is contained in an element we call the element a "crack element."

On the other hand, it is quite conceivable that through interaction of closely spaced cracks, binder fibers or ligaments form, which tear from each other under large deformations (cf. figure 46); the distinguishing feature of such an element would be that it responds with tearing as soon as the stress exceeds some given value. As a

consequence a tear element is not likely to sustain high stresses. We would expect that when cracks reach a certain size further fracture would occur in a tearing mode rather than a crack mode. One might expect thus that a crack element has to be changed into a tear element after the "crack" reaches a certain dimension.

Crack Element

i) Quasi-elastic properties

We define the (effective) Young's modulus of a crack element of unit area (i^{th} element) as

$$E_i = \frac{E_o}{1+\frac{2\pi}{A} c_i^2} \qquad A = 1 \tag{30}$$

where E_o is the modulus of the unfractured composite solid. E_i is, of course, only a "tensile modulus" measured normal to an existing crack; parallel to the crack the material exhibits a modulus E_o. Although a crack induced anisotropy exists we neglect this fact and treat the element as if it possessed isotropic properties. An effective Poisson's ratio for the element is obtained by calculating the effective bulk modulus of a hollow sphere whose inner and outer diameter are $2c_i$ and 2ℓ (= 1), respectively; from this effective bulk modulus and the modulus E_o one determines the effective Poisson's ratio ($K^* \Rightarrow \infty$ for the unfractured incompressible solid)

$$\nu_i = \begin{cases} \dfrac{2-3(c_i/\ell)^3}{4-3(c_i/\ell)^3} & \dfrac{c_i}{\ell} \leq \left(\dfrac{2}{3}\right)^{\frac{1}{3}} \\ 0 & \dfrac{c_i}{\ell} > \left(\dfrac{2}{3}\right)^{\frac{1}{3}} \end{cases} \tag{31}$$

Note that since the crack sizes c_i are functions of time both the effective modulus and the effective Poisson's ratio are functions of time.

ii) Rate of crack growth

With regard to failure properties of the composite the law governing the fracture process is most important. We need not review here theories dealing with crack growth but refer the reader to a recent review (Knauss, 1973). If chemical reaction rate theory is a viable idea governing macroscopic crack propagation then this would be the place to insert such a growth law into our later calculations. As may be gaged from the just referenced review, the calculations of crack propagation rates based on chemical reaction rate concepts is a formidable task at best. We therefore employ a power law for the rate of crack propagation which relates the stresses at the tip to the crack growth rate. Let K be the stress intensity factor for a crack and let $\dot{c}$ be the rate of crack propagation, then we can write [Greensmith, 1964], [Knauss, 1969],

$$\dot{c} \begin{cases} = b(K-K_o)^m & K \geq K_o \\ = 0 & K < K_o \end{cases} \tag{32}$$

where b, m and K_o are constants. K_o corresponds to the limit of stress intensity below which the crack will not propagate. The constants b and m are derived from fracture tests (crack propagation tests) on binder material, if possible; otherwise they have to be chosen by fitting computations to measured properties of the composite propellant.

Tear Element

i) Quasi-elastic properties

In figure 46 let the "leg" of a tear element be $\ell_o(t)$* in the undeformed state and in the extended state equal to $\ell(t)$; furthermore let $\lambda(t)$ be the extension ratio

$$\lambda(t) = \ell(t)/\ell_o(t) \tag{33}$$

Before the tear element has been stretched to produce some tear growth let the length of a "leg" be equal to unity, i.e., $\ell_o(0) = 1$. Then any time after tearing has occurred the overall strain of the tear element is

$$\varepsilon_o = \ell_o(t)\,[\lambda(t) - 1] \tag{34}$$

Let the stress pulling the "legs" apart be σ. We then define an instantaneous modulus

$$E(t) = \frac{\sigma}{\ell_o(t)[\lambda(t)-1]} \tag{35}$$

Now the stress-strain behavior of one "leg" by itself is a property of the elastomer itself. We have therefore the relation between the stress $\sigma(t)$ and the extension ratio $\lambda(t)$

$$\{\lambda(t)-1\} = \text{Function of } \{\sigma(t)\} \tag{36}$$

In order to approximate (36) we attempted to use a strain energy

---

*$\ell_o(t)$ is a function of t because the time-dependent tearing changes the length of the "leg."

function for elastomers proposed by Hart-Smith [Hart-Smith]. After performing tests with SBR and attempting to incorporate the Hart-Smith formulation we decided that the simple relation

$$\lambda - 1 = \frac{\sigma}{c_1 + c_2\sigma} \quad ; \quad c_1,\ c_2 = \text{constants} \tag{37}$$

was a reasonably accurate description of uniaxial elastomer tensile description and perhaps sufficient for our purposes. If we now note for reference that

$$\ell_o(t) \doteq 1 + \int_o^t \dot{e}(t)dt \tag{38}$$

we can write with the use of (35) and (37)

$$E(t) = \frac{c_1 + c_2\sigma(t)}{\ell_o(t)} \tag{39}$$

as a crude estimate for the effective modulus of a tear element. The values of the constants c_1 and c_2 were estimated from the uniaxial extension curve of a propellant binder used in the chemical aging studies at the Lockheed Propulsion Company; they were $c_1 = 47$ and $c_2 = 9$.

We have no rational way to estimate a value of Poisson's ratio for this type of element. In view of the rather crude modelling of a binder tearing behavior by a linearly elastic constitutive "law" for the element a guess at an appropriate value of Poisson's ratio seems consistent with the degree of approximation used so far. We thus chose $\nu = 0.45$.

ii) Rate of tear growth

Since the force F in figure 46b is carried essentially by the tearing material at the tip of the tear, the rate of tear growth should

be a function of this force or of the stress. In view of the work on the tearing of rubber conducted at the British Rubber Producers' Research Association [Thomas] we approximate the tear rate by the power law relation

$$\dot{c} \begin{cases} = c_{t1} (\sigma - \sigma_o)^{m_t} & \sigma \geq \sigma_o \\ \\ = 0 & \sigma < \sigma_o \end{cases} \tag{40}$$

with σ_o, c_{t1} and m_t constants, and σ the tensile stress in the tear element.

8. Damage Calculations

As soon as it became apparent that the characterization of damage would be attempted in connection with the non-linear constitutive behavior of the propellant we conducted extensive tests on how the tensile modulus during unloading depends on the maximum strain achieved during any load cycle. We furthermore examined how the average modulus in a small cyclic excursion around a point (σ, ε) on the unloading path depends on the strain ε and on the maximum strain achieved in the total past deformation history of the sample. Some of this information was documented earlier in this report. The remainder of the tests were conducted with the expectation of deriving information on the distribution of initial flaws and on the approximate amount of growth they would exhibit under load. This information did not materialize on an experimental basis alone.

Influenced by these tests we turned first to the attempt to model the constant strain-rate loading and unloading test. In retrospect it would seem wiser, perhaps, to have started with the relaxation test, by which the rate of relaxation of the model could have determined the rate parameters for the flaw growth equations (32) and (40). One might argue that a creep test would have been more informative yet, since in that test the stress would remain constant, and since then the crack growth rate would be exhibited directly since it is tied to the stress in the elements via (32) and (40). Here it should be remembered, however, that the stress in each element is not related in a simple way to the macroscopically applied stress in our model. In particular, the stress in each element is <u>not</u> proportional to the gross applied stress.

a. Effect of Intrinsic Material Properties

Since we are attempting to use linearly elastic theory for the stress analysis portion of our work it is clear that the specification of, say, the modulus of the unfractured material determines largely the stress-strain behavior of the composite. Alternately, if we specify a stress for the partially fractured solid the corresponding strain can be adjusted easily through an appropriate device of the "elastic moduli" entering the calculations. We have, therefore, not laid emphasis on physically realistic magnitudes of stress and strain. Just as a point of information, the strains tended to be on the order of 10% of physically realistic values. In our figures we have therefore plotted stress and strain in arbitrary units.

b. Constant Strain-rate Histories

It would be natural to analyze the effect of varying the material parameters which enter the computational scheme outlined in figure 45. Such an analysis would yield information on how sensitive the failure accumulation would be to variation in these parameters and would obviously yield information on how to best fit the computational scheme to measured propellant response. As an initial attempt we chose parameters not by fitting the properties of the composite propellant with the computational response, but by deducing reasonable parameters from the behavior of elastomer behavior not "reinforced" with filler particles as available either from available publications or from data developed in our laboratory on earlier programs. In the rate equations (32) and (40) we have assumed that the crack speed is reducible by the WLF-time-temperature reduction

scheme. Through this assumption the time-temperature behavior of the failure process, and thus of the "failure properties," is automatically determined.

There is little sense in reproducing all the calculated stress-strain diagrams along with the damage factors since many yielded unrealistic behavior because of unrealistically chosen parameters. In the following calculations the tear elements were generated from the crack elements; when cracks had reached a size of 75% of the (unit) element dimension, a transfer was effected which designated the element to the set of tear elements. In doing so it was necessary to make certain that the effective modulus at the instant of element re-assignment was the same for the crack and for the tear element because otherwise a discontinuity in the stress-strain diagram would have resulted.*

In figure 47 we show computations of the stress-strain behavior, for which only the power of the crack or tear propagation rate law was varied. The distribution of the initial flaw sizes is shown as an insert. Figure 48 gives an example of a strain history involving restressing which shows the characteristic lowering of the modulus as a result of stress cycling. We shall discuss the effect of stress or strain cycling in more detail later.

Figure 49 shows a comparison of a calculated and measured stress-strain cycle on TPH 1011 propellant, indicating that modelling

---

*Such a possible discontinuity could not occur if one were to formulate the whole problem in terms of an incremental stress-strain law.

of the damaged propellant is entirely possible with the crack and tear elements.

9. Repetitive Cycling (Fatigue)

We turn next to the calculation of damage in repetitive load cycles. We use first the same initial crack size distribution as shown inset in figure 47. We define the damage by the summation of the total fracture or flaw area in the composite, normalized by the maximum internal fracture area that can be obtained. We call this ratio the damage function "D."

In figure 50 we show the stress-strain behavior along with the damage function. Time increases in the direction of the arrows. It is clear from that graph that the accumulation of damage per cycle decreases with increasing cycle number. This is to be interpreted as the result of the lowering of the stress in the cycling process, which in turn is the result of accumulated fractures in the material.

A series of computations as documented in figure 50 was made in which the threshold for crack propagation was varied, holding all other parameters constant. The result was such that only the first (leading) cycle was affected. If the threshold was high, damage was deferred until late in the first loading cycle and it occurred then rather rapidly. Subsequent load cycles differed little. There is little value in reproducing all these curves since they appear like those in figure 50 with variations which are hardly noticeable on that plot scale.

A second series of calculations was performed in which the distribution of initial flaw sizes was varied. Figure 51 shows the "effect" of this initial distribution on the damage function. The

influence is surprisingly low.

a. Failure Concept

It is appropriate at this point to emphasize (once more) that we are not presenting a rupture criterion for propellants but a means of keeping track of physically accumulated damage. Instead of predicting when a particular geometry (say a test specimen) generates a macroscopically observable crack we compound only the small scale crack damage. Whether "ultimate failure" by macroscopic crack growth is imminent must be defined or determined in terms of the damage function. If one defines D = 1 as the ultimate failure, it is possible to produce a conservative design by working with an ultimate allowable value of, say, 0.9 or 0.95. Thus the value of the damage function provides information on how safe a structure is under extreme loading conditions.

b. Experiments

Because a considerable amount of effort was spent initially on studying a method by which the concept of chemical reaction rates in propellants could be tested, the coordination of the calculations with experiments suffered. In anticipation of the analytical developments cyclic strain tests in uniaxial tension were conducted at different temperatures. The tests were executed on an Instron tester by providing constant rate of straining during the loading and unloading part of each cycle as shown in figure 52. The lower value of the strain ($t > 0$) was chosen different from zero so that the specimen would not experience a compression. In figure 53 we show a typical load-time trace of such a test. The remaining data are

recorded only in the form of the maximum value of the stress in each cycle.

c. Failure Evidence

During the tests a close watch was kept on the development of cracks or other macroscopic flaws which could lead to ultimate fracture. Cracks were usually observed to occur in three locations within the uniformly stressed test section of the specimen: "surface" cracks on the wide face of the specimen (1/2" dimensions in figure 9); "corner" cracks, and lastly, "edge" cracks which appeared over the thickness of the specimen. Corner cracks usually developed later into edge cracks. There seemed to be a tendency for surface cracks (on the order of 1/32") to appear first, and their appearance occurred usually before 5 or 10% of the specimen life had passed. Some time later corner cracks of the same order of magnitude developed and still later edge cracks would appear although the latter did not always occur. Once these small cracks had appeared they seemed to remain stagnant until about half of the specimen life time had passed; they then started to grow slowly. Often multiple cracks would grow on the specimen. In figure 53 we give a typical record of a cyclic stress-time trace. Only the maximum and minimum stress is traced since the cycles were spaced so closely on the time axis that the detailed stress-time plot would simply blacken the area between the maximum and the minimum shown.

As may be gathered from the rather early appearance of cracks, their development and thus ultimate rupture of the tensile specimen is subject to considerable statistical variation associated

with the microstructure. However if we plot the maximum stress in each cycle as normalized by the maximum stress achieved in each subsequent cycle, then the resulting plot should represent a measure of the damage incurred in each cycle. We have done this for tests at three different temperatures in figures 54-56. It turns out that these curves are all nearly the same.

In the same graphs we have shown the prediction of the flaw growth theory presented here. The heavy black line corresponds to the cyclic stress-strain history plotted in figure 10. According to figure 50 the propellant is already 97% damaged at the end of the 5th cycle. If we recall now that the appearance of cracks on the tensile specimens occurred rather early in the cycle history it is, perhaps, not unreasonable that most of the "lifetime" of the propellant is illusory.

We cannot claim that the failure accumulation model has so far been optimized where such deduced statements must be considered absolute fact. However, there seems to be, so far, no major inconsistency in the predictions of the theory which would not warrant a further exploitation of the flaw growth concept and the coupled effect it impresses on the constitutive and failure problems of solid propellants.

10. Biaxial Experimental Investigations

As a part of this program, a biaxial test device was constructed and biaxial tests were performed on TPH 1011 specimens. The purpose of the investigation was to generate experimental data that would extend the understanding of the damage process on propellant from the uniaxial case which was studied here and in other works to the more general case that would be expected in actual hardware situations.

a. Biaxial Test Apparatus and Specimens

The biaxial test apparatus was designed to be used in conjunction with an Instron test machine. A front view of the device is shown in figure 57 and a rear view in figure 58. The principle of the device is that the Instron cross bar displacement is converted into the displacement and rotation of a set of specimen grips by means of two independent lever arms. The relative amounts of displacement and rotation seen by the specimen are controlled by movable pivot points. The degree of control includes as a range pure translation or pure rotation or a combination of these. The displacement and rotation that can be obtained versus the Instron cross bar displacement is shown in figures 59 and 60, respectively. The test fixture was dimensioned to allow it to be placed in a Missimer temperature cabinet for temperature environments of from -50° C to +50° C.

The specimen used in the test fixture is essentially a cylinder where the dimensions can be selected within a broad range to satisfy the requirements of the particular test. For the biaxial tests

performed here, the cylinders were machined from blocks of TPH 1011. The cylinders had wall thicknesses of 0.125 inches and 2 inch diameters. The cylinders were 2 inches long, although the gage length was only 1 inch as aluminum end fittings were bonded on each end and used an inch of cylinder length. Rings that were 1/16 inch thick were fitted snugly against the cylinder's inner wall. These rings were stacked to match the gage length and were free to rotate. Their purpose was to constrain the necking of the test specimen and thereby insure that the radial strain would remain zero for the duration of the test. The test specimen, end fittings and rings are shown in figure 61. An assembled test specimen, which when tested is bolted into the biaxial test fixture, is shown in figure 62. The ends were bonded with epocy adhesive BFG A-1273B. A special load cell was designed for use in the biaxial tests. It was similar in shape to the test specimen but constructed from brass and steel and instrumented with two strain gage full bridges. The load cell was bolted to the test specimen and loaded in series with it. During the tests, the axial load and torque from the load cell were monitored continuously with time. The strain rates were linear functions of the Instron crossbar movement setting.

b. Biaxial Strain States

When uniaxial tests are conducted on a material such as a propellant, the control parameters are strain rate and temperature, which, of course, substantially affect the stress history and fracture strength of the material as has been shown earlier. In the case of biaxial tests, an additional control parameter, namely, a

description of the state of stress or strain, is added to the previous two. Because the loading device used in this effort inputs a rotation which is a linear function of the axial displacement, it is natural to think of the added parameter as a shear rate about the specimen axes. This natural and simple idea, though, is not completely adequate to the task of evaluating the effect of the state of strain. For example, assume that two room temperature biaxial tests are to be run. In one case the axial strain rate equals the shear strain rate and in the other case the axial rate is twice that of the shear rate. The question then arises: under what conditions are these two tests comparable. Should the axial rate be equal in each test or should the shear rate be equal. There are, of course, a number of relationships that could be used as a basis of establishing some form of equivalency. In searching for a plausible criterion, one naturally considers the possibility of using principal strains.

We recall that tight fitting rings are placed in the test specimen to insure that the radial strain remains zero. Since the axial strain and the shear strain can be arbitrarily chosen, we see that the principal strains can be easily determined. For convenience, a Mohr's circle is shown in figure 63 with typical strains shown at some instant. We shall require the axial strain to be tensile since we are interested in the lower values of stress that will cause fracture and we wish to avoid the complication of buckling. A consequence of tensile axial strain and null radial strain is the following set of inequalities:

$$\epsilon_{11} > 0 \qquad \epsilon_{22} \leq 0$$

$$|\epsilon_{22}| \leq |\epsilon_{11}| \tag{41}$$

These relationships suggest that the principal tensile strain rate would represent a reasonable basis of establishing equivalency between tests. This selection is partly motivated by the belief that tensile stress or strains dominate the failure process. Subsequent test results, particularly the shear tests, seem to reinforce this opinion. Our need to adequately describe the state of stress is now partially satisfied by using the principal tensile strain rate. A second parameter is needed to fully specify the state of strain (i. e., a control on the other principal strain). A reasonable selection is to have the principal strains proportional (e. g., $\dot{\epsilon}_{22} = \dot{\epsilon}_{11} \tan\delta$). These criteria are represented in figure 64 where four radial load paths are shown. They correspond to values of δ of 0, 15, 30 and 45 degrees. The first and last of these correspond to pure tension and pure shear, respectively.

c. Biaxial Test Results

Table 1 lists the 18 biaxial tests that were performed and the corresponding test conditions. The test conditions were established by the type of information that could be useful in understanding the stress-strain behavior and fracture characteristics of TPH 1011. Three of the tests which varied in either strain rate or test temperature or both were performed at a uniaxial strain state. The purpose of these tests was to evaluate the biaxial specimen configuration by

Test Number	ε_{11} ("/"/min)	δ^* (degrees)	T(^oC)
1	0.1	0	23
2	0.1	45	23
3	0.1	15	23
4	0.1	30	23
5	0.1	30	23
6	0.1	45	23
7	1.0	0	23
8	1.0	15	23
9	1.0	30	23
10	1.0	45	23
11	0.1	15	0
12	0.1	0	0
13	0.1	30	0
14	0.1	45	-20
15	0.1	45	0
16	1.0	45	23
17	1.0	30	23
18	1.0	15	23

* $\varepsilon_{22} = \varepsilon_{11} \tan \delta$

Table 1. Biaxial Test Conditions

comparing the test results to dogbone specimen test results for the closest equivalent test conditions. The results are shown in figures 65, 66 and 67. The plots show stress versus time which from knowing the constant strain rate could easily be converted to stress-strain plots. In each of the cases presented, the loading curves are in reasonable agreement except the dogbone specimen fails at higher stress level. This might be expected as the closest comparable dogbone specimen test had a 40 percent higher strain rate. An additional possible cause for the higher failure stress results from the stress concentration that is developed by the aluminum end fittings on the cylindrical propellant specimens. The dogbone specimen is, of course, designed to minimize the effect of grips, but in so doing, special care must be exercised in calculating the appropriate strains. It might be possible to alleviate the stress concentrations from the end fittings by locally increasing specimen wall thicknesses, but the problem of calculating the equivalent biaxial strain history would be very difficult. Despite these shortcomings, the results of the uniaxial tests are in general agreement with what would be expected from knowledge of the dogbone specimen tests. In all of the uniaxial tests, the shear stress recorded from the load cell was negligible.

Because of the number of available specimens and the motivation to determine repeatability, it was decided to limit the testing to a comparison of two temperatures and two strain rates for a given state of strain. The data is presented in figures 68, 69 and 70 for the load path corresponding to an angle of 15 degrees shown in figure 64 . It is interesting to note that although the axial stress reached

a peak and was decreasing during the later stages of the test, the shear stress increased monotonically. The high-strain-rate test was repeated and the shear stress histories for the two tests were identical. Failure, in these as well as the other tests, was established when there was a severe drop in the developed stress. This was usually accompanied by one or more large fractures. In practically all of the tests with the exception of the pure shear tests, fracture surfaces were observed at the edge of an end fitting. It was not uncommon though to detect fractures opening away from a fitting. The next set of tests corresponds to a load path angle of 30 degrees in principal strain space. The test results are shown in figures 71, 72 and 73. Except for the difference in state of strain the observations concerning the 15 degree tests apply.

The most interesting series of tests were the 45 degree or pure shear tests. The stress histories are shown in figures 74, 75, 76, and 77. The most obvious feature of these tests is that an axial compressive stress is developed when only torque is applied to specimen. This was observed on all six of the pure shear tests. It was also noted that all but one of the test specimens initially experienced a small tension stress before going into compression. The only difference detected in that one anomaly was that a very slight compression preload was applied to specimen number 2 while a very slight tension preload was applied to all of the other shear specimens. A slight preload (e.g., 2 psi) is practically unavoidable since for the shear test, no axial displacement of the speciment grips is permitted and a slight specimen elongation occurs as the bolts holding the

specimen are tightened. Two possible explanations for the compression arise from past experience with related materials. Recent shear tests on sand at GALCIT indicated the development of compression stresses. The explanation was that the sand particles rotated under the applied shear force and the irregular sand particles "rolled" against other irregular particles. The result may be considered as the reverse of compaction. Since TPH 1011 is 80 per cent particulate, a similar phenomena could explain the appearance of compression. Another possible explanation might be the behavior of the polymer chains or ligaments when subjected to shear stress. It is well known, for example, that rubbery materials exhibit negative coefficients of thermal expansion. The compressive stresses observed in these experiments may stem from the same character as do the unusual thermal properties.

Figure 78 shows a typical shear test failure. It is interesting to note that the fracture is aligned nearly perpendicular to the principal tension stress. The fracture always appeared aligned in this manner. As the test was continued, the fracture ran to an end piece interface and proceeded circumferentially as shown in figure 79.

11. Failure by Crack Propagation in Propellants

Earlier in this report we have described how failure of propellant progresses from the growth of many flaws through their coalescence to form a macroscopic crack. The same processes that lead to the formation of a macroscopic crack operate also in the inhomogeneous stress field at the tip of such a crack.

Let us consider the material at the tip of a crack in a block of propellant under stress such that the crack tends to propagate in its own plane. The material at the tip (shown dotted in figure 80a) will "disintegrate" or lose its cohesive forces during the crack propagation as a result of the localized high stresses at the crack tip. For illustrative purposes let us make the very crude assumption that the crack tip stresses are simulated by a tensile specimen of the shape shown in figure 80b. Because of the variable cross section the stresses at the waist are highest. Now consider that somehow the specimen was stressed to a certain state without rupturing at the waist but such that rupturing could be imminent. If we suppose that the material exhibits the uniaxial stress-strain characteristics shown in figure 81, then this hypothetical state may place the net section stresses of the waist specimen on this curve; for instance, the narrowest section may be at point A and the sections B and C at appropriate points on the stress-strain curve.

Suppose we now hold the displacement of the waist specimen fixed; this does not actually correspond to the condition on the material at the crack tip, for which the waist specimen is supposed to be an analogue, but this condition simplifies the following argument.

Under fixed end conditions on the y-displacement we ask whether it is possible that the energy stored in the outer portions of the specimen can be used to do work on the central section and thereby bring the central section from the state A (figure 81) to the stress free state D which would correspond to rupture. We deal thus with a plastic instability. If the ends of the specimen are not fixed but loaded by constant tractions then the instability is imminent as soon as the stress at the thinnest section obtains the maximum value because from then on the external constant forces can supply the work necessary to strain the material near the waist to the end point on the stress-strain curve at point D. If the end conditions on the waist specimen are without constant displacement or constant force, but say an elastic constraint, then the work done by this elastic agent must be considered in determining the condition for instability.

What we have described so far would correspond to a solid whose mechanical response does not depend on deformation rate. In reality both the loading and unloading behavior of propellant is rate dependent, although it seems to be a good approximation - on the basis of the unloading studies at different strain rates - that unloading is rather insensitive to unloading rates.

Disregarding such complications introduced by rates, it is clear that the propagation of a crack involves an exchange of the energy stored in the material at large and a small domain at the crack tip. For a linearly (visco)elastic solid this energy exchange can be calculated provided one assumes that the rupture work (equivalent to loading past the point A in figure 81) is confined to

a very narrow region along the axis of crack propagation (Knauss, 1973a and b). The ability to perform this analysis derives from the relative case with which a linearly viscoelastic stress and deformation analysis can be performed.

For a non-linear viscoelastic solid such as a solid propellant one encounters difficulties which are similar to those one meets when dealing with ductile solids, except that the latter present a smaller problem than propellants because of lack of rate sensitivity. The problem with solid propellants is thus basically that their properties of progressive strength degradation - and thereby its ultimate properties - are infinitely coupled with the stress field around the crack tip. Thus if one develops a model of crack propagation based on the representation of non-linear constitutive response as modelled here, it is necessary to perform the requisite stress analysis for the same non-linear viscoelastic material; at the present time it is not possible to perform this stress analysis primarily because the non-linear constitutive behavior is still not sufficiently well understood. If one were satisfied with an approximate representation of the material behavior, an analysis structured on incremental plasticity characterization with time as a parameter becomes possible, however the procedure seems exorbitantly expensive.

Before suggesting two possibilities of approximate crack propagation (instability) analysis we remark on an approach to the problem of crack propagation explored earlier (Knauss 1963). We had in mind during the proposal stage to consider that the crack propagation could be calculated on the following basis: we assume

that the material ahead of the crack tip consists of uniaxially tensile mirco-specimens aligned normal to the crack axis. The surrounding material exerts stresses on these uniaxial specimens which are given by the stresses on the prolongation of the crack axis in a linearly elastic or viscoelastic solid. If the crack propagates these tensile specimens each experience a certain stress history which leads to their rupture and thus to crack propagation.

During the literature surveys it was found that Barenblatt, et al. [Barenblatt, Entov and Salganik, 1966-1971] had worked out in part a similar model in which the tensile specimens are supposed to rupture according to Zhurkov's rate law [Zhurkov]. The execution of that model met with extreme mathematical difficulties which left the investigation with only qualitative results that are obvious from physical intuition alone.

Two Suggested Procedures for Crack Propagation Determination.

1) If a propellant can be reasonably well approximated by a linearly viscoelastic solid then the results of the crack propagation studies for linearly viscoelastic solids [Knauss, 1973 a and b] may be applicable. Moreover the procedures proposed by Greensmith and Thomas [Greensmith, 1960], [Thomas] may prove useful with an appropriate material characterization for fracture. Particulars are discussed in detail in the references and need not be repeated here.

2) If a propellant has a strongly non-linearly viscoelastic response - as most practical propellants do - recourse may be taken to currently available computer programs dealing with the fracture

of rate-independent plastic behavior. We make this suggestion with the following observation in mind: one observes that the rate dependence of propellants is strongly noticeable only if rates vary by orders of magnitude; generally the properties do not vary greatly in a limited range of deformation histories. Suppose one determines the average response in a particular range of deformation rates as if the material were a ductile solid. In doing so it would be necessary to take into account the type of load history which the material will approximately experience at the crack tip in the practical design problem at hand. One can then perform the "plasticity characterization" for a similar load history and using these properties, a fracture analysis geared to ductile solids.

12. Summary and Conclusions

The initial intent of this study was the examination of the applicability of the equations of chemical reaction rates to the fracture description of solid propellants. A critical literature review soon showed that the use of chemical reaction rate laws (absolute reaction rate laws) in connection with molecular concepts was not completely sound. In effect what is lacking in most current treatments by reaction rate theory applied to polymer fracture is a sound physical model of the rupture process. Rather than use the reaction rate equations and develop a curve-fitting procedure, the effort was turned to identifying the physical processes of fracture growth in propellants and to model these processes.

Having determined that the growth of cracks and voids either within the binder matrix or at binder-particle interfaces was the factor determining propellant life, it appeared necessary to develop an experimental technique to trace this void growth directly. This was attempted via a high frequency (10-16 kcps) electromechanical device which, however, failed to provide unique answers. Therefore we turned to the non-linear constitutive behavior as a measure for the internal damage sustained by the propellant during any load history. It became thus necessary to connect the flaw or crack growth with the macroscopically measurable stress-strain behavior of the propellant.

To this end a simple model is proposed: It divides the solid into elements each of which contains an initially small flaw; the flaws or cracks in the elements are aligned normal to the direction of

maximal tension and follow some size distribution. The elements together contribute a composite solid whose average properties depend on the deformation properties of the individual, flawed elements. The size of the flaws, in turn, depend on the entire past load history through a rate law derived from the fracture mechanics of viscoelastic solids. If reaction rate laws are applicable, they would substitute for the fracture rate law to determine how the size of the flaws depends on the load history.

The fracture concept yields thus simultaneously information on the amount of damage incurred in the form of flaw or crack growth as well as the material properties (stress-strain behavior) as a result of flaw growth.

It is our considered opinion that currently practiced methods of failure prediction in solid propellant rocket motors lead to poor results because of an inadequate description of the mutual dependence of the failure process and constitutive behavior on each other. To improve the predictability of propellant failure it appears absolutely necessary to devise a technique which traces the flaw-damage directly. Similarly it will be equally necessary to employ non-linear stress analysis in motor failure prediction. This requirement follows from the fact that the rate of failure accumulation can be very sensitive to small changes in the applied stresses. Hence relatively small errors induced by a linear stress analysis for a constitutively non-linear solid will lead to gross errors in failure prediction.

Considering the simplicity of the proposed physical model the agreement with experiments is very good. This observation applies to both single loadings - unloading cycles and to repetitive

loading loading-unloading in uniaxial strain histories.

Under strain cycling between fixed (tensile) strain limits the rate of damage accumulation is highest initially and decreases with further cycling.

Since the model allows a continuous accounting of the internal damage, a method exists by which one determines how close the material is to complete failure. Total failure is defined when the flaws have grown to their maximum size which is determined by the size of the element in which they are contained.

Under biaxial loadings the failure accumulation appears to follow the same process as in uniaxial tension. This observation follows from the comparison of experimental data in the uniaxial and biaxial strain state, where the latter was conducted for different ratios of the principal strains.

REFERENCES

Barenblatt, G. I., Entov, V. M. and Salganik, R. L., "Kinetics of Crack Propagation, General Conditions: Cracks Approaching Equilibrium Cracks," Mechanics of Solids (Mekhanika Tverdogo Tela) 1, English Version p. 82, 1966; AMR 23 (1970), Rev. 4398.

_____, "Kinetics of Crack Propagation: Conditions of Fracture and Longterm Strength," ibid 1, English version p. 76, 1966; AMR 24 (1971), Rev. 316.

_____,"Kinetics of Crack Propagation: A Note on the Rule of Summation of Damageabilities," ibid 2, English version p. 148, 1967.

_____, "Kinetics of Crack Propagation: Fluctuation Fracture," ibid 2, English version p. 122, 1967; AMR 24 (1971), Rev. 6811.

_____, "Some Problems of the Kinetics of Crack Propagation," Inelastic Behavior of Solids, Materials Science and Engineering Series, Kanninen, M. F., et al. editors, McGraw-Hill, 1970.

Budiansky, B., "On the Elastic Moduli of Some Heterogeneous Materials," J. Mech. Phys. of Solids, Vol. 13, pp. 223-227, 1965.

Busse, W. F., Lessig, E. T., Loughborough, D. L., "Fatigue of Fabrics," J. Appl. Physics, Vol. 13, pp. 715-724, 1942.

Campbell, D., Peterlin, A., "Free Radical Formation in Uniaxially Stressed Nylon," Polymer Letters, Vol. 6, pp. 481-485, 1968.

Cantey, D., "Solid Propellant Structural Integrity Investigation - Dynamic Response and Failure Mechanisms," Report AFRPL-TDR-54-32 (LP 618-F) 1954.

Cartwright, R. V., "Modelling Fatigue Failure in Urethane Elastomers - A New Approach," J. Elastoplastics, Vol. 3, pp. 249-270, 1971.

Devries, K. L., Simonson, E. R., Williams, M. L., "A Micro-Macro Correlation of Ozone-Induced Fracture in Rubber," Journal of Applied Polymer Science, 14, p. 3049, 1970a.

_____, Farris, R. J., "Strain Inhomogeneities, Molecular Chain Scission and Stress-Deformation in Polymers," International Journal of Fracture Mechanics, 6, p. 411, 1970b; AMR 24 (1971) Rev. 6814.

REFERENCES (Cont'd)

_____, Roylance, D. K., Williams, M. L., "Formation of Free Radicals During Mechanical Degradation of Elastomers," Polymer Letters, Vol. 9, pp. 605-609, 1971a.

_____, Roylance, D. K., Williams, M. L., "An Experimental Investigation of Some Models of Polymer Fracture," International Journal of Fracture Mechanics, Vol. 7, pp. 197-202, 1971b; AMR 25 (1972), Rev. 3703.

_____, Loyd, B. A., Williams, M. L., "Reaction-Rate Model for Fracture in Polymeric Fibers," J. Appl. Phys., Vol. 42, No. 12, pp. 4644-4653, 1971c.

Eshelby, J. D., "The Determination of the Elastic Field of an Ellipsoidal Inclusion, and Related Problems," Proceedings of the Royal Society of London, Series A, Vol. 241, p. 376, 1957.

Farris, R. J., "The Character of the Stress-Strain Function for Solid Propellants," Transactions of the Society for Rheology, Vol. 12, pp. 281-301, 1968a.

_____, "The Influence of Vacuola Formation on the Response and Failure of Highly Filled Polymers," Transactions of the Society for Rheology, Vol. 12, pp. 315-334, 1968b.

_____, "Homogeneous Constitutive Equations for Materials with Permanent Memory," Ph. D. Thesis, Dept. of Civil Engineering, University of Utah, Salt Lake City, June 1970.

Graham, P. H., Robinson, C. N., Henderson, C. B., "Analysis of Dilatational Failure of Heterogeneous Materials by Reaction Rate Theory," International Journal Fracture Mechanics, Vol. 5, No. 1, pp. 57-62, 1969; AMR 23 (1970), Rev. 5344.

Greensmith, H. W., Mullins, L., and Thomas, A. G., "Rupture of Rubber," Transactions of the Society of Rheology, 4, p. 179, 1960.

_____, "Rupture of Rubber, XI, Tensile Rupture and Crack Growth in a Non-Crystallizing Rubber," Journal of Applied Polymer Science, 8, p. 1113, 1964.

Hart-Smith, L. J., "Elasticity Parameters for Finite Deformations of Rubber-Like Materials," Zeitschrift fur Angewandte Mathematik und Physik, V. 17, pp. 608-626, 1966.

Henderson, C. B., Graham, P. A., Robinson, C. N., A Comparison of Reaction Rate Models for the Fracture of Solids," International Journal Fracture Mechanics, Vol. 6, No. 1, pp. 33-40, 1970; AMR 23 (1970), Rev. 8705.

REFERENCES (Cont'd)

Il'yushin, A. A., Ogibalov, P. M., "Criteria of the Long Time Strength of Polymers," Polymer Mechanics (Mechanika Polymesor), Vol. 2, No. 6, English Version, pp. 828-832, 1966.

Kausch (Blecken von Schmeling), H. H., Hsiao, C. C., "Behavior of Elastic Networks of Various Degrees of Orientation in the Kinetic Theory of Fracture," Journal of Applied Physics, Vol. 39, No. 11, pp. 4915-4919, 1968.

_____, "A Note on the Paper of V. R. Regel and A. M. Leksovsky "A Study of Fatigue within the Framework of the Kinetic Concept of Fracture,'" International Journal of Fracture Mechanics, Vol. 5, No. 1, pp. 9-11, 1969. AMR 23 (1970), Rev. 291.

_____, "On a Fracture Criterion for High Polymers Derived from the Kinetic Theory of Fracture," Materialprufung, Vol. 12, No. 3, pp. 77-81, 1970a.

_____, "Recent Developments in the Kinetic Theory of Fracture of Polymers," Kolloid-Zeitschrift und Zeitschrift fur Polymere. Vol. 236, No. 1, pp. 48-58, 1970b, AMR 24 (1971) Rev. 3520.

_____, Becht, J., "Uber Spannungsrelaxation und Zeitabhangige elastische Bruchvorgange in orientierten Fasern," Rheologica Acta, Vol. 9, No. 1, pp. 137-144, 1970c.

_____, "The Role of Network Orientation and Microstructure in Fracture Initiation," Polymer Science Symposia, No. 32, John Wiley and Sons, Inc., pp. 1-44, 1971.

Knauss, W. G., "The Time Dependent Fracture of Viscoelastic Materials," Proceedings First International Conference on Fracture, Vol. 2, p. 1139, Sendai Japan, 1965. (See also Ph. D. Thesis, Calif. Inst. of Tech., Pasadena, 1963).

_____, "Stable and Unstable Crack Growth in Viscoelastic Media," Transactions of the Society of Rheology, 13, p. 291, 1969.

_____, "The Mechanics of Polymer Fracture," Applied Mechanics Reviews, 26, No. 1, p. 1-17, 1973a.

_____, "Mechanics of Fracture in Polymeric Solids," California Institute of Technology, Graduate Aeronautical Laboratories, Pasadena, California. To appear in the Proceedings of the Third International Conference on Fracture, Munich, April, 1973b.

REFERENCES (Cont'd)

Prevorsek, D., Lyons, W. J., "Fatigue Fracture in Fibrous Polymers as a Brittle Crack-Nucleation Process," Journal Applied Physics, Vol. 35, No. 11, pp. 3152-3164, 1964; AMR 18 (1965), Rev. 2792.

Pucik, T. A., "Elastostatic Interaction of Cracks in the Infinite Plane," Ph.D. Thesis, California Institute of Technology, Pasadena, California, June 1972.

Roylance, D. K., DeVries, K. L., Williams, M. L., "Fracture Detection in Polymers by Electron Paramagnetic Resonance," Fracture 1969, Proceedings of the Second International Conference on Fracture, Brighton, England, April 1969, Pratt, P. L. ed., Chapman and Hall, Ltd., London, p. 551, 1969.

Regel, V. R., Leksovsky, A. M., "A Study of Fatigue within the Framework of the Kinetic Concept of Fracture," International Journal of Fracture Mechanics, Vol. 3, pp. 99-109, 1967; AMR 21 (1968), Rev. 4182.

Short, D. A., Anderson, O. L., "Dependence of Ultimate Strength of Glass Under Constant Load on Temperature, Ambient Atmosphere, and Time," Journal of the American Ceramic Society, Vol. 36, No. 12, pp. 416-424, 1953.

Thomas, A. G., "Rupture of Rubber VI. Further Experiments on the Tear Criterion," Journal of Applied Polymer Science, 3 p. 168. 1960.

Tobolsky, A., Eyring, H., "Mechanical Properties of Polymeric Materials," Journal of Chemical Physics, 11, pp. 125-134, 1943.

Williams, M. L., DeVries, K. L., "An EPR Investigation of Newly Formed Fracture Surfaces," Sagamore Army Materials Research Conference Proceedings, Surfaces and Interfaces, Syracuse University Press, 1968.

Zhukov, S. N., "Kinetic Concept of the Strength of Solids," International Journal of Fracture Mechanics, Vol. 1, No. 4, pp. 311-323, 1965; AMR 20 (1967), Rev. 4080.

APPENDIX A. Review of Literature on Reaction Rate Theory Applied to the Fracture of Solids

For the purpose of our immediate discussion it is useful to think of an amorphous polymer as a tangled bundle of long, intertwined and flexible strings of atoms. According to whether we consider, respectively, a crosslinked or uncrosslinked material, these chains of atoms may, or may not, be connected to each other at several points along their length. At temperatures above the glass transition, segments of entangled chains are in more or less vigorous thermal motion and at temperatures below the glass transition this motion of large chain segments is impaired or virtually precluded. When a macroscopic state of deformation is imposed on a polymeric solid, molecular rearrangement occurs. Due to the relatively high thermal mobility of the polymer chain segments above the glass transition temperature this reorganization is easier and quicker above than below the glass transition temperature; below the glass transition a given macroscopic deformation (history) has to be accommodated by a much more tightly arranged molecular assemblage.

This difference in the rapidity with which molecular rearrangement can occur has two practical and important consequences. First, since the conformation of polymer chains is statistical in nature, the forces experienced by individual molecule chains (or chain segments) upon macroscopic deformation are also not uniformly distributed [A1-A3]. However, because of the greater mobility of polymer chains above the glass transition the chances are also

greater that the macroscopic stress is more evenly distributed over many polymer chains than would be the case below the glass transition [A4] ; below this latter temperature one would expect, therefore, that some chains will break rather early in any loading history, while others need to be oriented first through a molecular reorientation process before they rupture [A4]. Thus molecular orientation and chain rupture occur simultaneously, and occur one as the result of the other below the glass transition temperature; above the glass transition temperature, orientation tends to precede bond rupture. Second, when radicals are formed in the rupture of a polymer chain above the glass transition temperature, the thermal motion of the "loose" ends allows a high chance of recombination with other radical chain ends. Consequently, radicals do not exist long enough to be easily traced with current experimental techniques [A5, A6]. The opposite tends to be true when the temperature is below the glass transition temperature; therefore detailed studies of molecular fracture are performed on solids well within the glassy state. Although molecular rupture has been interpreted qualitatively as being either a process primarily of flow [A7-A9], of orientation [A10-A13], or of bond rupture [A14-A16], these phenomena are not easily separated. To eliminate the time dependent flow during the molecular orientation process in order to study the time dependence of the bond rupture process by itself, one would favor the study of highly pre-oriented films and fibers. It is doubtful, however, that such pre-oriented materials are so uniform in their molecular arrangement that time dependent flow and orientation cannot occur. Nevertheless,

pre-oriented polymers are studied extensively in the glassy state [A3, A4, A13, A16-A21] to reduce polymer chain orientation during stressing and to thereby further enhance the number of radicals formed under stress in a unit of volume.

An additional point needs to be made regarding the temporal separation of the molecular rearrangement and chain rupture. It is sometimes contended [A4] or implied [A11-A13, A16, A22] that in the glassy state molecular motion is so impaired that the time dependence of observed chain ruptures is direct evidence of the time dependence of the bond rupture, rather than evidence of any molcular rearrangement history. While it is true that under stresses producing infinitesimal strains the molecular motion is essentially "frozen" in the glassy state, a dilatational tensile stress component, large enough to (nearly) promote total failure, may facilitate molecular motion just as a large hydrostatic pressure will inhibit it [A23]. Indeed, studies with the electron microscope [A24, A25] indicate visibly that extensive molecular rearrangement is inseparably connected with the molecular chain rupture process, and may well be the process controlling time dependent fracture in (glassy) polymers. As we shall see presently, bond rupture is modeled on the theory of chemical reaction rates, which builds into the modeling process an exponential relation between time and applied stress. Since the rheology of polymers basically obeys also relations which are exponential in time, such modeling can hardly differentiate between bond rupture and time dependent molecular rearrangement processes.

The quantitative description of molecular rupture in polymers

is today considered almost entirely within the framework of the theory of rate processes [A26] with obvious parallels to the application of rate theory to metal flow [A27-A31] and the fracture of inorganic glasses [A14]. In view of the above-mentioned competition of the molecular flow and rupture processes in the failure of polymers, it is difficult at best to argue that the application of reaction rate theory to polymer fracture on the molecular level is clearly sound. Postulated by allusion to quantum mechanical principles, this description is based on several assumptions. First, one treats the process as if it were representable by a typical, average chain segment existing in very large numbers. In this average representation one is only concerned with the bookkeeping of broken and unbroken bonds under the exclusion of any spatial interaction between two or more sites where chain rupture occurs. The pool of elements from which one draws broken or unbroken bonds for this bookkeeping is taken variously as a unit volume of a macroscopic test specimen [A5, A20, A32, A33], a unit cross sectional area [A8, A9], or a microscopic domain which develops into a microscopic flaw [A3, A14, A34, A35]. Second, the rate at which the number of unbroken bonds N* diminishes is, in its simplest form [A3, A8, A9, A12, A13], assumed proportional to the number of unbroken bonds, i.e.,

$$\frac{dN^*}{dt} = -PN^* \qquad \text{(A1)}$$

with P being a rate factor to be discussed shortly, and with more elaborate relations [A8, A14, A34, A35] accounting for possible reformation of bonds. Third, the rate factor P is taken proportional

to the probability [A9, A14, A34-36] that a molecular bond will break due to thermal fluctuation when it is under a tensile force. Thus,

$$P = \frac{1}{\tau_o} \exp\left\{ - \left[A_o - F(\sigma)\right] / kT_{ab} \right\} \qquad (A2)$$

where k, T_{ab}, A_o are, respectively, Boltzmann's constant, the absolute temperature and the activation energy. τ_o is a constant [A11] or inversely proportional to the temperature T [A8, A10, A14] and $F(\sigma)$ is a function of the applied (uniaxial) stress σ. $F(\sigma)$ is assumed to equal $\lambda_1 \cdot \sigma$ [A16, A22]; or $\lambda_2 \sigma/N$ [A8, A9, A14]; or the strain energy density for an assumed linearly elastic solid [A35]; or, for a viscoelastic solid, the free energy density functional of the stress history [A20, A34]. λ_1 and λ_2 are constants. Under these rather arbitrary constraints on $F(\sigma)$ equations [A1] and [A2] predict bond rupture, even in the absence of a stress σ when $F(\sigma) = 0$; that implication contradicts experimental evidence [A16] and therefore [A1] is usually applied only under conditions of "sufficiently high stress." In practice the somewhat uncertain term in quotation marks means merely that equation [A1] is deemed applicable when the theoretical results based on its integration fit the experimental findings. At low stress levels the net rate of bond rupture can be reduced by assuming that bonds can reform again [A8, A14, A34, A35] although it is highly questionable that these bonds reform into a stretched state. These formulations admit the vanishing of (net) bond rupture only for vanishing (tensile) stresses; for non-zero stresses the rupture of bonds, and thus presumably the gross fracture process, continues. One

can show from a continuum viewpoint that a non-vanishing stress state with some principal tensile component larger than some positive minimum exists in order for gross crack propagation to occur. Rate theory by itself -- as proposed to date -- does not allow for such a non-zero limit on the stress for fracture. In relating bond rupture to the fracture on the macroscopic scale, its occurrence must be argued on continuum mechanical grounds [A34, A35], by requiring that a sufficient number of bonds have to fracture locally to produce a recognizable surface.

In an extensive study covering some 50 metallic and non-metallic materials Zhurkov and co-workers [A15, A16, A22, A37, A38] have found that the time-to-rupture, τ^*, of fibers or strips subjected to (uniaxial) constant true stress, σ, was given by the simple relation

$$\tau^* = \tau_o \exp\{(A_o - \lambda_1\sigma)/kT\} \qquad \text{(A3)}$$

with τ_o, A_o, λ_1, k and T_{ab} as already defined. A somewhat surprising result of these investigations was that apparently for all materials τ_o was on the order of the molecular oscillation period of 10^{-13} sec., and E_o was equal to the heat of sublimation for metals and equal to the interatomic bond energy for polymers [A16]. In order to examine for polymers the implications of this sweeping result, Zhurkov studied the production of radicals in polymers as a result of bond rupture through exciting their electron paramagnetic resonance (EPR) [A16, A38] and found that the rate of radical production was proportional to exp ($\alpha \cdot \sigma$), α a constant.

Since Zhurkov's EPR studies imply that radicals are produced at a constant rate under application of constant stress, DeVries, Roylance and Williams [A4, A5] examined bond rupture as a result of different stress histories; they could not corroborate Zhurkov's results in general, the best agreement being achieved for the special history of a constant (engineering) stress rate [A5]. Zhurkov's impressive findings appear thus to be the somewhat fortuitous result of a particular test method.

The picture of molecular bond rupture that emerges from these recent studies by DeVries et al. [A4, A5, 19, A20] is one of increasing complexity. Current trends are towards a resolution of the bond rupture process which is more detailed than that reflected by equations (A1) or (A3). Use of EPR has become a standard tool [A39, A40] and permits even the identification of the rupture sites in molecules [A4], the average number of rupture sites per molecule [A4, A18], as well as the separation distance of radicals when a bond ruptures [A18]; it also confirmed the guess [A34, A35] that newly generated surface at the supermolecular level is proportional to the number of bonds broken [A41]. Evolution of gases during fracture has become another tool for investigating molecular chain rupture [A42]. Information on how the molecule chains are stressed to different degrees in the bulk polymer is being obtained both by improved analytical modeling of the non-uniform distribution of forces acting on molecule chains [A20] and by direct, experimental examination through infrared spectroscopy [A1], or, at the supramolecular scale, by low-angle x-ray scattering [A43]. The interaction by

which chain rupture sites influence each other, both with regard to time sequence and relative spatial separation seems very hard to determine. Current experimental techniques give access to spatially averaged quantities and it appears that information on spatially distinct events must be attacked by designing the molecular structure of test material for this purpose.

This trend in refinement of the molecular aspects of failure spells, in a sense, a move away from a continuum mechanical formulation of the fracture problem. While a global but simple rate concept like that advanced by Zhurkov et al. [A16] allows its incorporation into a continuum mechanical analysis [A44-A49] -- provided it is universally valid -- the information to be derived in the future from molecular studies is likely to be more precise with regard to molecular parameters but less informative with respect to the analysis of fracture from a continuum mechanical viewpoint.

References to Appendix A

[A1] Zhurkov, S. N.; Vettegren, V. I.; Korsukov, V. E.; Novak, I. I.; Infrared Spectroscopie Study of the Chemical Bonds in Stressed Polymers. Paper 47 in Fracture 1969. Proceedings of the Second International Conference on Fracture, Brighton, England, April 1969. Chapman and Hall, Ltd., London, p. 545, 1969.

[A2] DeVries, K. L.; Farris, R. J.; Strain Inhomogeneities, Molecular Chain Scission and Stress-Deformation in Polymers. International Journal of Fracture Mechanics, Vol. 6, No. 4, p. 411, 1970.

[A3] DeVries, K. L.; Lloyd, B. A.; Williams, M. L.; Reaction-rate Model for Fracture in Polymeric Fibers. Journal of Applied Physics, Vol. 42, No. 12, p. 4644, 1971.

[A4] Roylance, D. K.; DeVries, K. L.; Williams, M. L.; Fracture Detection in Polymers by Electron Paramagnetic Resonance. Paper No. 48 in Fracture 1969, Proceedings of the Second International Conference on Fracture, Brighton, England, April 1969. Chapman and Hall, Ltd., London, p. 551, 1969.

[A5] Williams, M. L.; DeVries, K. L.; Electron Paramagnetic Resonance Measurement of Strain Rate and Cyclic Effects on Bond Rupture. Proceedings of the Fifth International Congress on Rheology, p. 139, 1968.

[A6] Becht, J.; DeVries, K. L.; Kausch, H. H.; On Some Aspects of Strength of Fibers. European Polymer Journal, Vol. 7, p. 105, 1971.

[A7] Busse, W. F.; Lessig, E. T.; Loughborough, D. L.; Larrick, L.; Fatigue of Fabrics, Journal of Applied Physics, Vol. 13, November, p. 715, 1942.

[A8] Tobolsky, A.; Eyring, H.; Mechanical Properties of Polymeric Materials. Journal of Chemical Physics, Vol. 11, March, p. 125, 1943.

[A9] Henderson, C. B.; Graham, P. H.; Robinson, C. N.; A Comparison of Reaction Rate Models for the Fracture of Solids. International Journal of Fracture Mechanics, Vol. 6, No. 1, p. 33, 1970.

[A10] Kausch, H. H.; Hsiao, C. C.; Behavior of Elastic Networks of Various Degrees of Orientation in The Kinetic Theory of Fracture, Journal of Applied Physics, Vol. 39, No. 11, p. 4915, 1968.

[A11] Kausch, H. H.; A Note on the Paper of V. R. Regel and A. M. Leksovsky "A Study of Fatigue within the Framework of the Kinetic Concept of Fracture." International Journal of Fracture Mechanics, Vol. 5, No. 1, P. 9, 1969.

[A12] Kausch, H. H.; Recent Developments in the Kinetic Theory of Fracture of Polymers. Kolloid-Zeitschrift und Zeitschrift für Polymere, Vol. 236, No. 1, p. 48, 1970.

[A13] Kausch, H. H.; The Role of Network Orientation and Microstructure in Fracture Initiation. Polymer Science Symposium, Journal of Polymer Science, No. 32, p. 1, 1971.

[A14] Stuart, D. A.; Anderson, O. L.; Dependence of Ultimate Strength of Glass under Constant Load on Temperature, Ambient Atmosphere and Time. Journal of the American Ceramic Society, Vol. 36, No. 12, p. 416, 1953.

[A15] Zhurkov, S. N.; Das Problem der Festigkeit fester Körper, Zeitschrift für Physikalische Chemie (Leipzig), Vol. 213, p. 183, 1960.

[A16] Zhurkov, S. N.; Kinetic Concept of the Strength of Solids. International Journal of Fracture Mechanics, Vol. 1, No. 4, p. 311, 1965.

[A17] Perepelkin, K. E.; Theoretical and Maximum Attainable Strength of Various Uniaxially Oriented Polymers (film, fibers). Mekhanika Polimerov, Vol. 2, No. 6, English version p. 845, 1966.

[A18] Campbell, D.; Peterlin, A.; Free-Radical Formation in Uniaxially Stressed Nylon. Polymer Letters, Vol. 6, p. 481, 1968.

[A19] Williams, M. L.; DeVries, K. L.; An EPR Investigation of Newly Formed Fracture Surfaces. Sagamore Army Materials Research Conference Proceedings: Surfaces and Interfaces II. Syracuse University Press, 1968.

[A20] DeVries, K. L.; Roylance, D. K.; Williams, M. L.; An Experimental Investigation of Some Models of Polymer Fracture. International Journal of Fracture Mechanics, Vol. 7, No. 2, p. 197, 1971.

[A21] DeVries, K. L.; Roylance, D. K.; Williams, M. L.; Formation of Free Radicals during Mechanical Degradation of Elastomers. Polymer Letters, Vol. 9, p. 605, 1971.

[A22] Zhurkov, S. N.; Sanfirova, T. P.; A Study of the Time and Temperature Dependences of Mechanical Strength. Soviet Physics Solid State (Fizika Tverdogo Tela), Vol. 2, No. 6, English version p. 933, 1960.

[A23] Quach, A.; Simha, R.; Pressure-Volume-Temperature Properties and Transition of Amorphous Polymers; Polystyrene and Poly(orthomethylstyrene). Journal of Applied Physics, Vol. 42, No. 12, p. 4592, 1971.

[A24] Keith, H. D.; Padden, F. J., Jr.; Vadimsky, R. G.; Intercrystalline Links: Critical Evaluation. Journal of Applied Physics, Vol. 42, No. 12, p. 4585, 1971.

[A25] Geil, P. H.; Morphological Aspects of the Deformation and Fracture of Crystalline Polymers. Fracture Processes in Polymeric Solids, Rosen, B., ed.; Interscience Publishers, John Wiley and Sons, New York, p. 551, 1964.

[A26] Glasstone, S.; Laidler, K. J.; Eyring, H.; The Theory of Rate Processes, McGraw-Hill, New York, 1941.

[A27] Prandtl, L.; Ein Gedankenmodell zur kinetischen Theorie des festen Körper; ZAMM, Vol. 8, p. 85, 1928. See also Ludwig Prandtl, Gesammelte Abhandlungen, Erster Teil; Springer, 1961.

[A28] Kauzmann, W.; Flow of Solid Metals from the Standpoint of the Chemical-Rate Theory, AIME Transactions, Vol. 143, p. 57, 1941.

[A29] Sherby, O. D.; Dorn, J. E.; Creep Correlations in Alpha Solid Solutions of Aluminum. Transactions AIME; Journal of Metals, Vol. 4, No. 9, p. 959, 1952.

[A30] Mukherjee, A. K.; Bird, J. E.; Dorn, J. E.; Experimental Correlations for High-Temperature Creep. Transactions of ASM, Vol. 62, p. 155, 1969.

[A31] Li, J. C. M.; Kinetics and Dynamics in Dislocation Plasticity. Dislocation Dynamics; Rosenfield, A. R.; Hahn, G. T.; Bement, A. L.; Jaffee, R. I.; editors. McGraw-Hill, 1968.

[A32] Bueche, F.; Tensile Strength of Plastics above the Glass Temperature. Journal of Applied Physics, Vol. 26, No. 9, p. 1133, 1955.

[A33] Bueche, F.; Tensile Strength of Plastics below the Glass Temperature. ibid., Vol. 28, p. 784, 1957.

[A34] Knauss, W. G.; The Time Dependent Fracture of Viscoelastic Materials. Proceedings of the First International Conference on Fracture, Vol. 2, p. 1139, 1965. See also Ph.D. Thesis, California Institute of Technology, Pasadena, California, 1963.

[A35] Prevorsek, D.; Lyons, W. J.; Fatigue Fracture in Fibrous Polymers as a Brittle, Crack-Nucleation Process. Journal of Applied Physics, Vol. 35, No. 11, p. 3152, 1964.

[A36] Graham, P. H.; Robinson, C. N.; Henderson, C. B.; Analysis of Dilatational Failure of Heterogeneous Materials by Reaction Rate Theory. International Journal of Fracture Mechanics, Vol. 5, No. 1, p. 57, 1969.

[A37] Zhurkov, S. N.; Narzullaev, B. N.; The Time-Dependence of the Strength of Solids. Zhurn. Tekhn. Fiz., Vol. 23, No. 10, English version p. 1677, 1953.

[A38] Zhurkov, S. N.; Savostin, A. Y.; Tomashevskii, E. E.; Electron Paramagnetic Resonance Study of the Polymer Degradation Mechanism. Soviet Phy. Diklady, Vol. 9, English version p. 986, 1965.

[A39] Pake, G. E.; Paramagnetic Resonance. W. A. Benjamin, Inc. New York, 1962.

[A40] Bershohn, M.; Baird, J. C.; An Introduction to Electron Paramagnetic Resonance. W. A. Benjamin, Inc. New York, 1966.

[A41] DeVries, K. L.; Simonson, E. R.; Williams, M. L.; A Micro-macro Correlation of Ozone-induced Fracture in Rubber. Journal of Applied Polymer Science, Vol. 14, p. 3049, 1970.

[A42] Andrews, E. H.; Reed, P. E.; Hydrogen Evolution from Natural Rubber during Tensile Tests. Polymer Letters, Vol. 5, p. 317, 1967.

[A43] Zhurkov, S. N.; Kuksenko, V. S.; Slutsker, A. I.; Submicrocrack Formation under Stress, Paper 46 in Fracture 1969. Proceedings of the Second International Conference on Fracture, Brighton, 1969. Pratt, P. L., ed.; Chapman and Hall, London, p. 531, 1969.

[A44] Barenblatt, G. I.; Entov, V. M.; Salganik, R. L.; Kinetics of Crack Propagation, General Considerations: Cracks Approaching Equilibrium Cracks; Mechanics of Solids (Mekhanika Tverdodo Tela) Vol. 1, No. 5, English version p. 82, 1966.

[A45] Barenblatt, G. I.; Entov, V. M.; Salganik, R. L.; Kinetics of Crack Propagation: Conditions of Fracture and Long-term Strength. ibid., Vol. 1, No. 6, English version p. 76, 1966.

[A46] Barenblatt, G. I.; Entov, V. M.; Salganik, R. L.; Kinetics of Crack Propagation: A Note on the Rule of Summation of Damageabilities. ibid., Vol. 2, No. 2, English version p. 148, 1967.

[A47] Barenblatt, G. I.; Entov, V. M.; Salganik, R. L.; Kinetics of Crack Propagation: Fluctuation Fracture. ibid., Vol. 2, No. 1, English version p. 122, 1967.

[A48] Barenblatt, G. I.; Entov, V. M.; Salganik, R. L.; Some Problems of the Kinetics of Crack Propagation in Inelastic Behavior of Solids, Materials Science and Engineering Series. Kanninen, M. F.; Adler, W. F.; Rosenfield, A. R.; Jaffee, R. I.; editors.

[A49] Barenblatt, G. I.; Entov, V. M.; Salganik, R. L.; On the Influence of Vibrational Heating on the Fracture Propagation in Polymeric Materials. Proceedings of the IUTAM Symposium in East Kilbride, June 25-28, 1968.

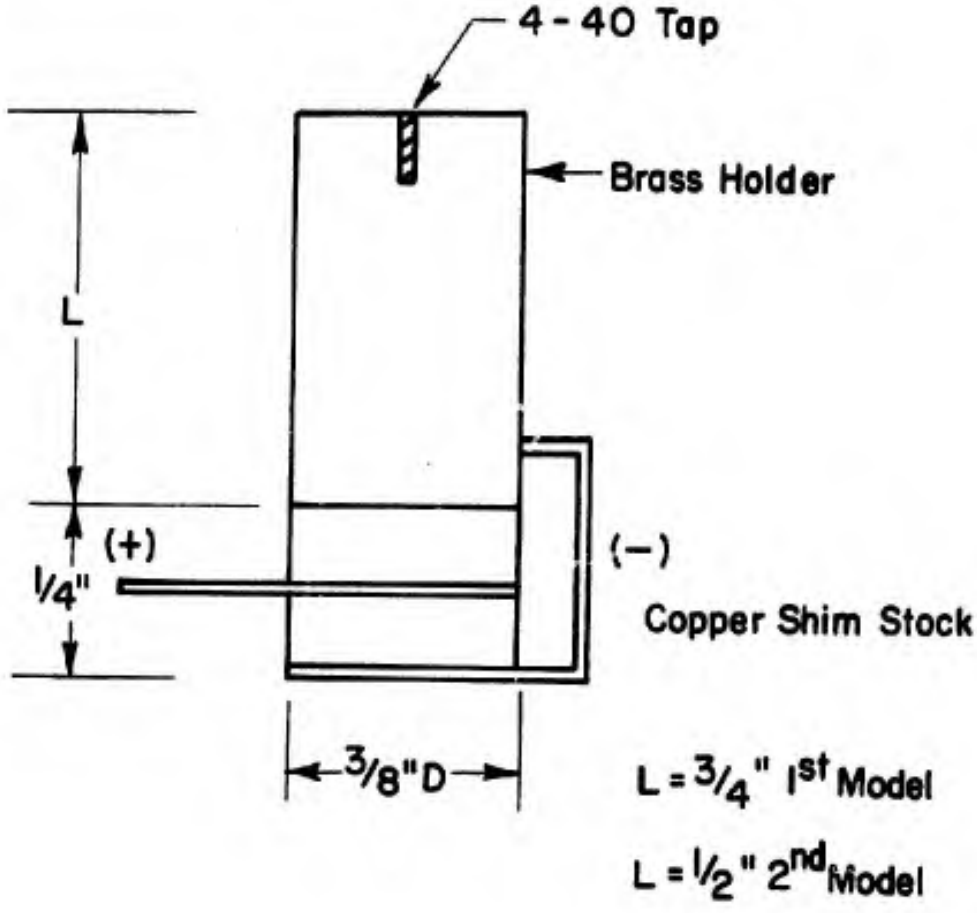

FIG.1 CONFIGURATION OF DRIVER AND RECEIVER

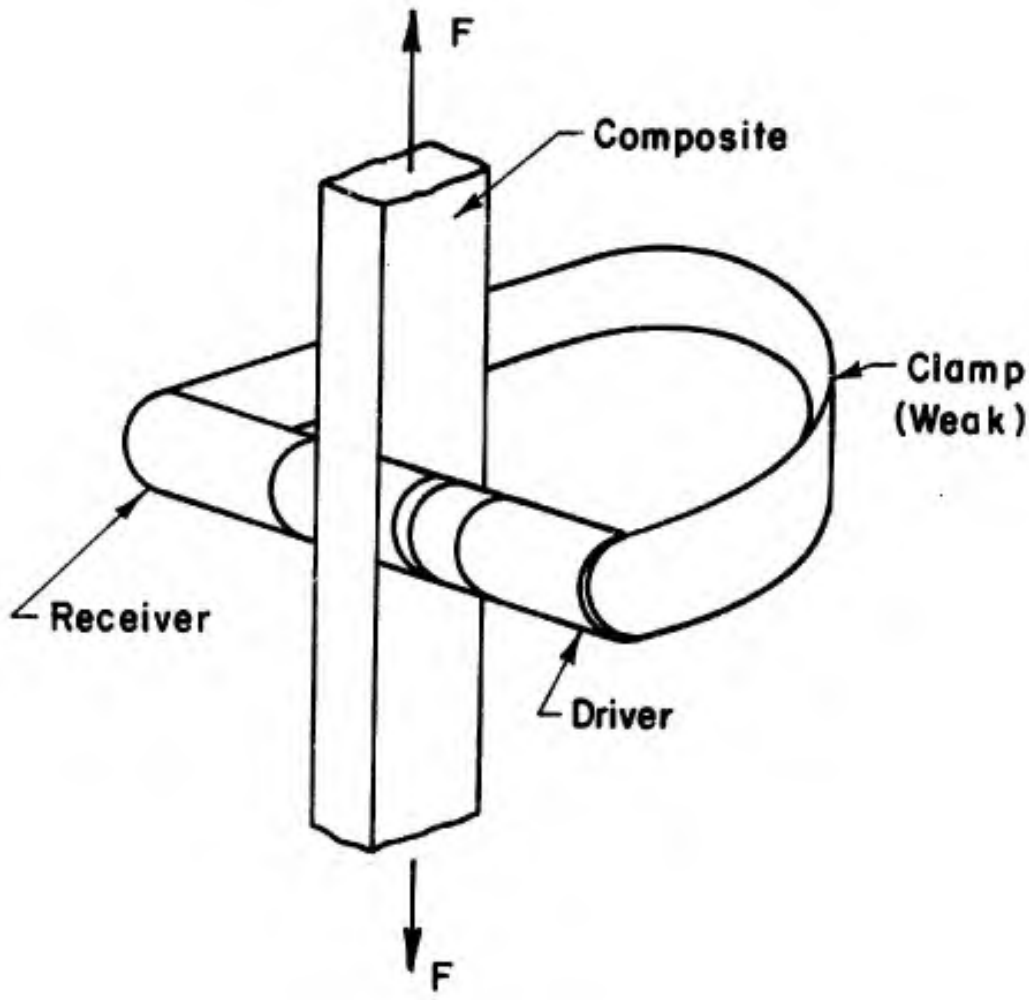

FIG. 2 DRIVER-RECEIVER ASSEMBLY MOUNTED ON PROPELLANT SPECIMEN

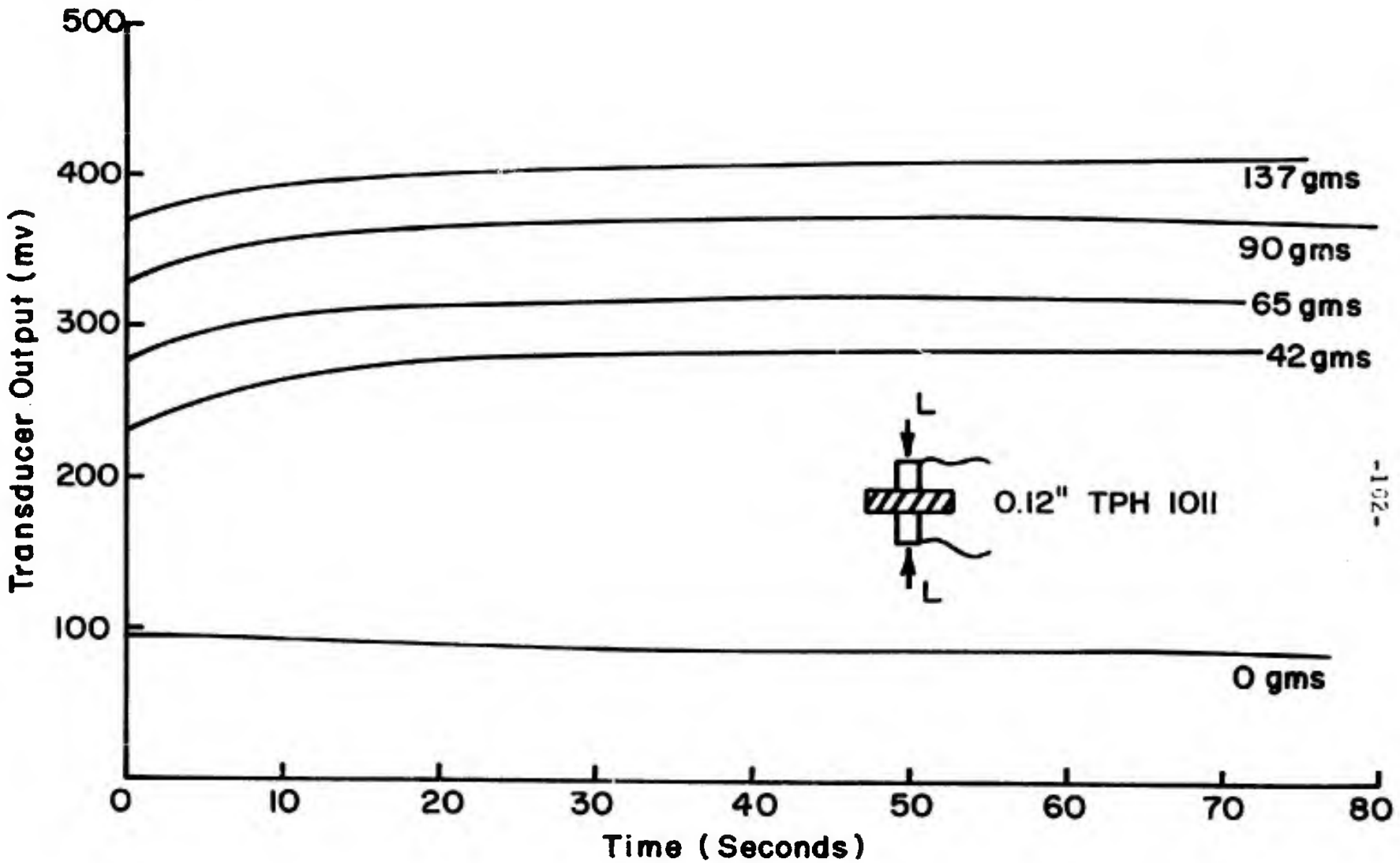

FIG. 3 REPRESENTATIVE TRANSDUCER OUTPUT FOR VARIOUS COMPRESSIVE LOADS L (16000 cps)

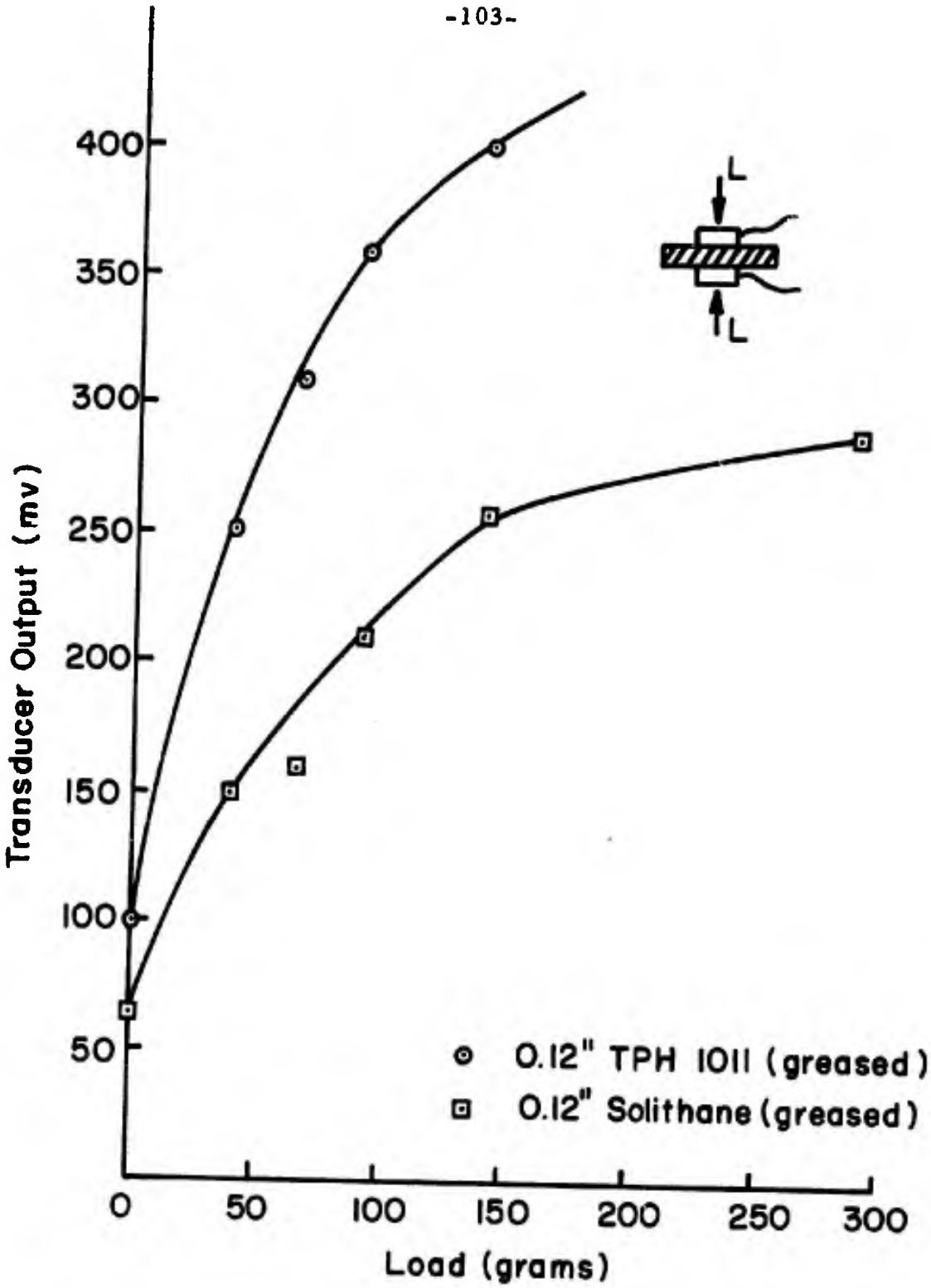

FIG. 4 TRANSDUCER OUTPUT VS. NORMAL LOAD NEARLY CONSTANT WITH TIME (16000cps)

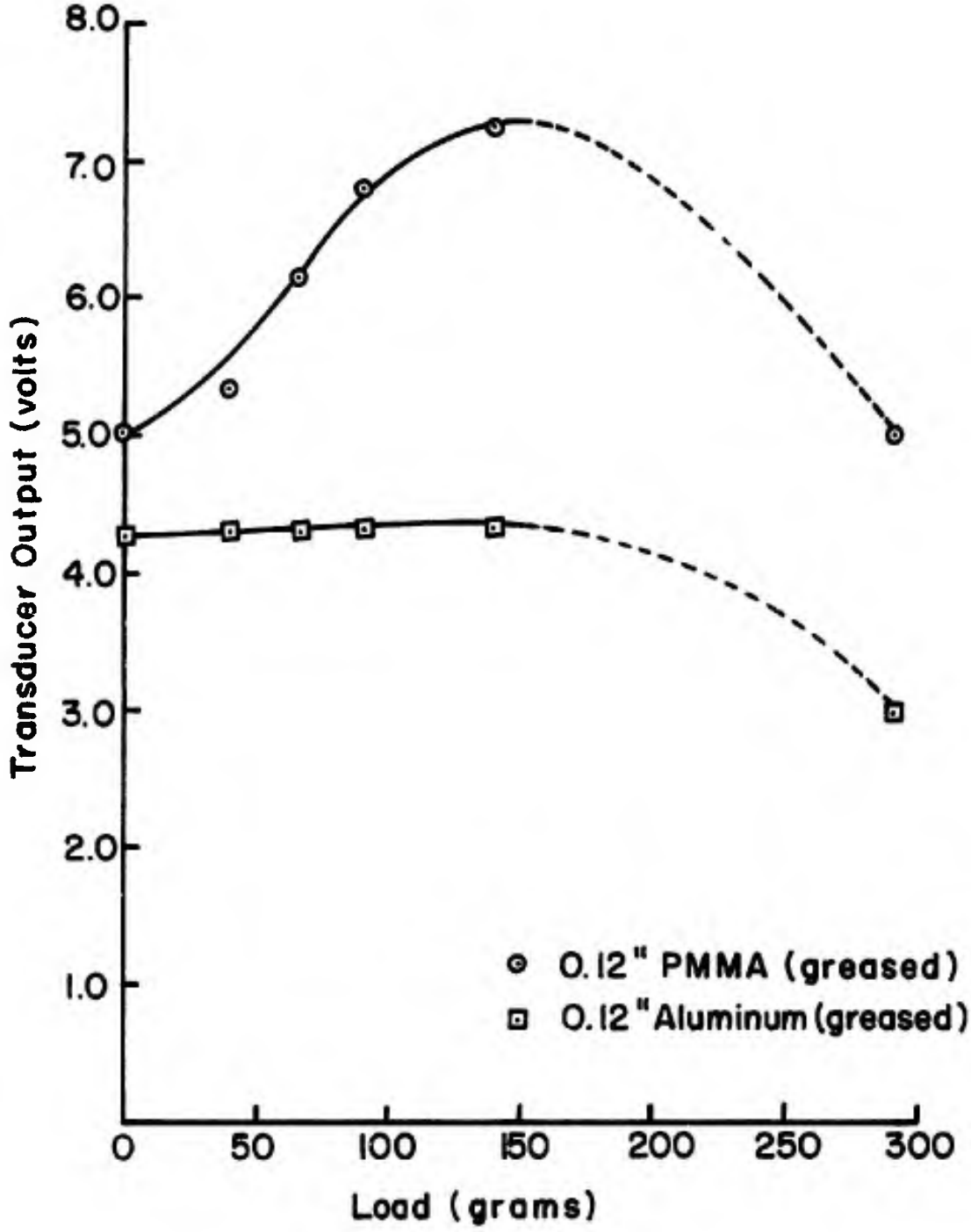

FIG. 5 TRANSDUCER OUTPUT VS. NORMAL LOAD NEARLY CONSTANT WITH TIME (16000 cps)

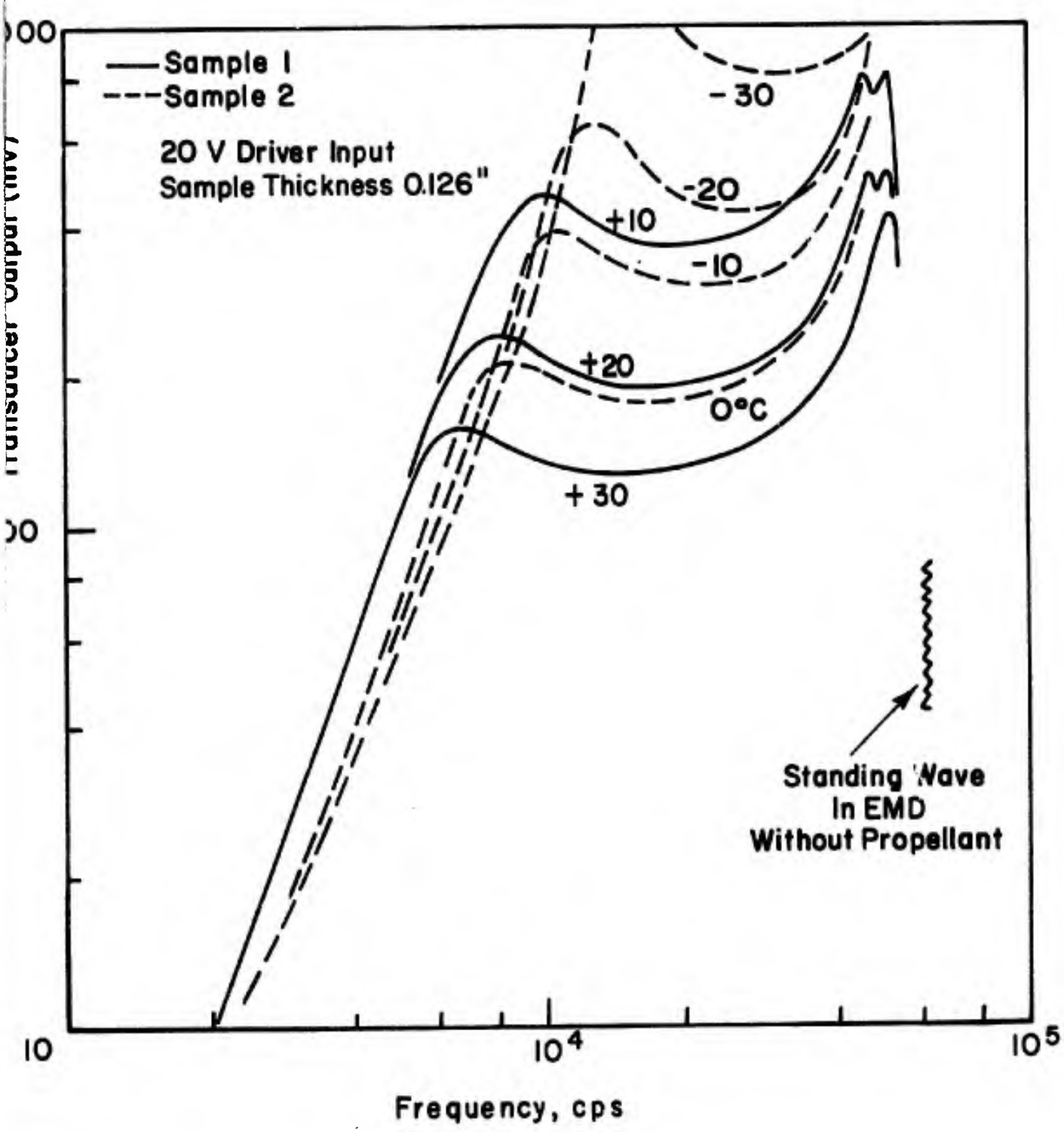

FIG. 6 FREQUENCY RESPONSE OF EMD AT DIFFERENT TEMPERATURES

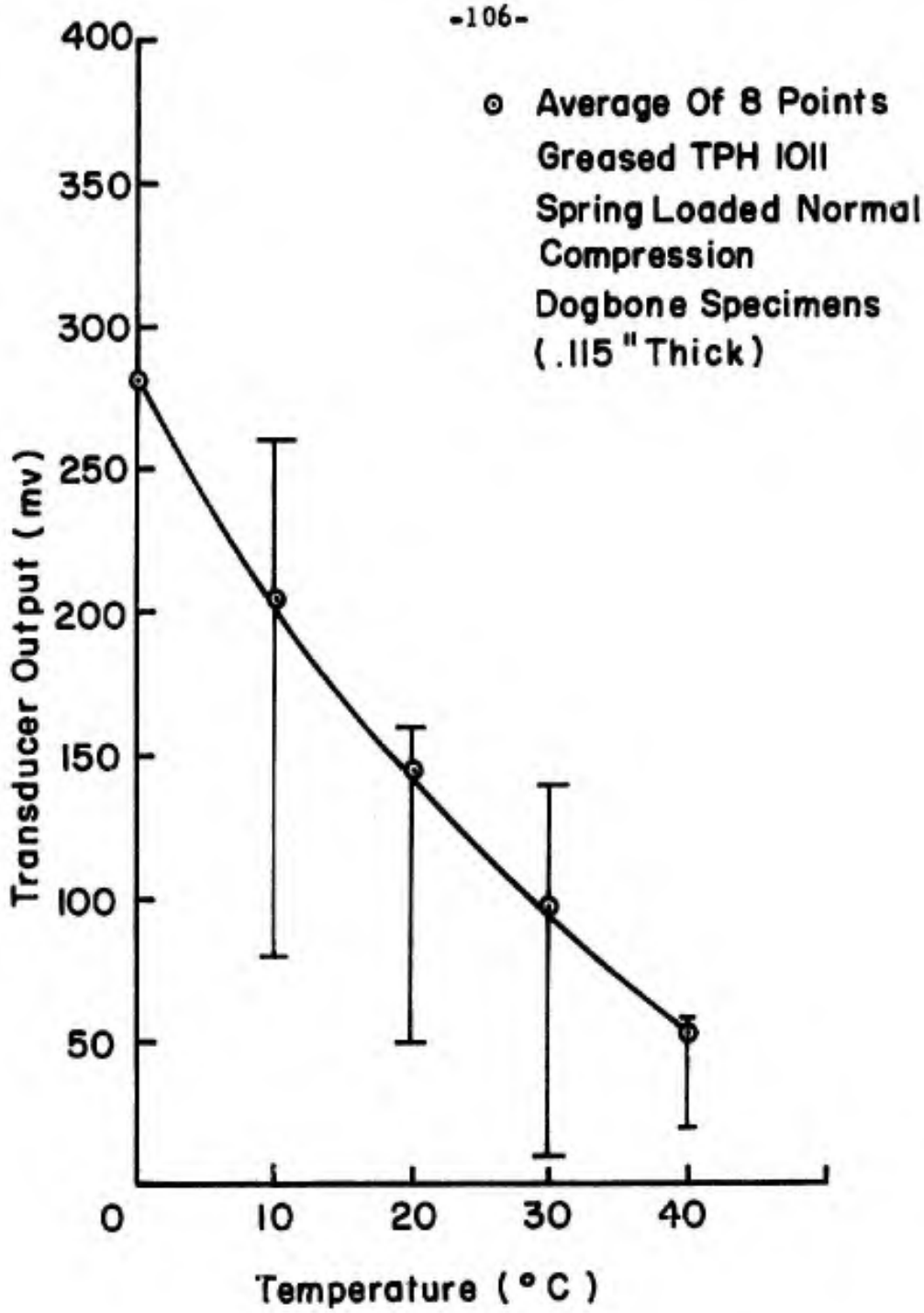

FIG. 7 TRANSDUCER OUTPUT VS. TEMPERATURE

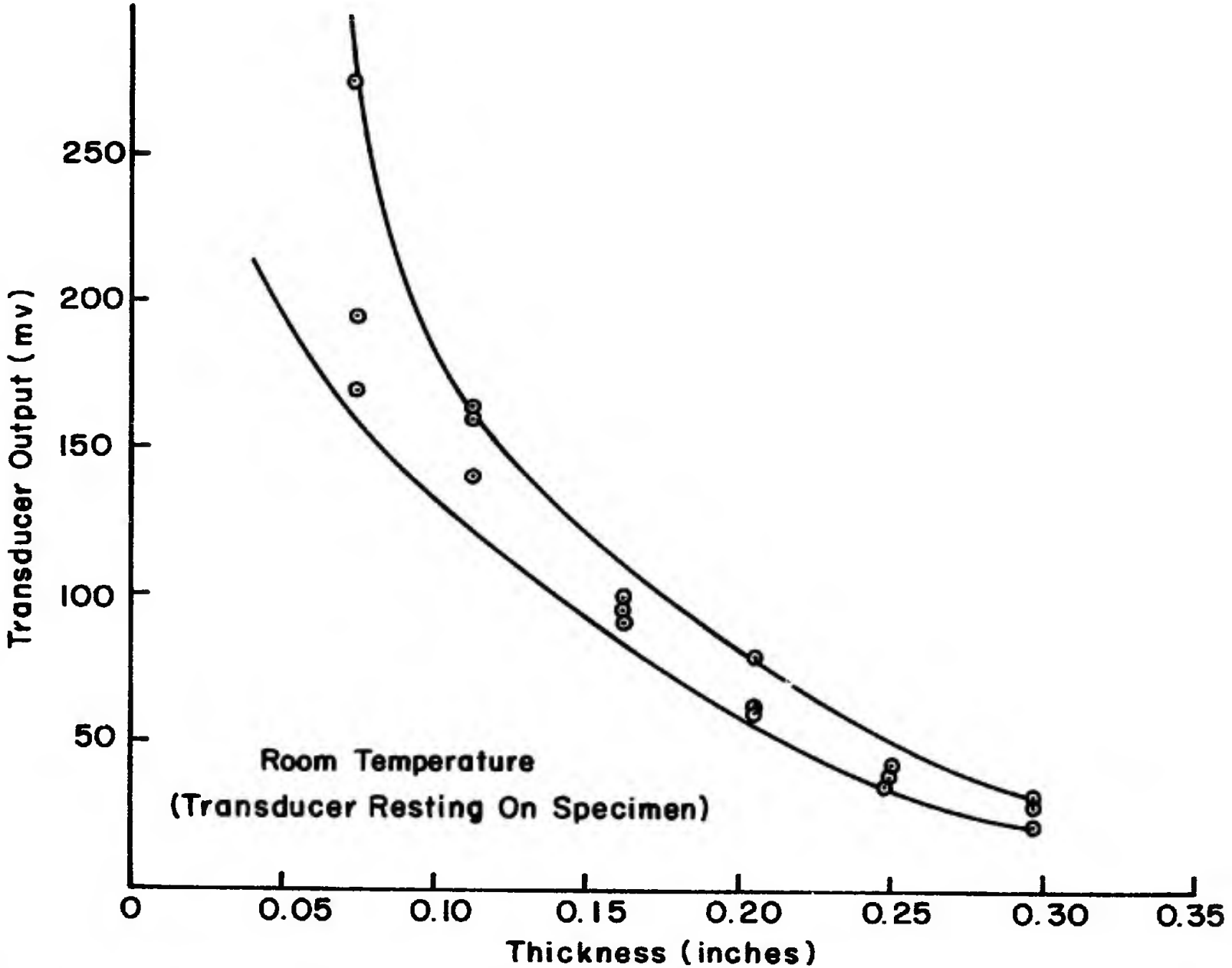

FIG. 8 VARIATION OF TRANSDUCER OUTPUT VS. SPECIMEN (TPH 1011) THICKNESS

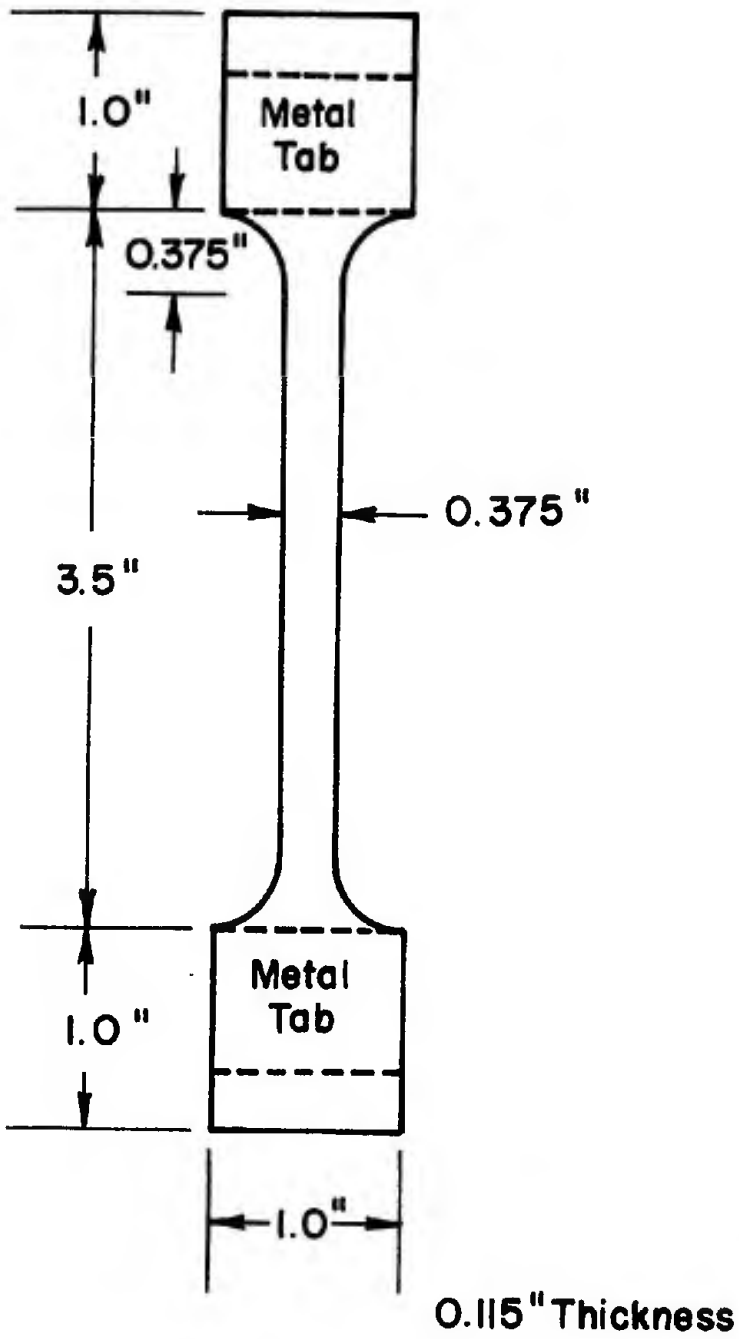

FIG.9 SPECIMEN CONFIGURATION

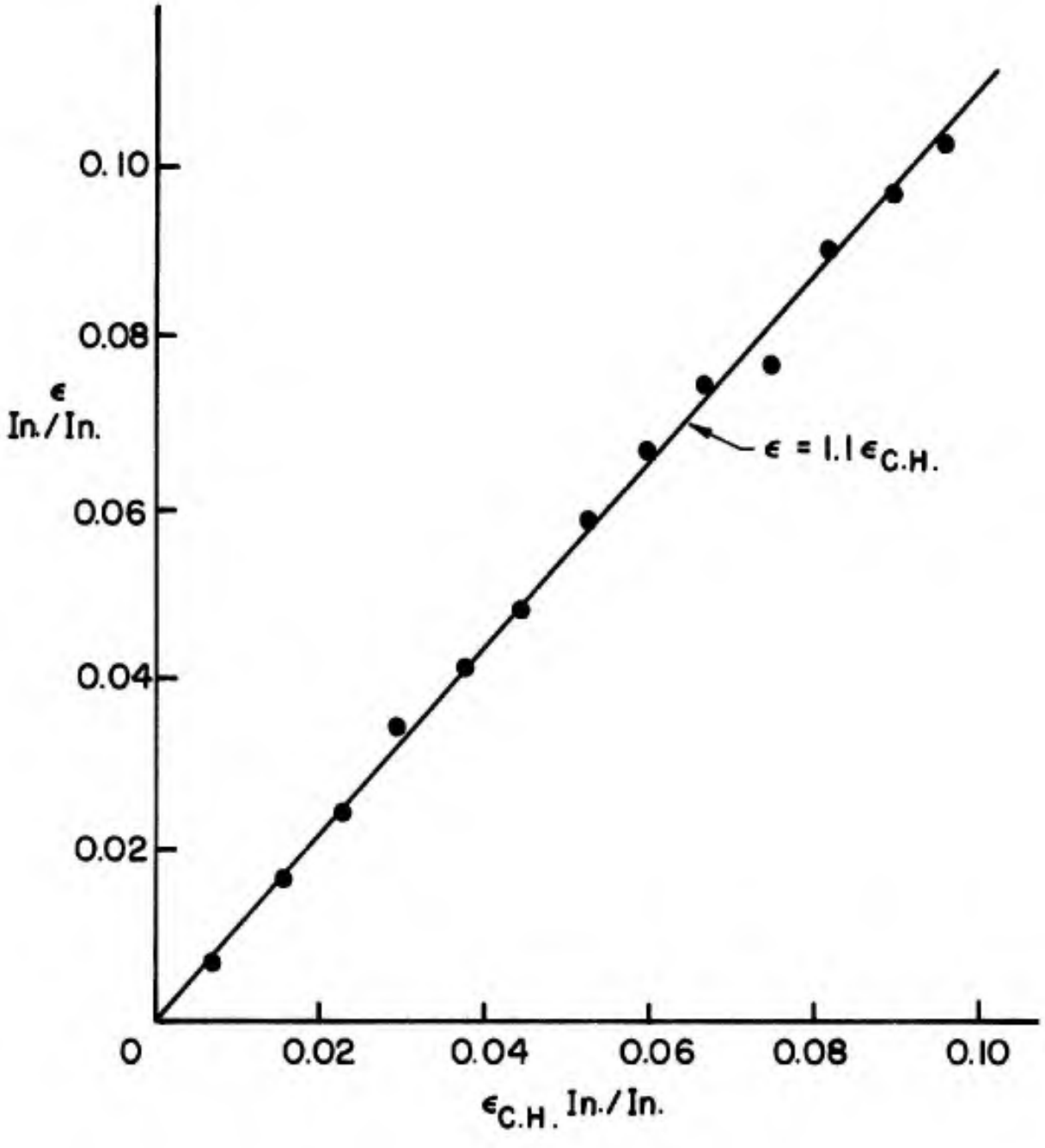

FIG. 10 TRUE STRAIN VS CROSS HEAD STRAIN

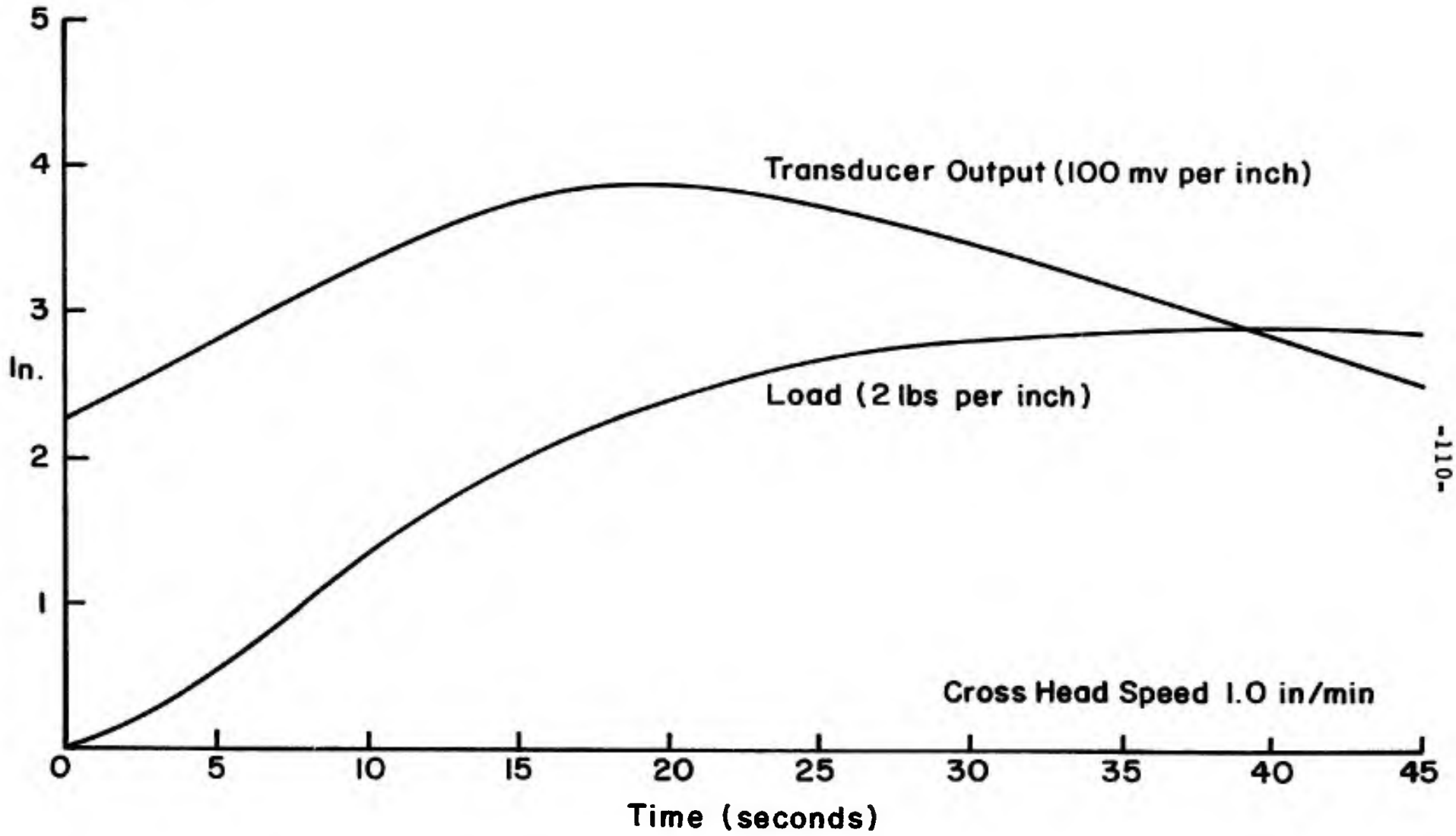

FIG. 11 REPRESENTATIVE DATA SAMPLE AT + 10 °C, TPH 1011

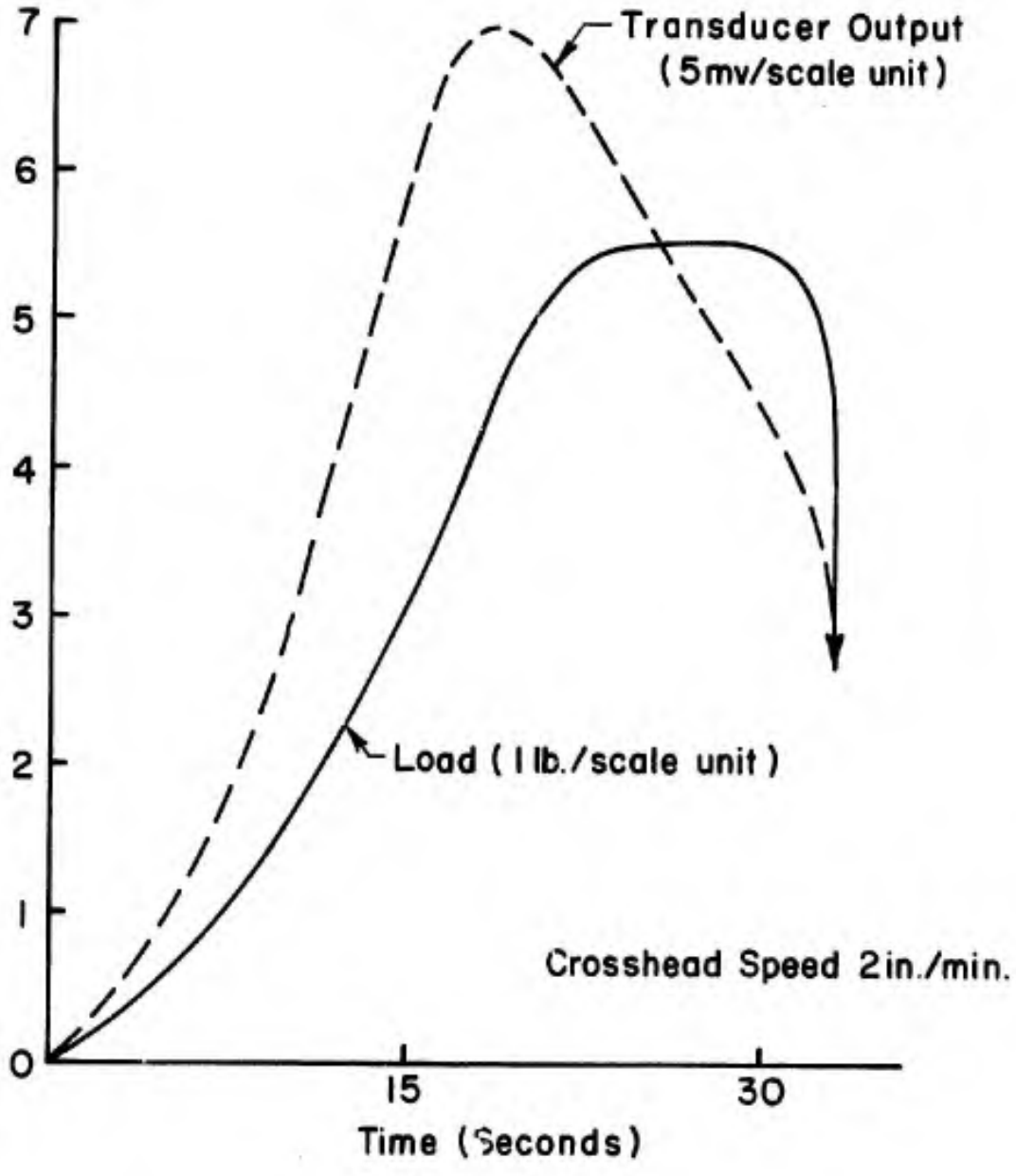

FIG.12 REPRESENTATIVE DATA SAMPLE OF TPH 1011 PROPELLANT, 25 °C, CONSTANT RATE OF EXTENSION TO FAILURE

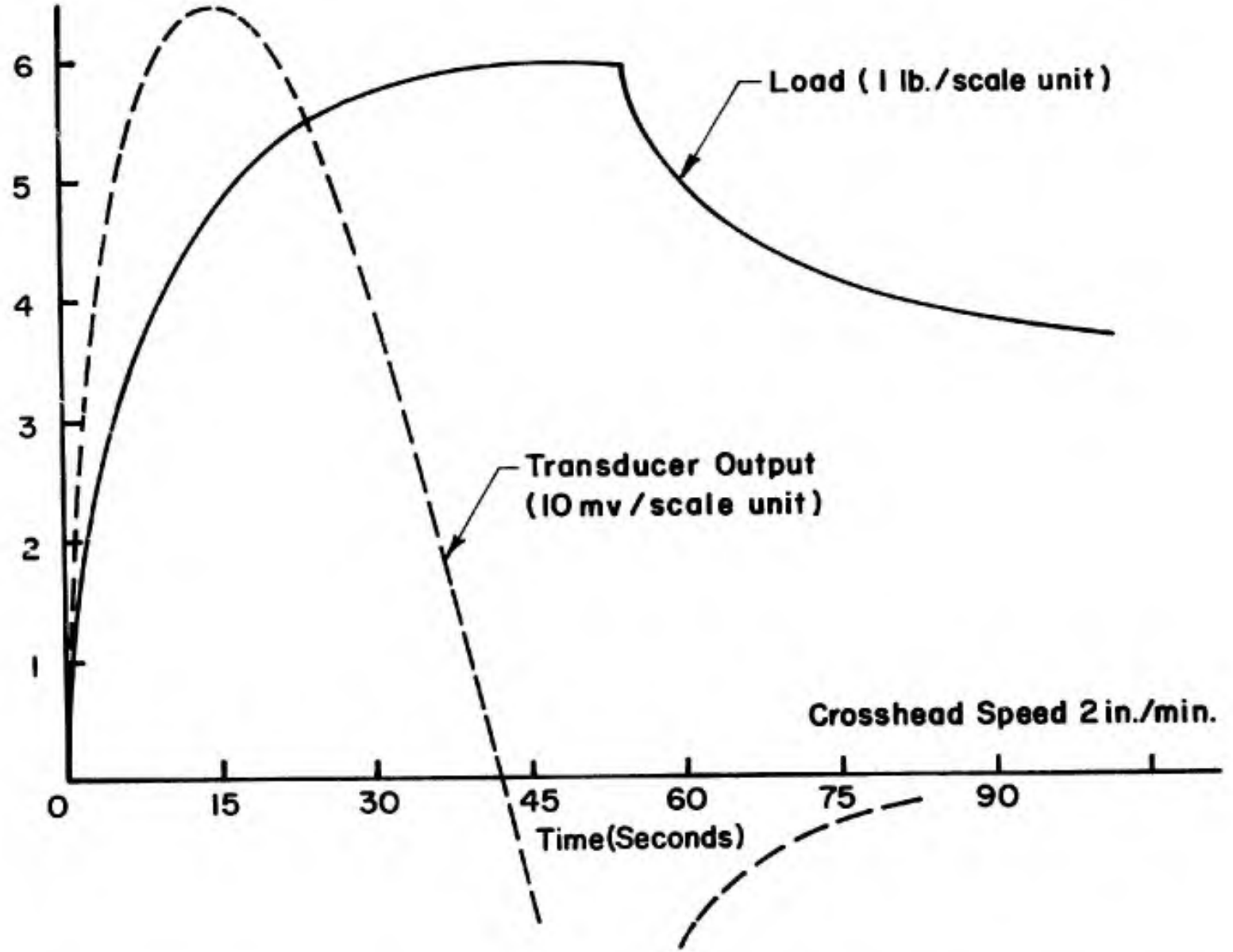

FIG. 13 REPRESENTATIVE DATA SAMPLE OF JPL 500 SERIES PROPELLANT, 25°C, CONSTANT RATE OF EXTENSION FOR ABOUT 55 SECONDS, STRAIN CONSTANT THEREAFTER

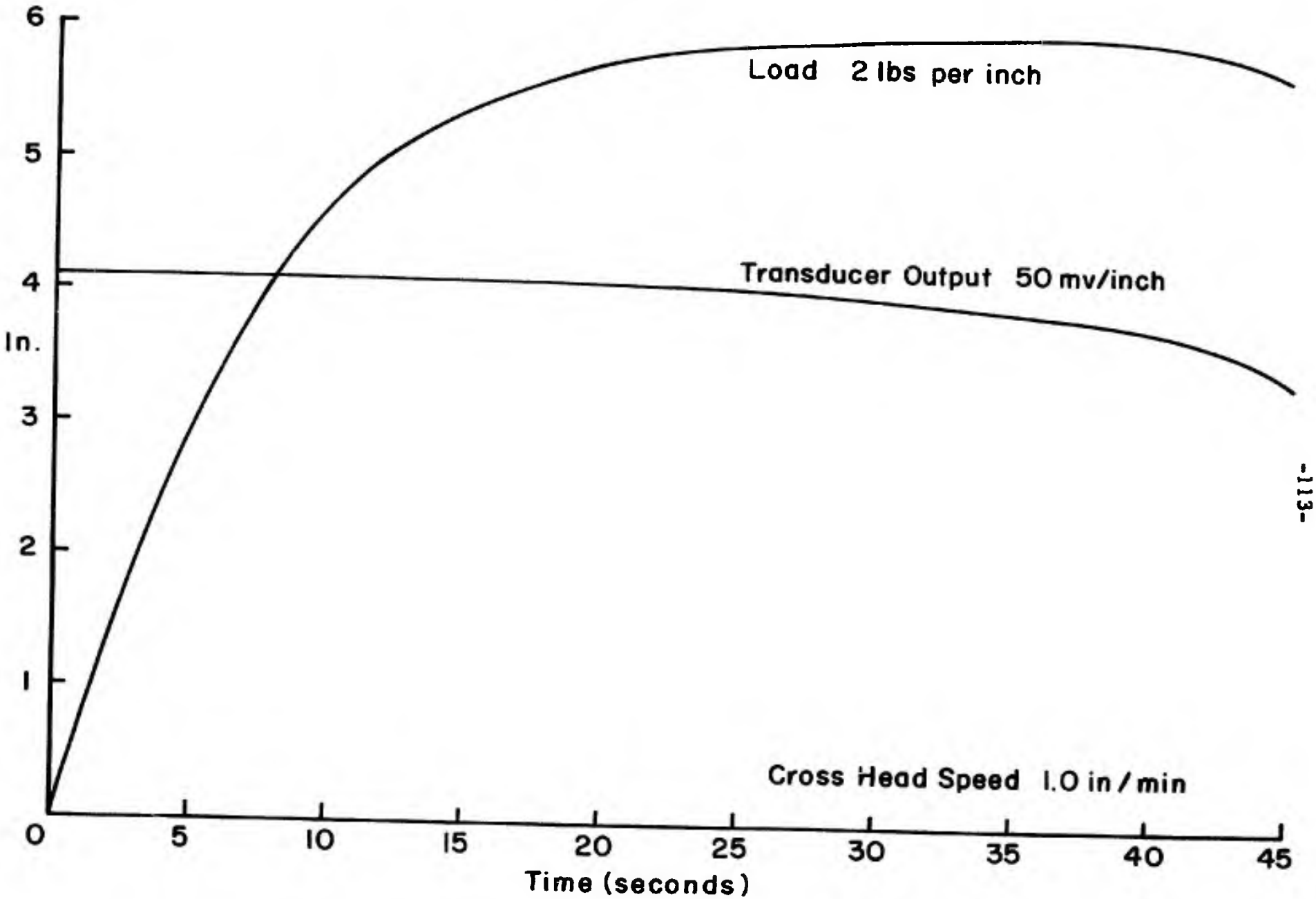

FIG.14 REPRESENTATIVE DATA SAMPLE AT - 20 ° C

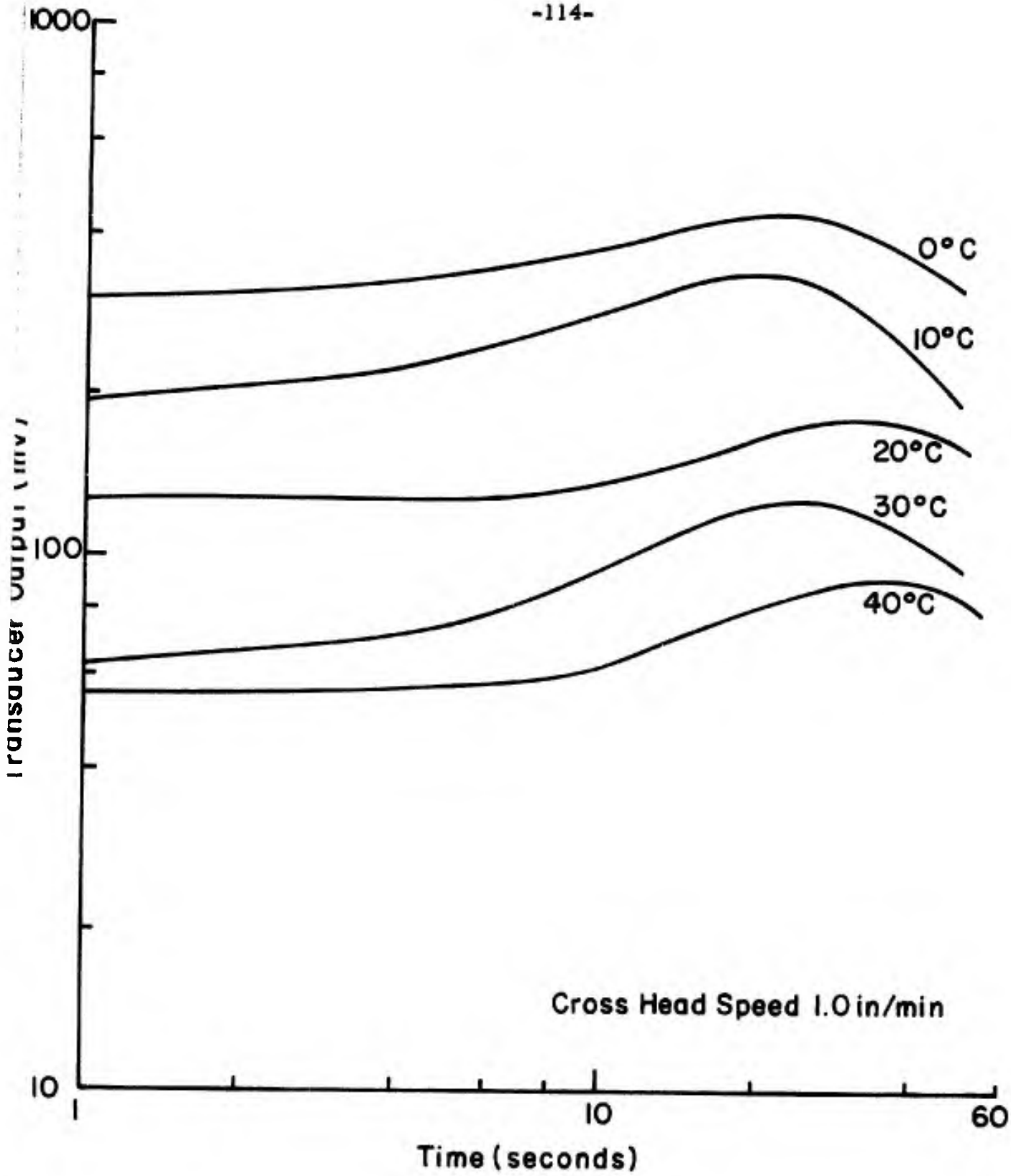

FIG. 15 TRANSDUCER OUTPUT VS TIME

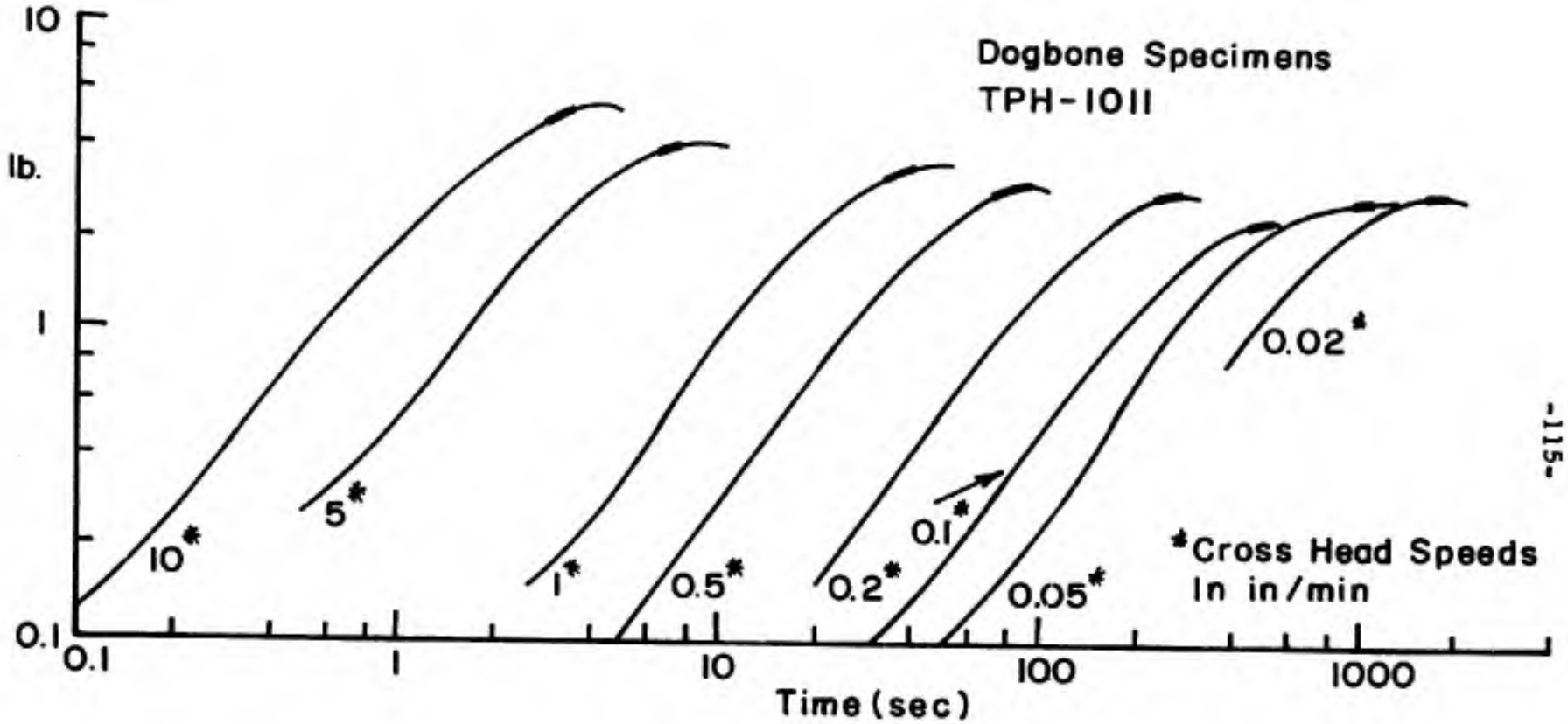

FIG.16 LOAD VS TIME AT 40° C

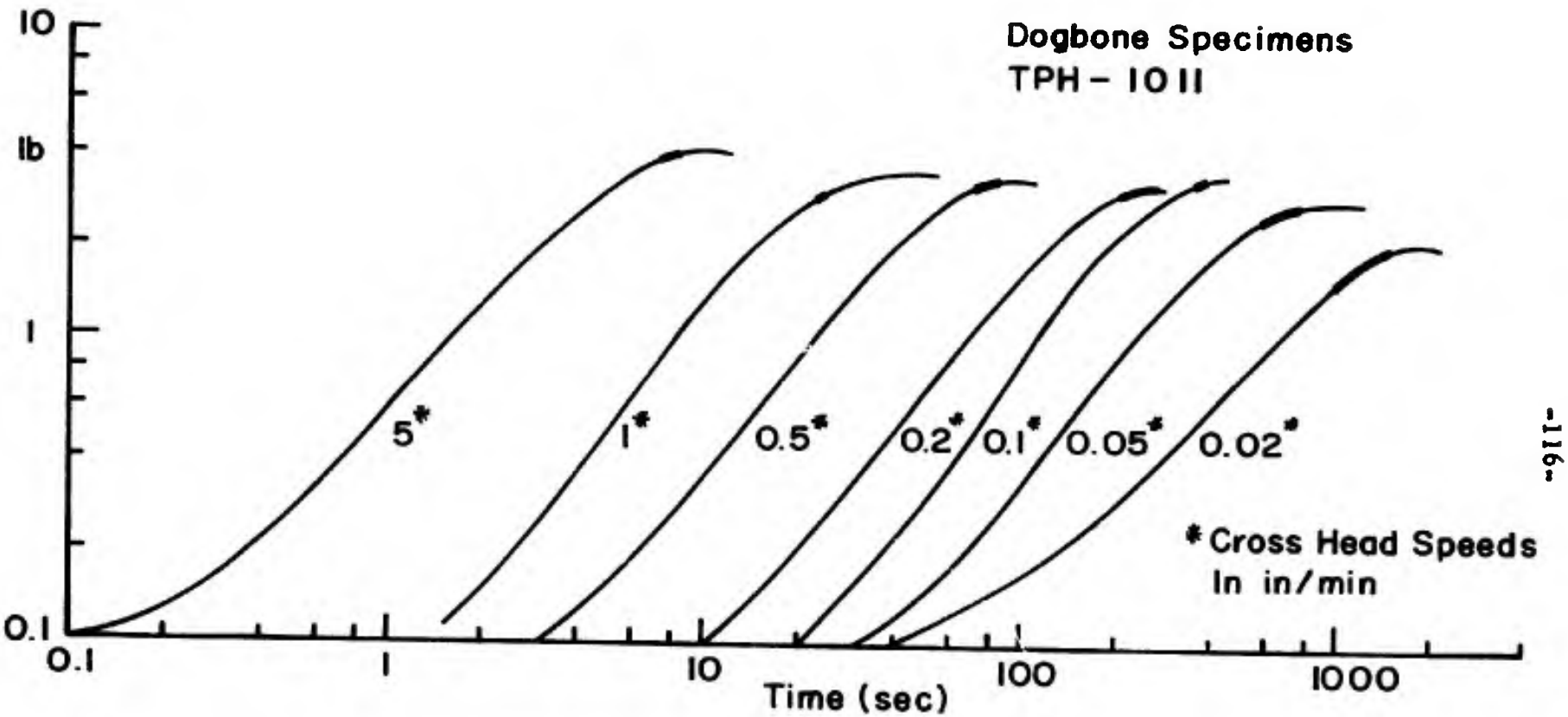

FIG. 17 LOAD VS TIME AT 30° C

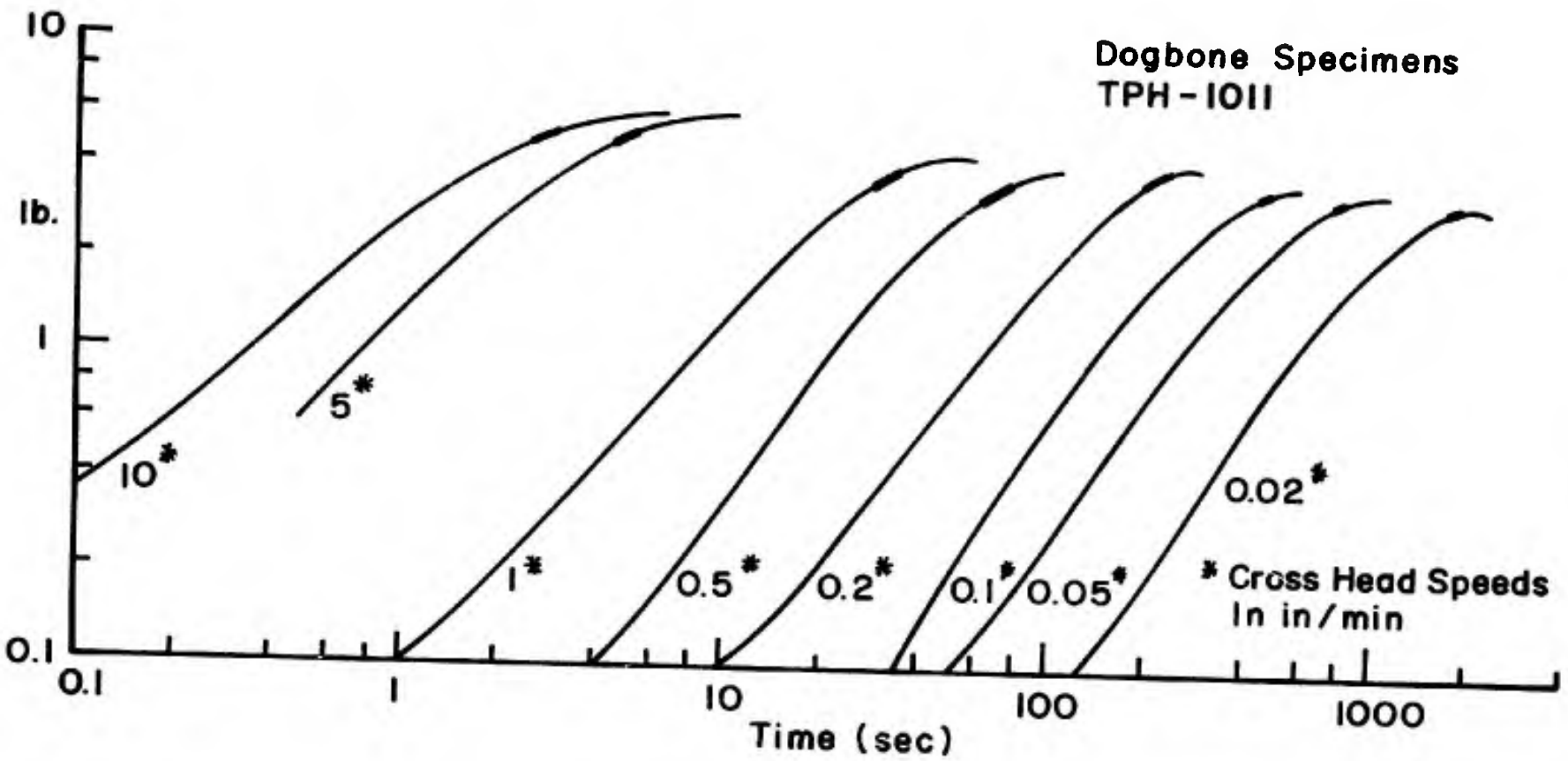

FIG. 18 LOAD VS TIME AT 20° C

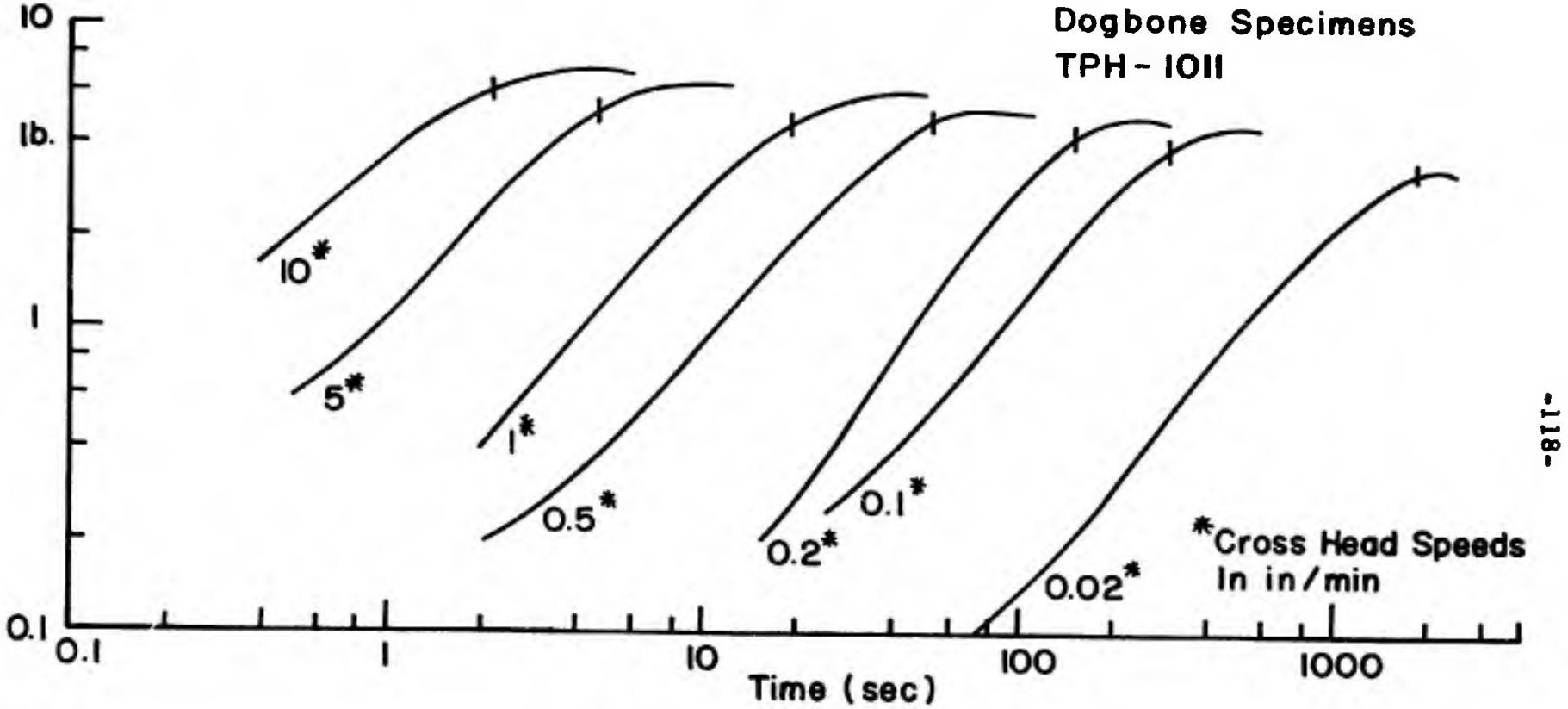

FIG. 19 LOAD VS TIME AT 10°C

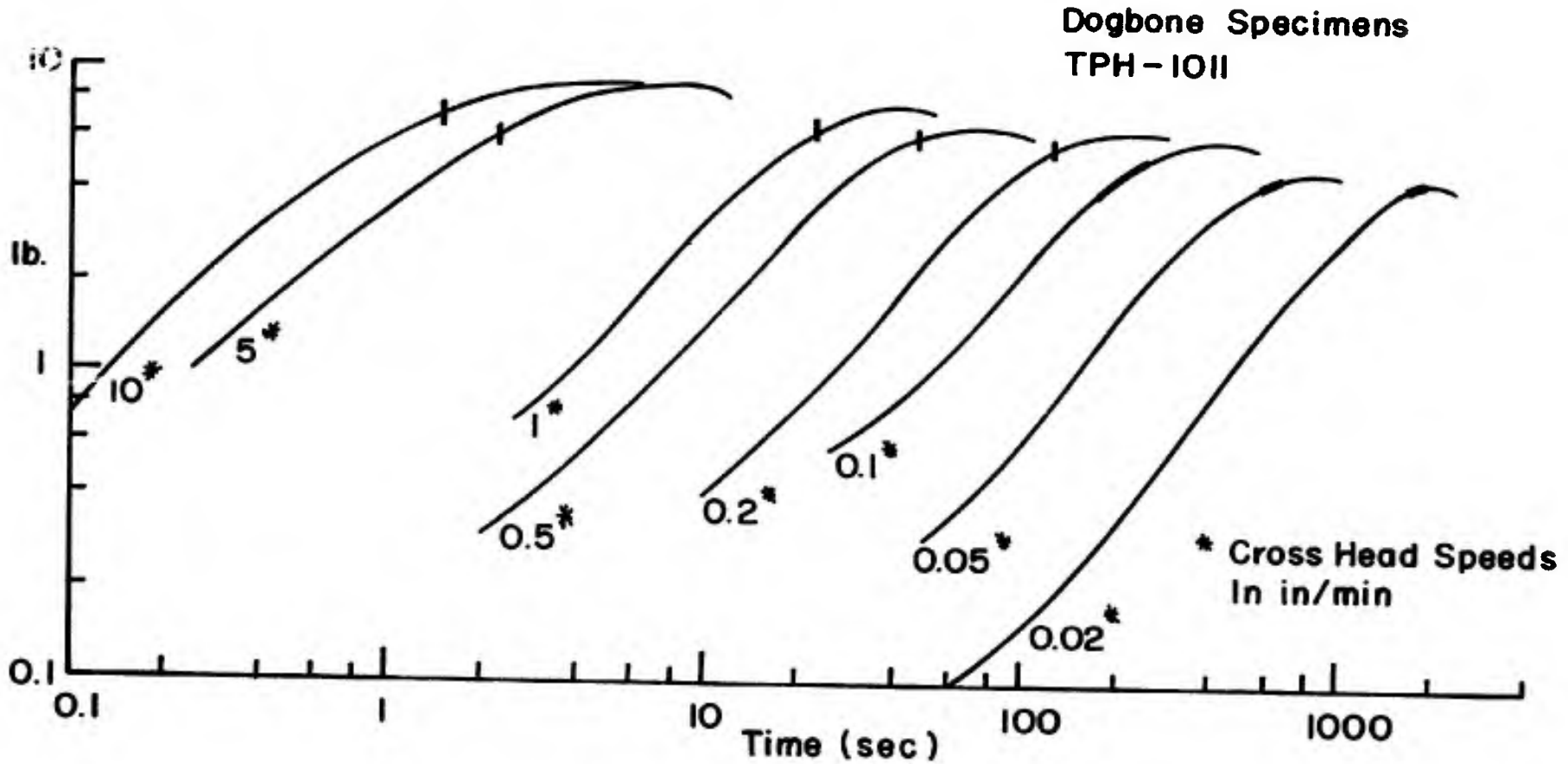

FIG. 20 LOAD VS TIME AT 0° C

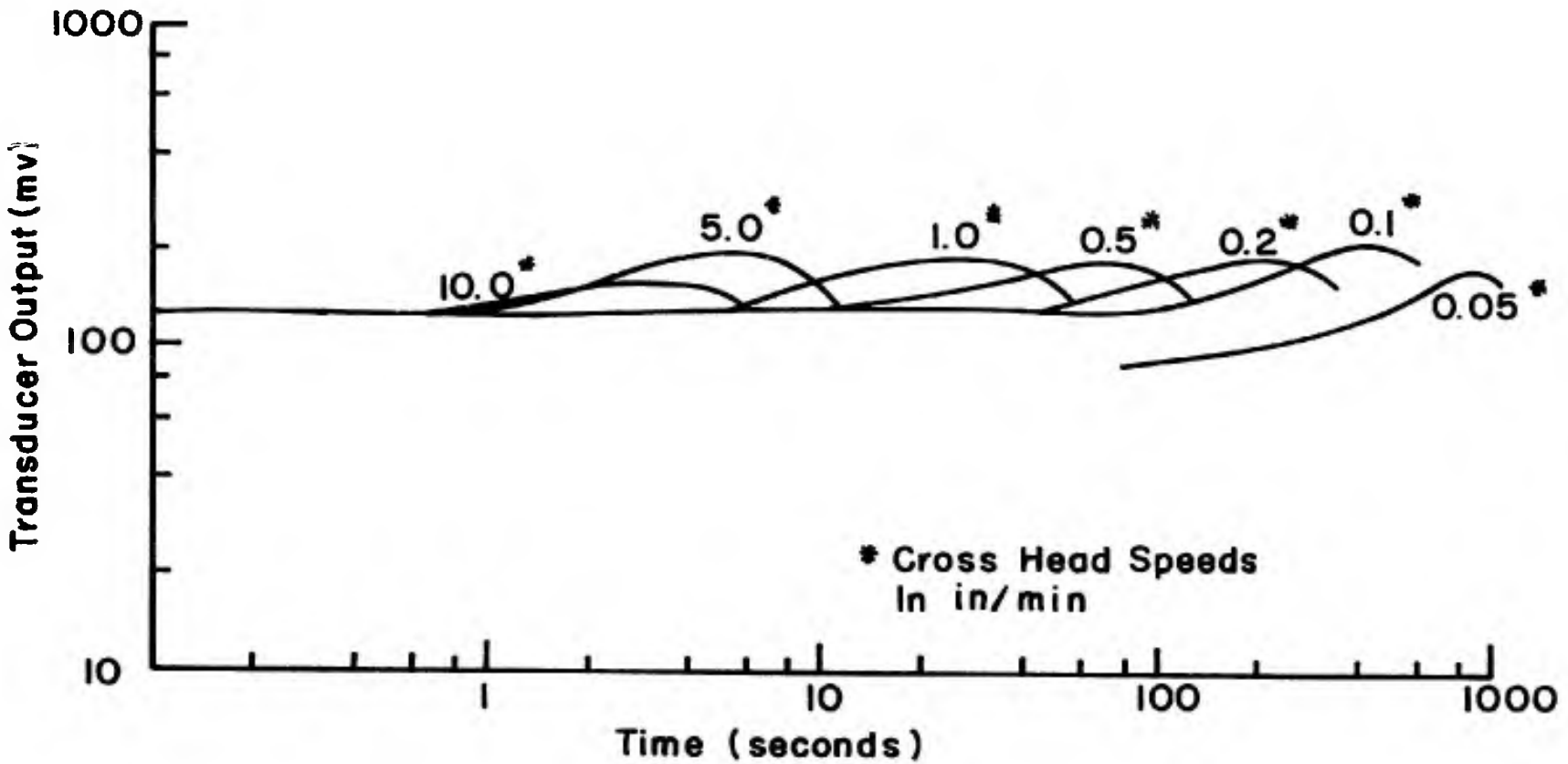

FIG. 21 TRANSDUCER OUTPUT VS TIME AT 20° C

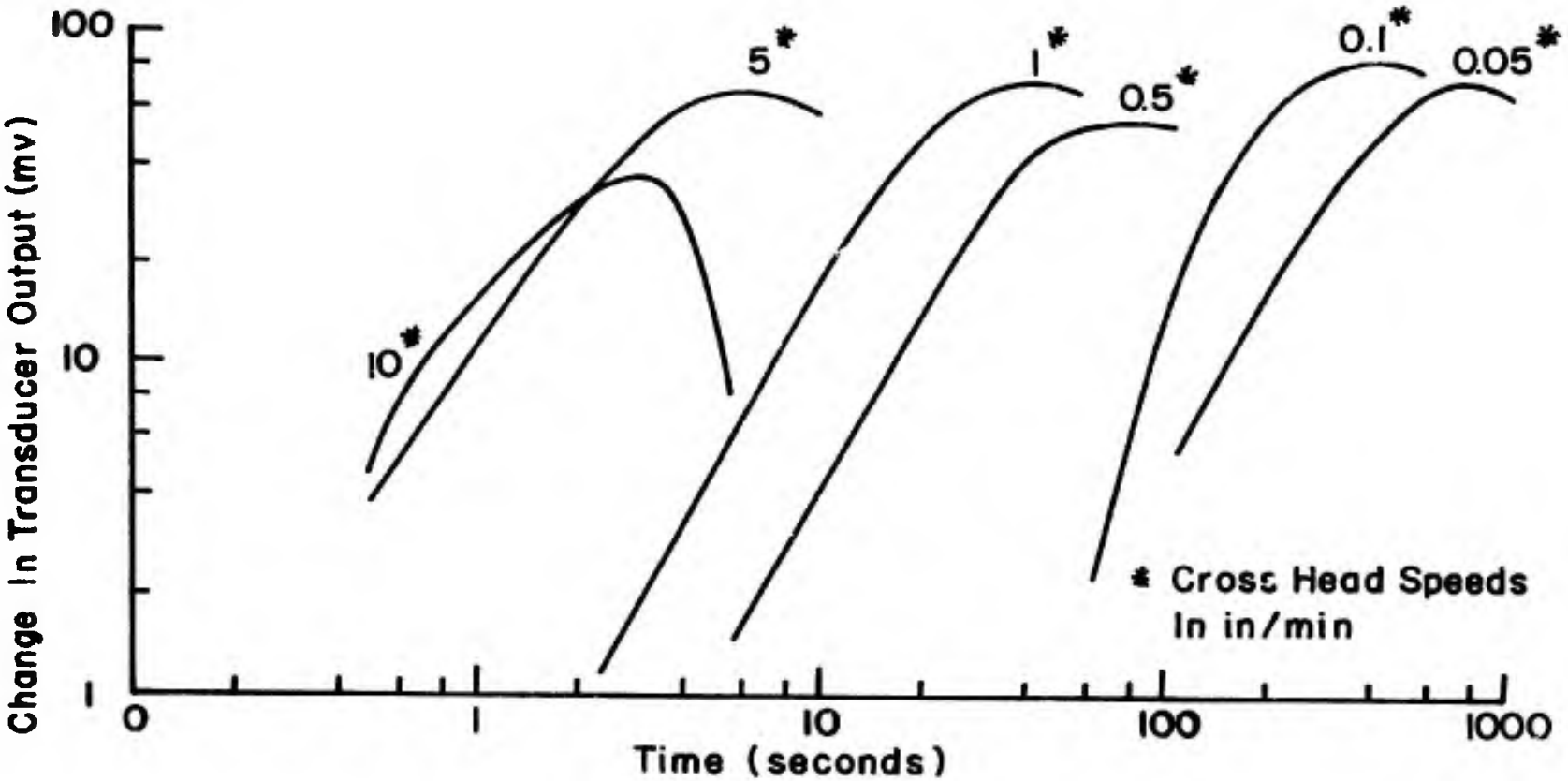

FIG.22 CHANGE IN TRANSDUCER OUTPUT VS TIME AT 20°C

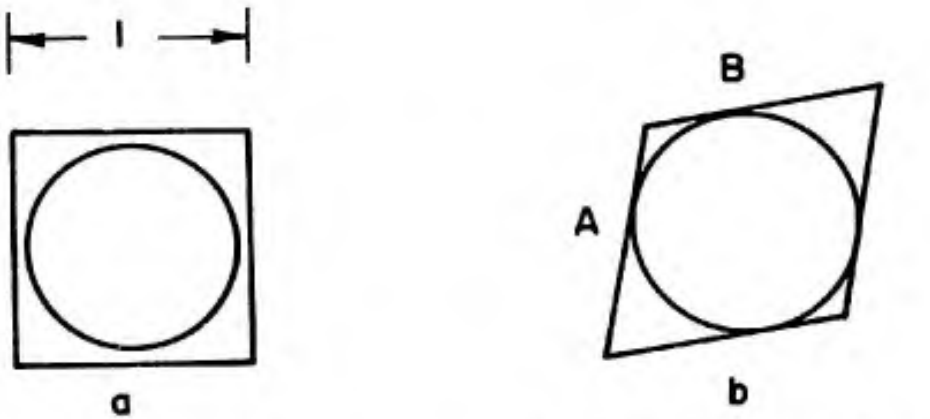

FIG. 23 UNIT CELL DEFORMATION LEADING TO LARGE STRAINS AT POINTS A AND B

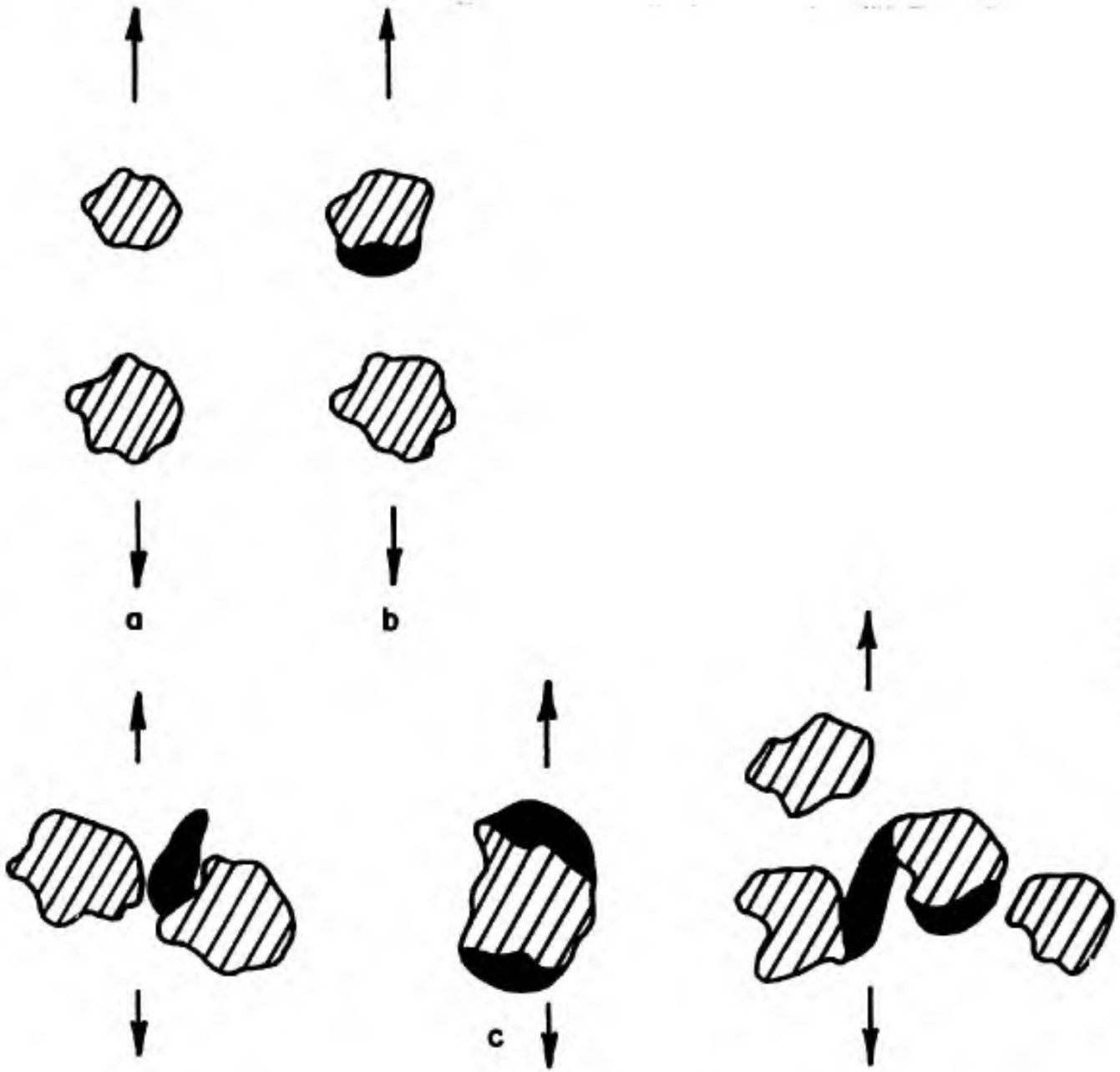

FIG. 24 EXAMPLES OF INTERPARTICULATE FRACTURES

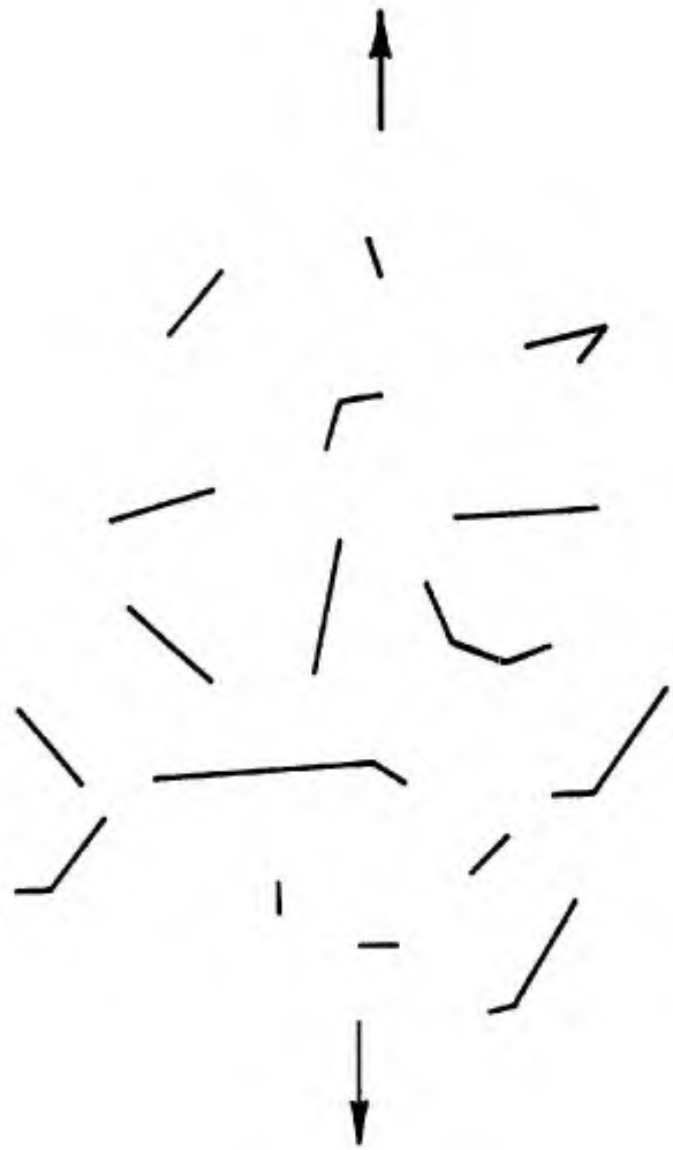

FIG. 25 FRACTURES IN PROPELLANT SAMPLE, 2-D ANALOG

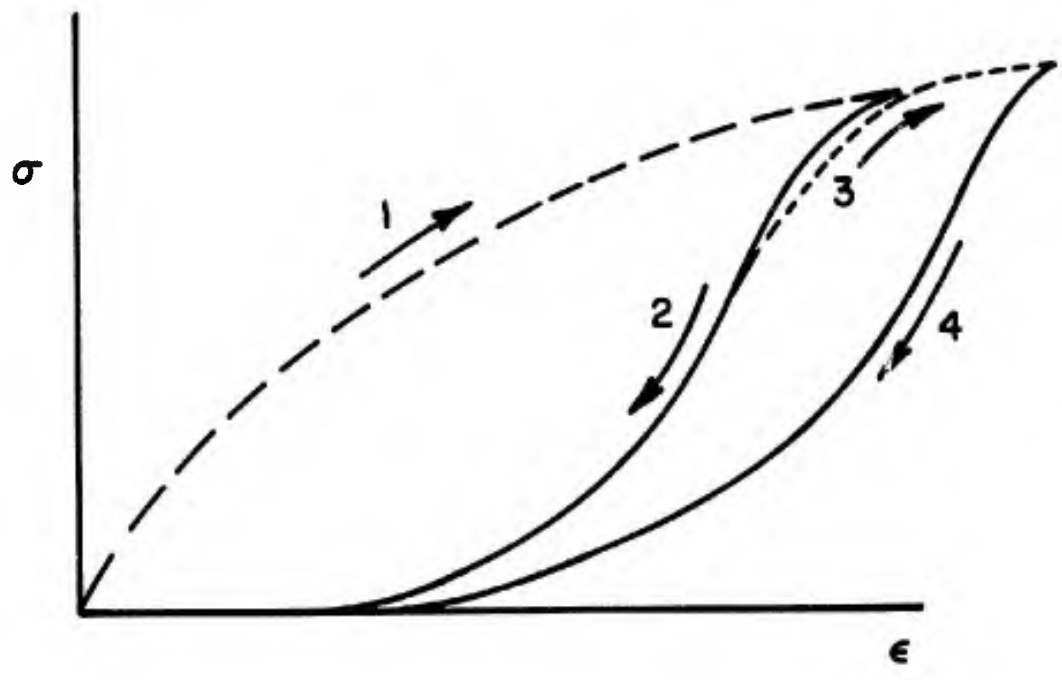

FIG. 26 UNIAXIAL LOADING AND UNLOADING STRESS STRAIN CURVES (NO TIME EFFECT)

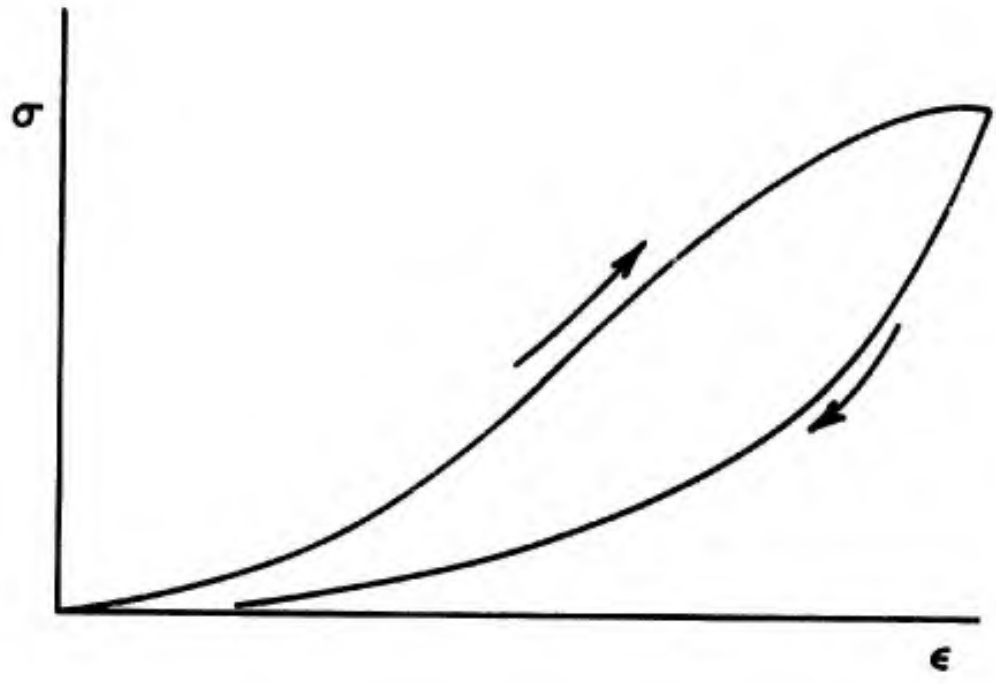

FIG. 27 LOADING AND UNLOADING OF A VISCOELASTIC BINDER

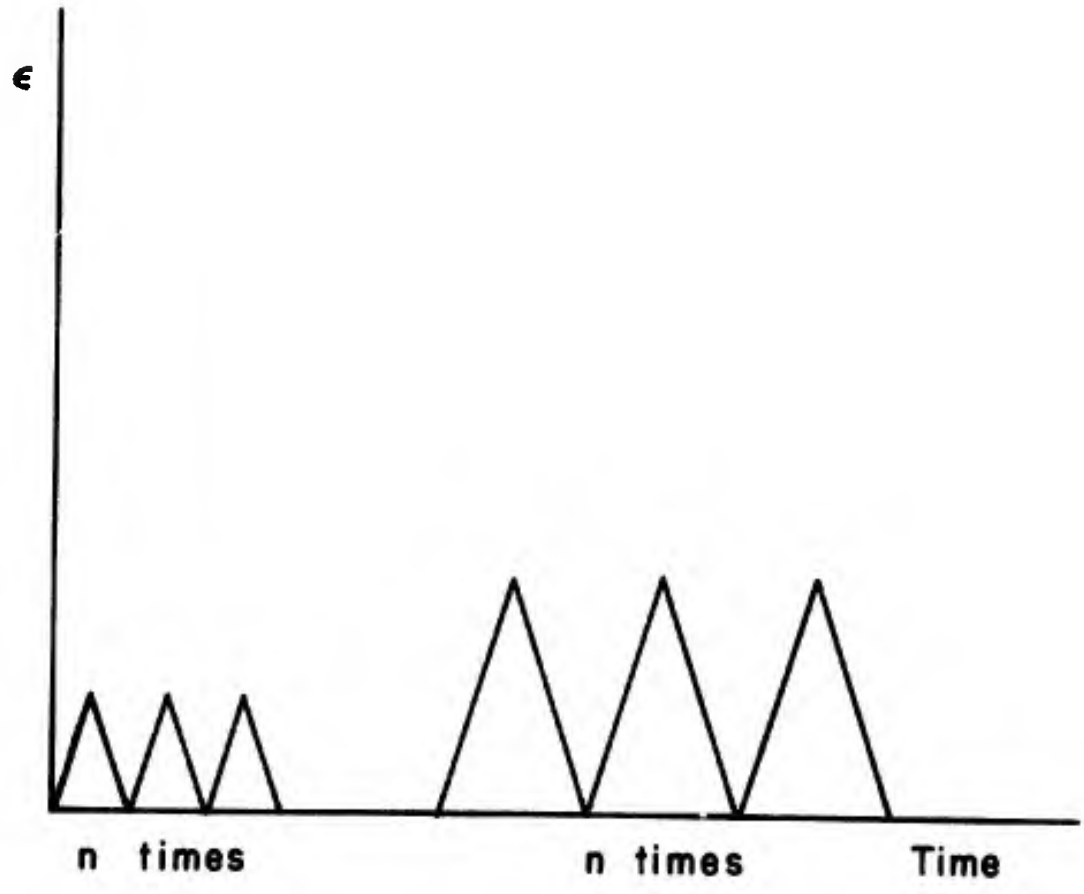

FIG. 28 CHARACTERIZATION OF CYCLIC STRAIN HISTORIES

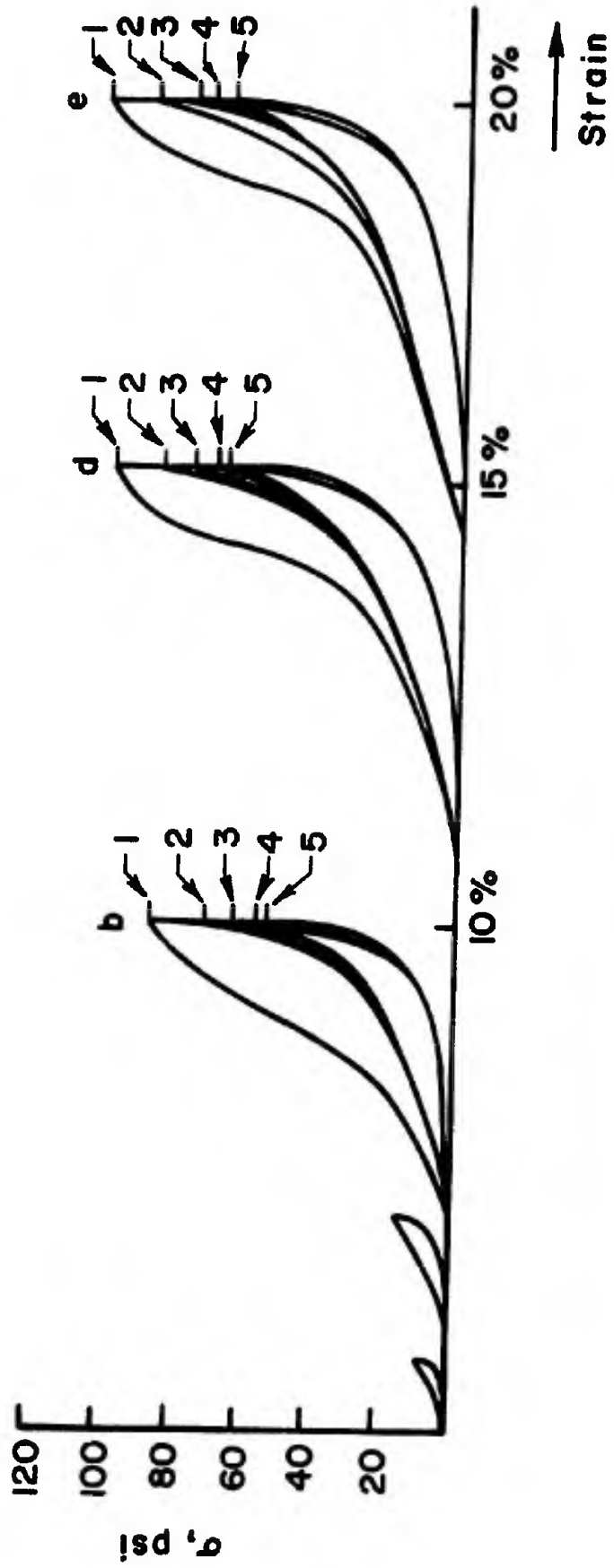

FIG. 29 EXCERPTS OF A CYCLE SEQUENCE

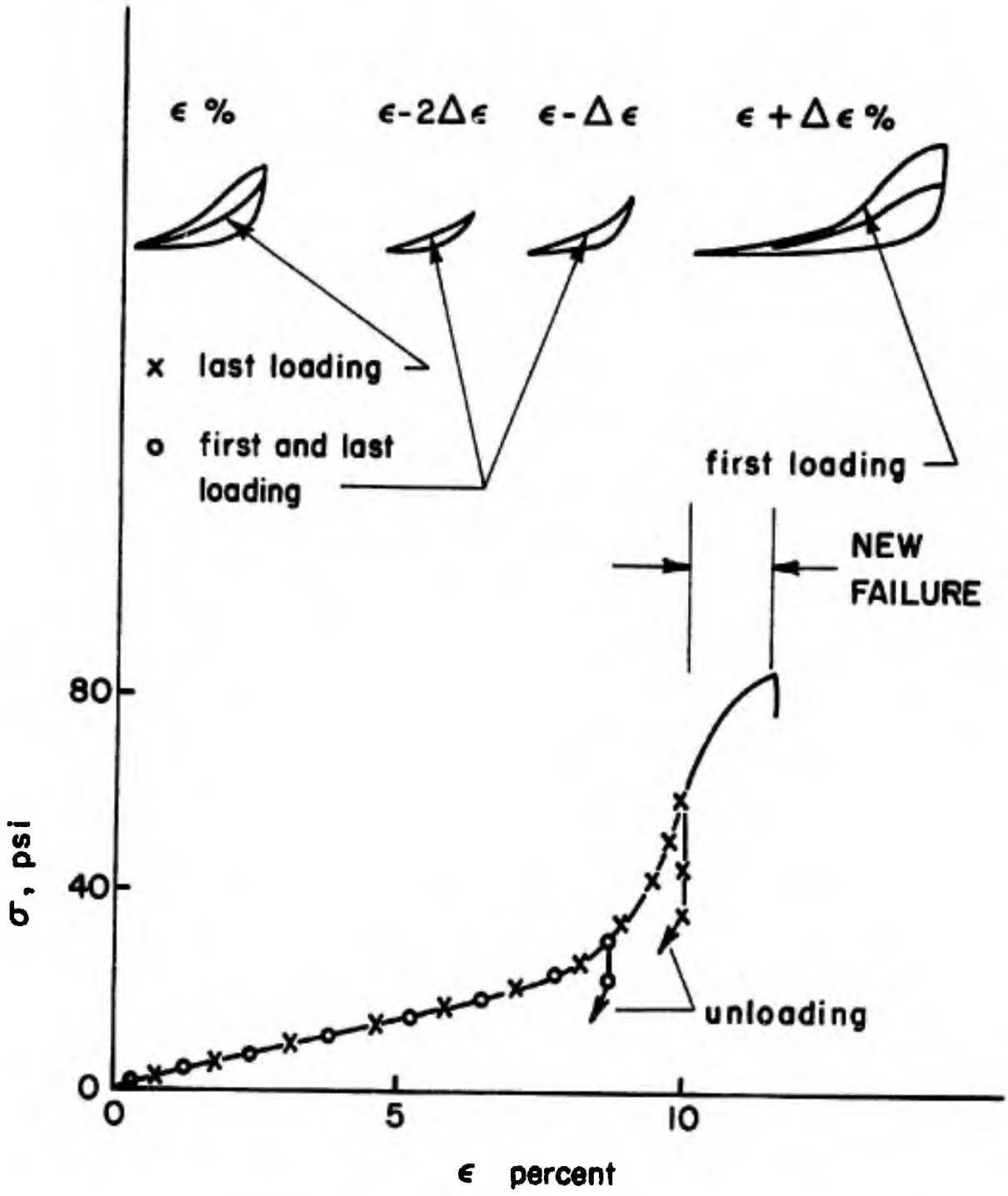

FIG. 30 SUPERPOSITION OF SUBSEQUENT, NON-LINEAR STRESS-STRAIN CURVES

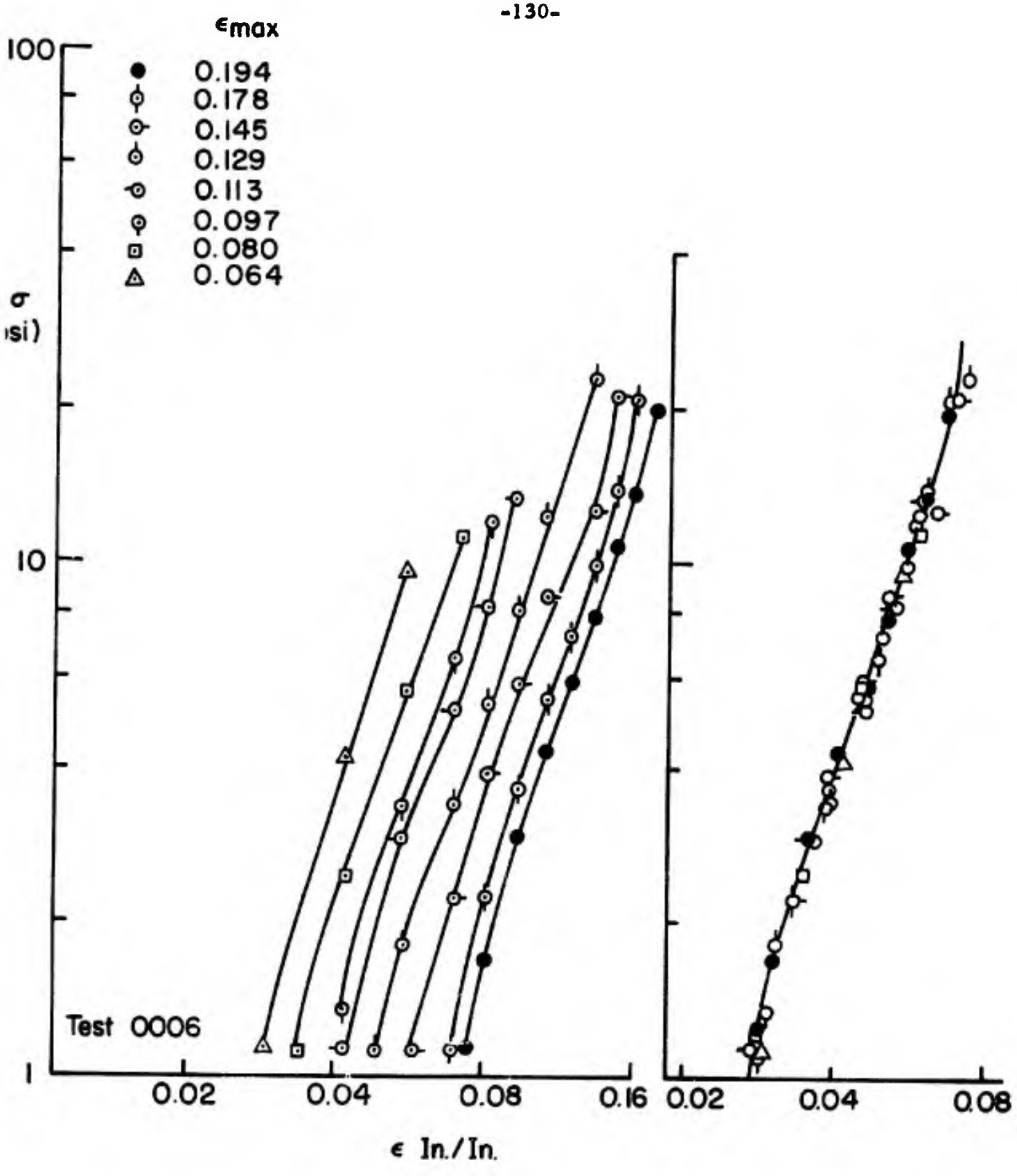

FIG. 31 STRESS-STRAIN CURVE FOR UNLOADING AFTER A SERIES OF CYCLES TPH 1011 (CROSSHEAD RATE 2"/MIN., 25°C)

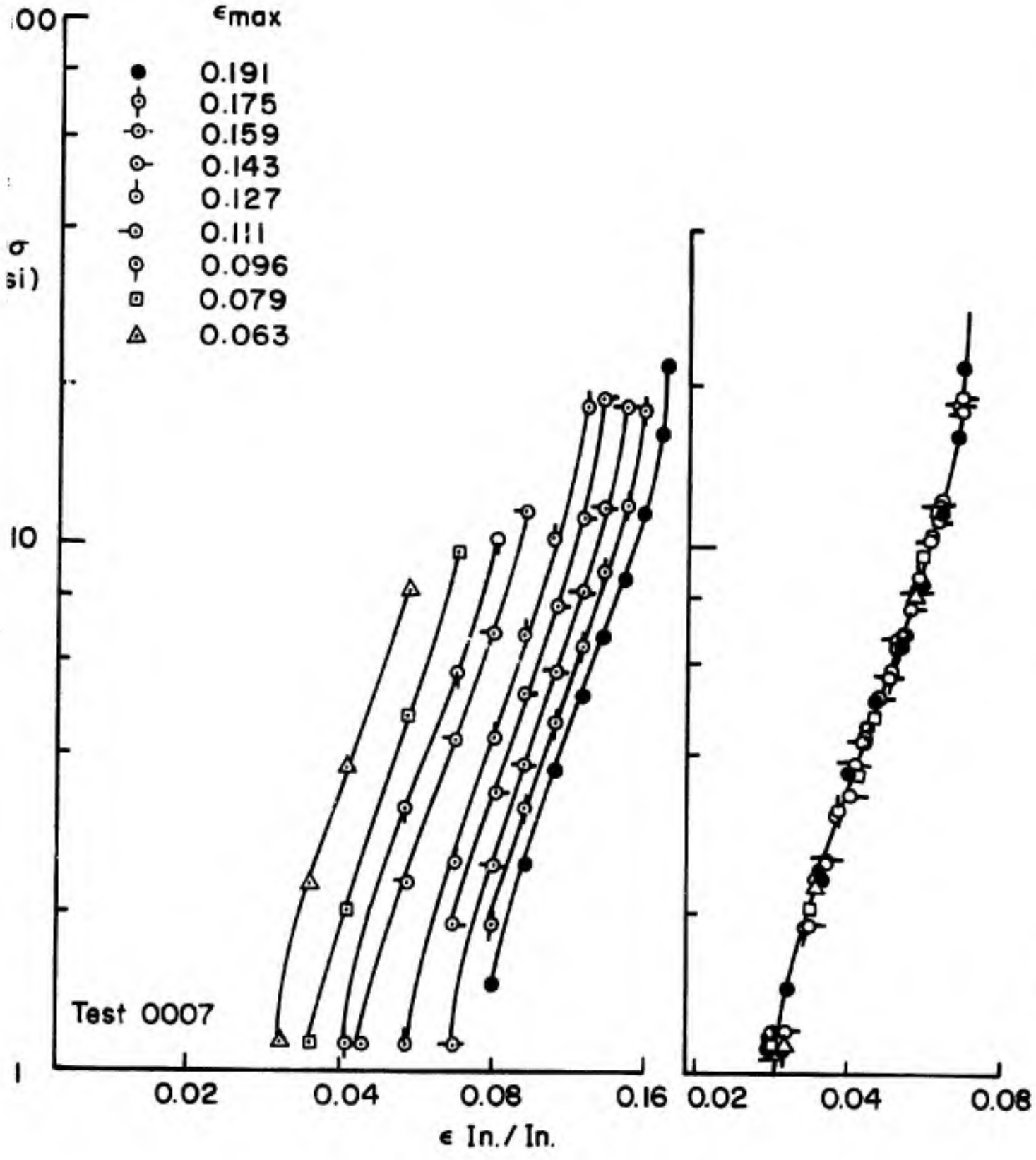

FIG. 32 STRESS-STRAIN CURVE FOR UNLOADING AFTER A SERIES OF CYCLES TPH 1011 (CROSSHEAD RATE 2"/MIN., 25°C)

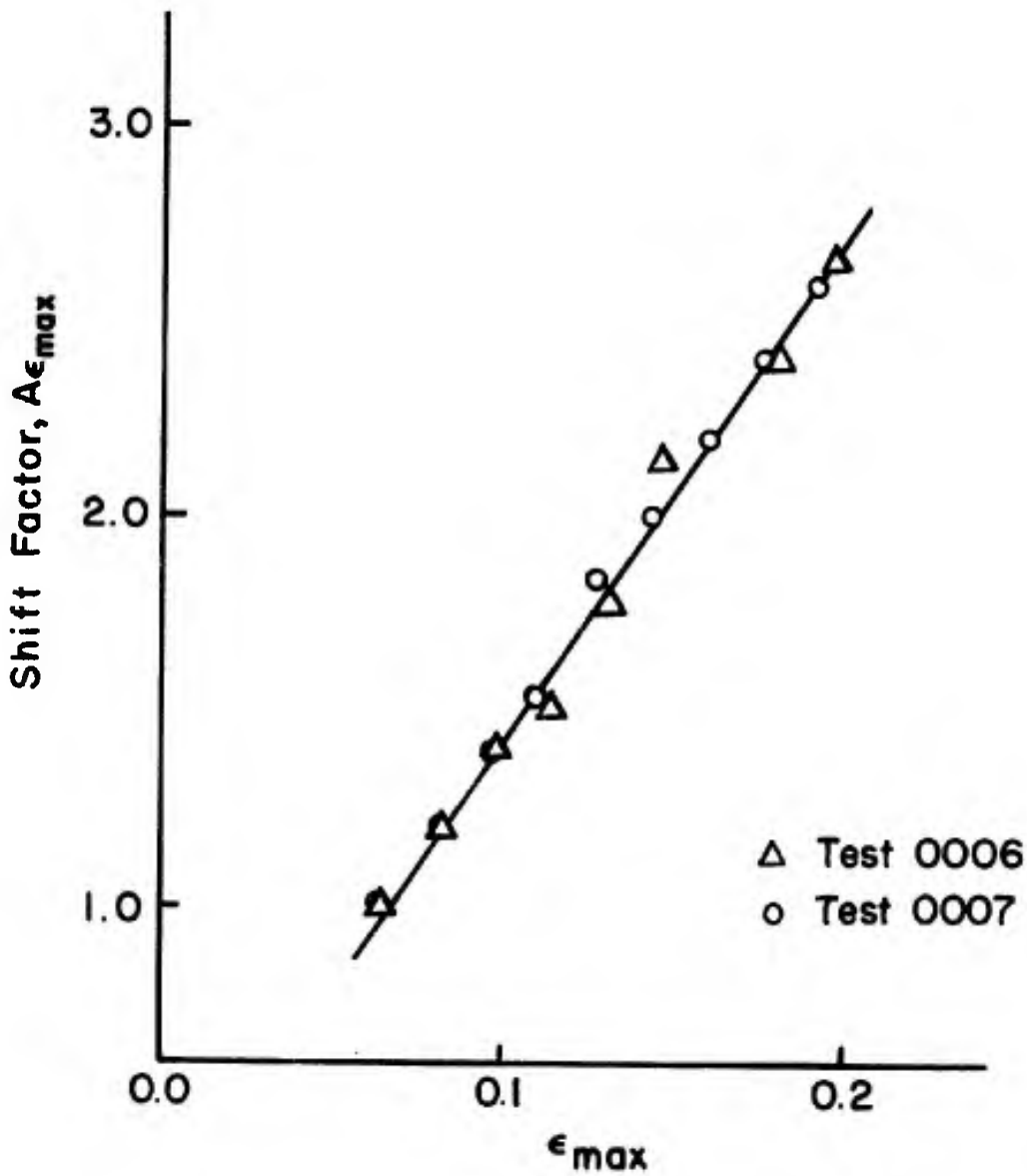

FIG.33 STRAIN SHIFT FACTOR $A_\epsilon(\epsilon_{max})$ TPH 1011

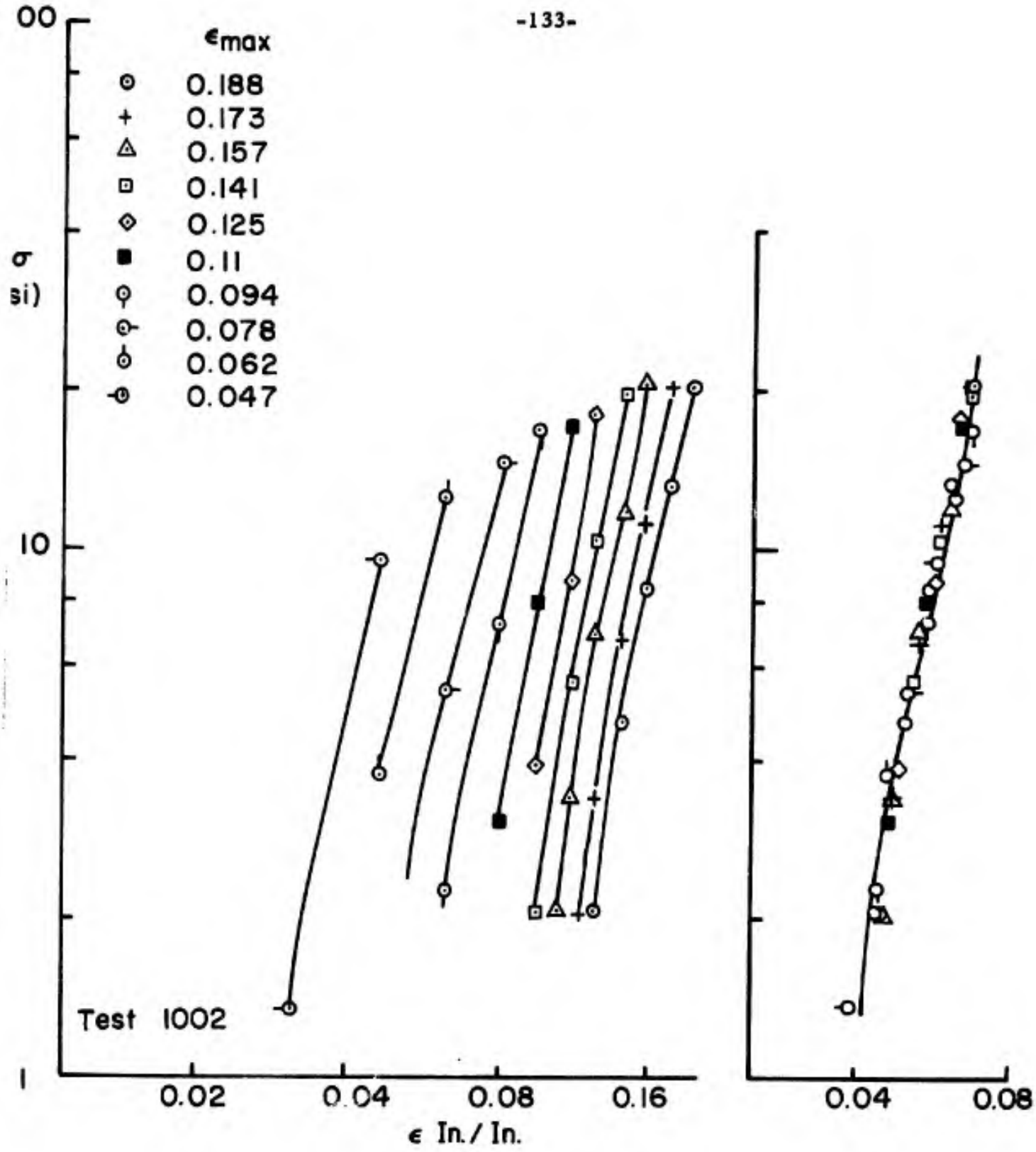

FIG. 34 STRESS-STRAIN CURVE FOR UNLOADING AFTER A SERIES OF CYCLES JPL 500 SERIES (CROSS HEAD RATE 2"/ MIN., 25° C)

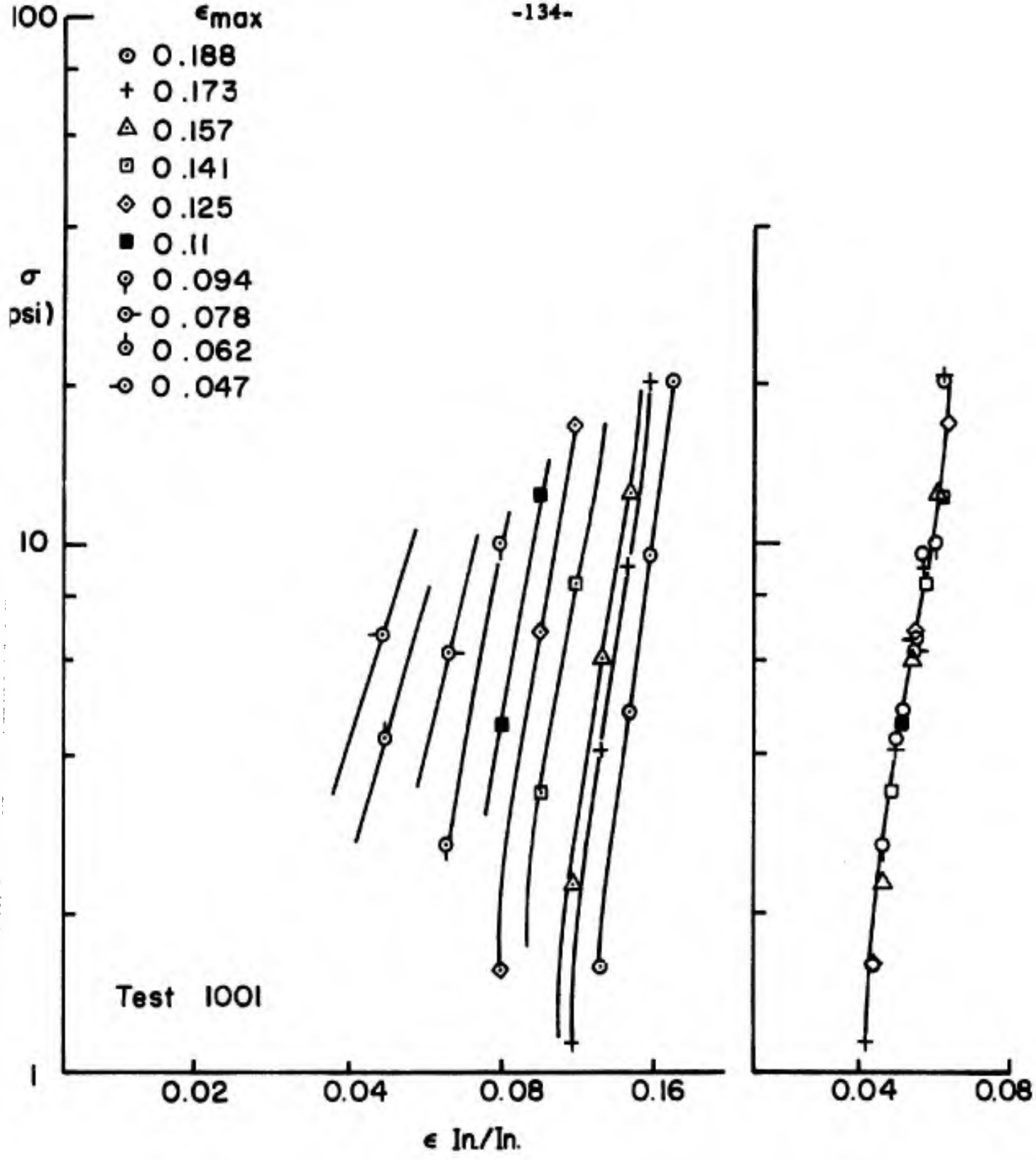

FIG. 35 STRESS-STRAIN CURVE FOR UNLOADING AFTER A SERIES OF CYCLES JPL 500 SERIES (CROSS HEAD RATE 2"/MIN., 25°C)

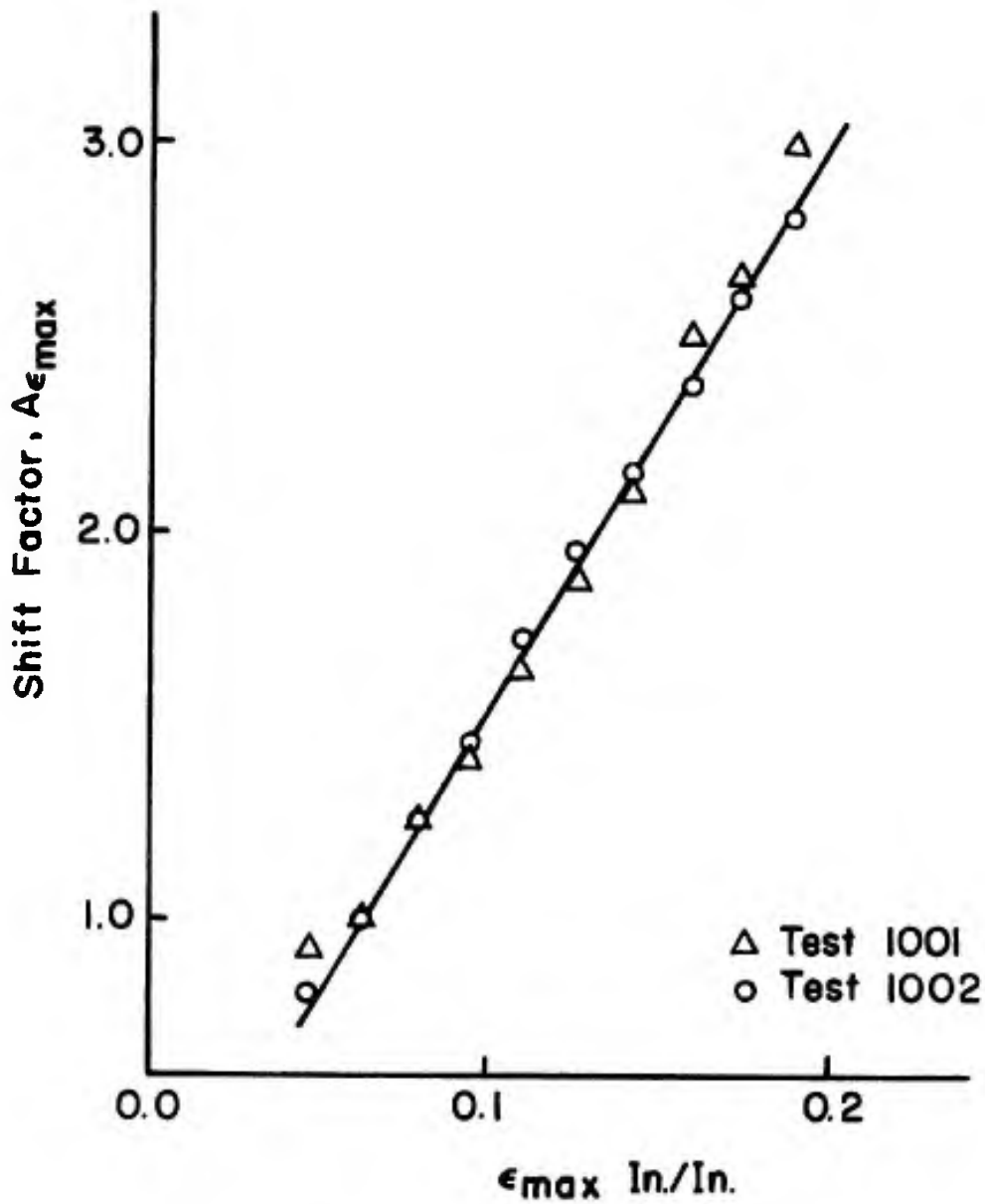

FIG. 36 STRAIN SHIFT FACTOR $A_\epsilon(\epsilon_{max})$ JPL 500 SERIES

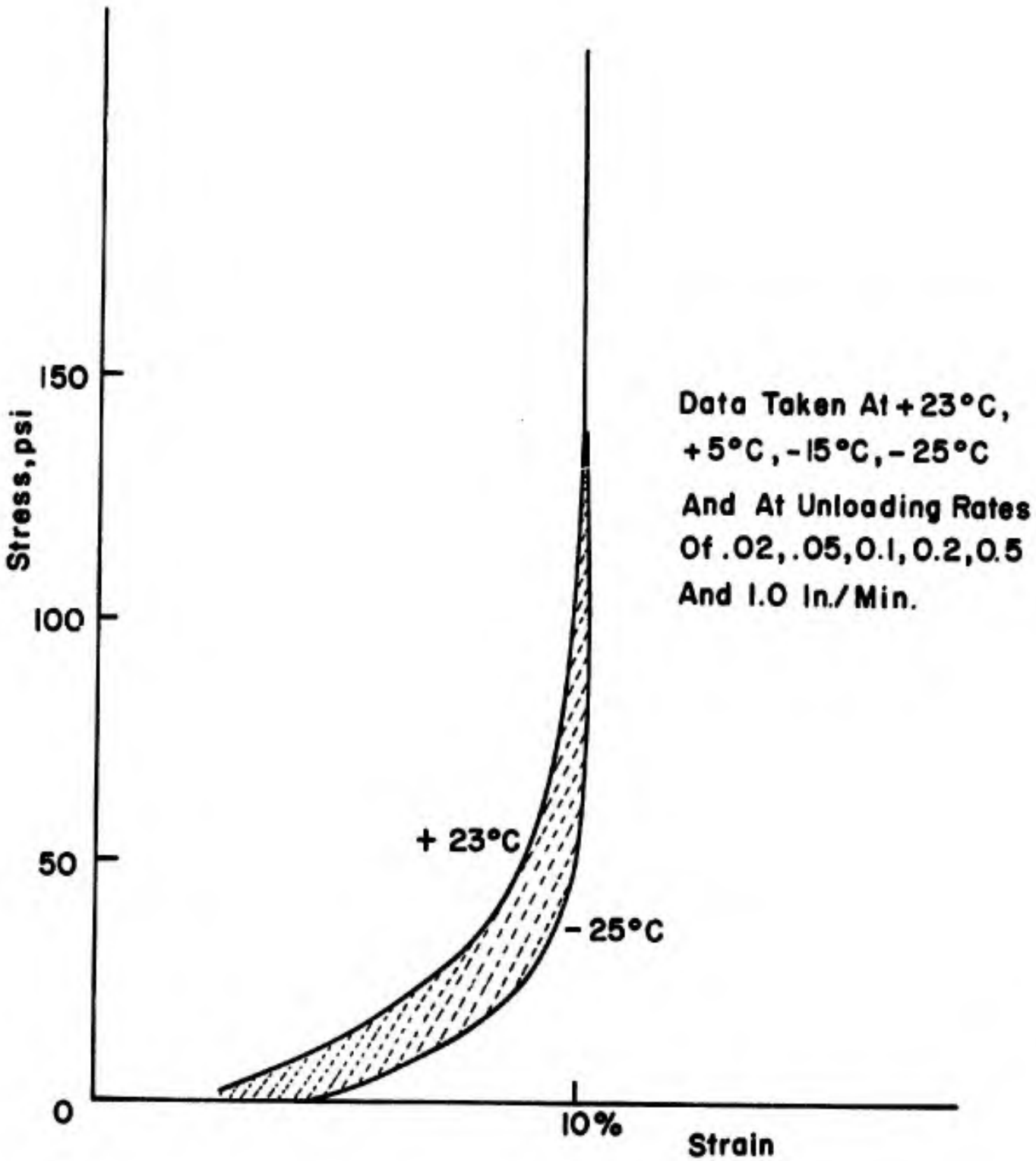

FIG. 37 UNLOADING STRESS STRAIN CURVES AT DIFFERENT RATES AND TEMPERATURES

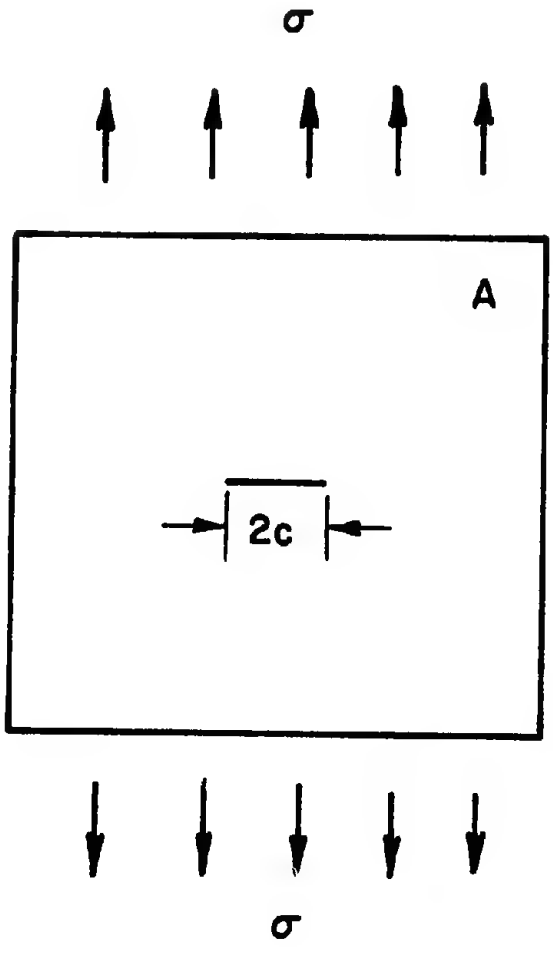

FIG. 38 CHARACTERISTIC CRACKED MATERIAL ELEMENT

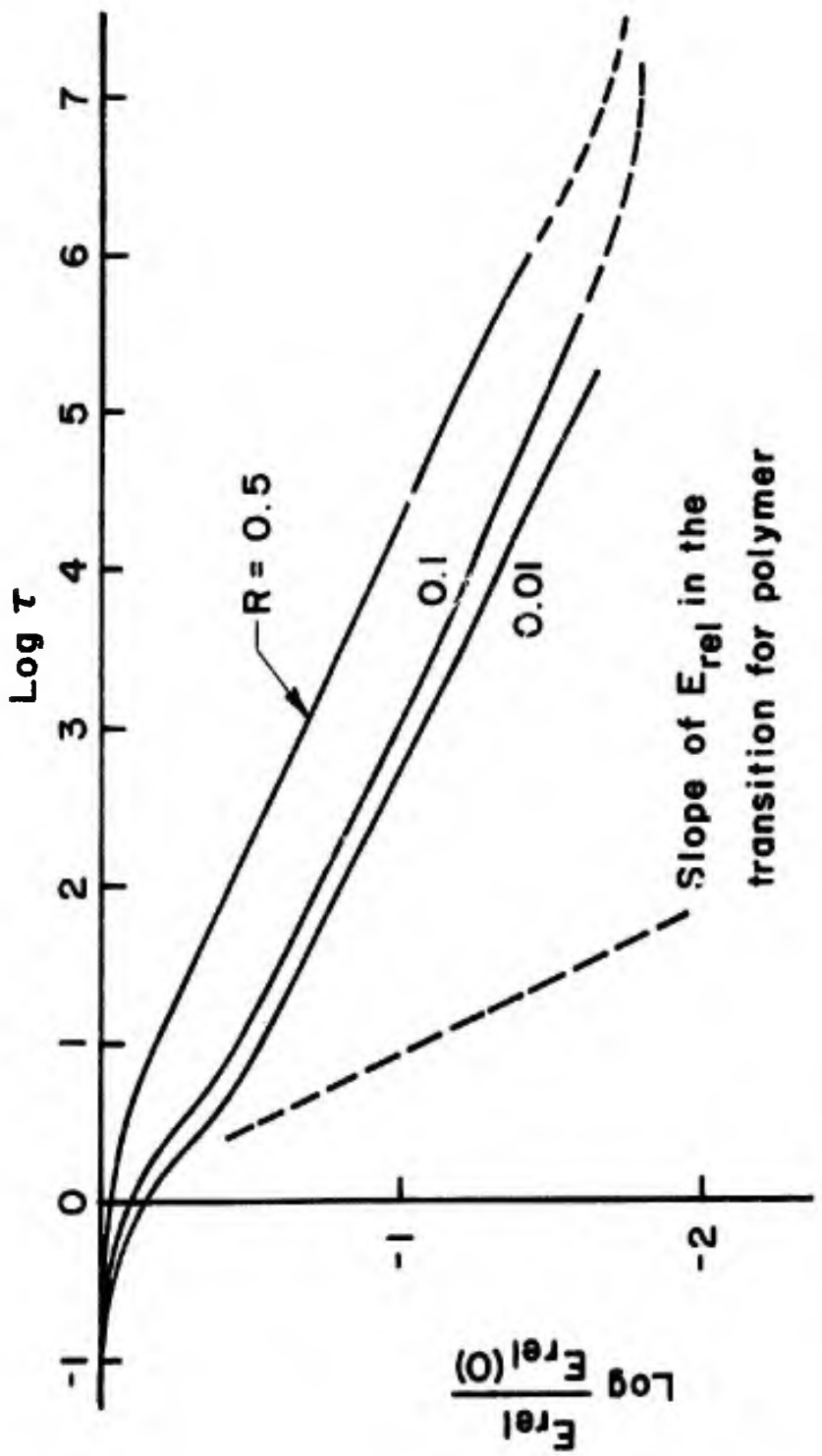

FIG. 39 RELAXATION MODULUS DUE TO FRACTURE

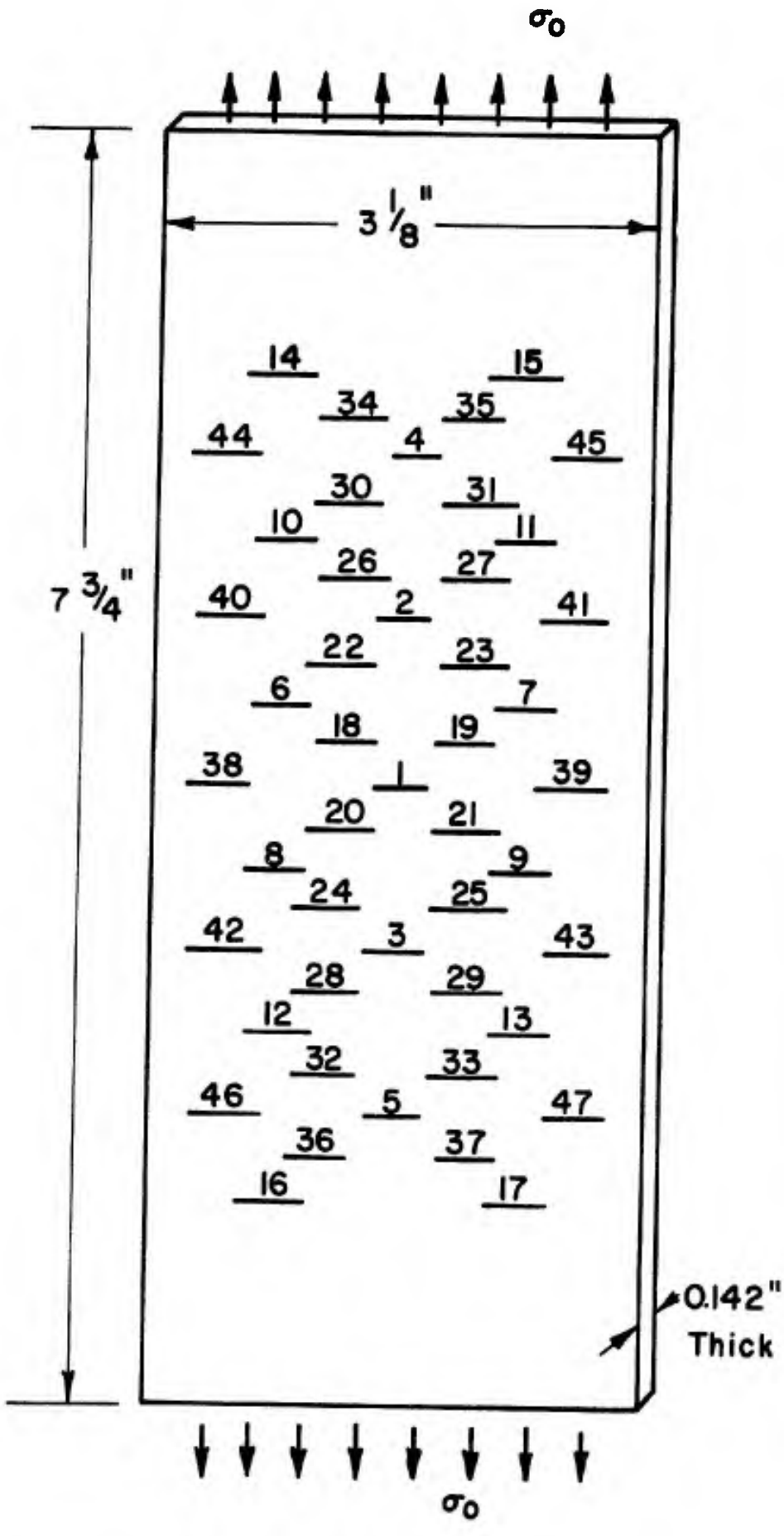

FIG. 40 CUT SEQUENCE IN EFFECTIVE MODULUS DETERMINATION

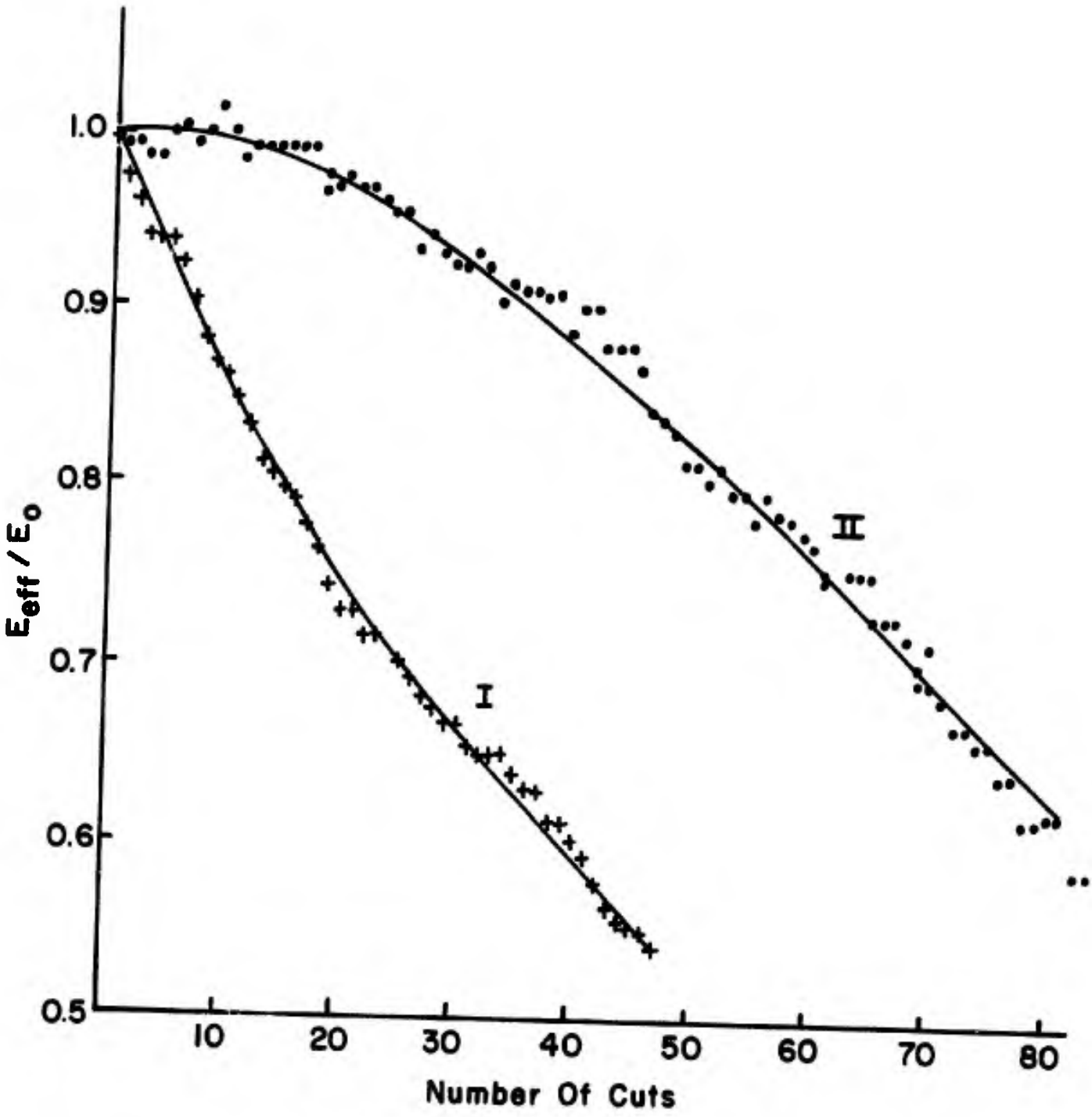

FIG. 41 EFFECTIVE MODULUS VS. NUMBER OF CUTS

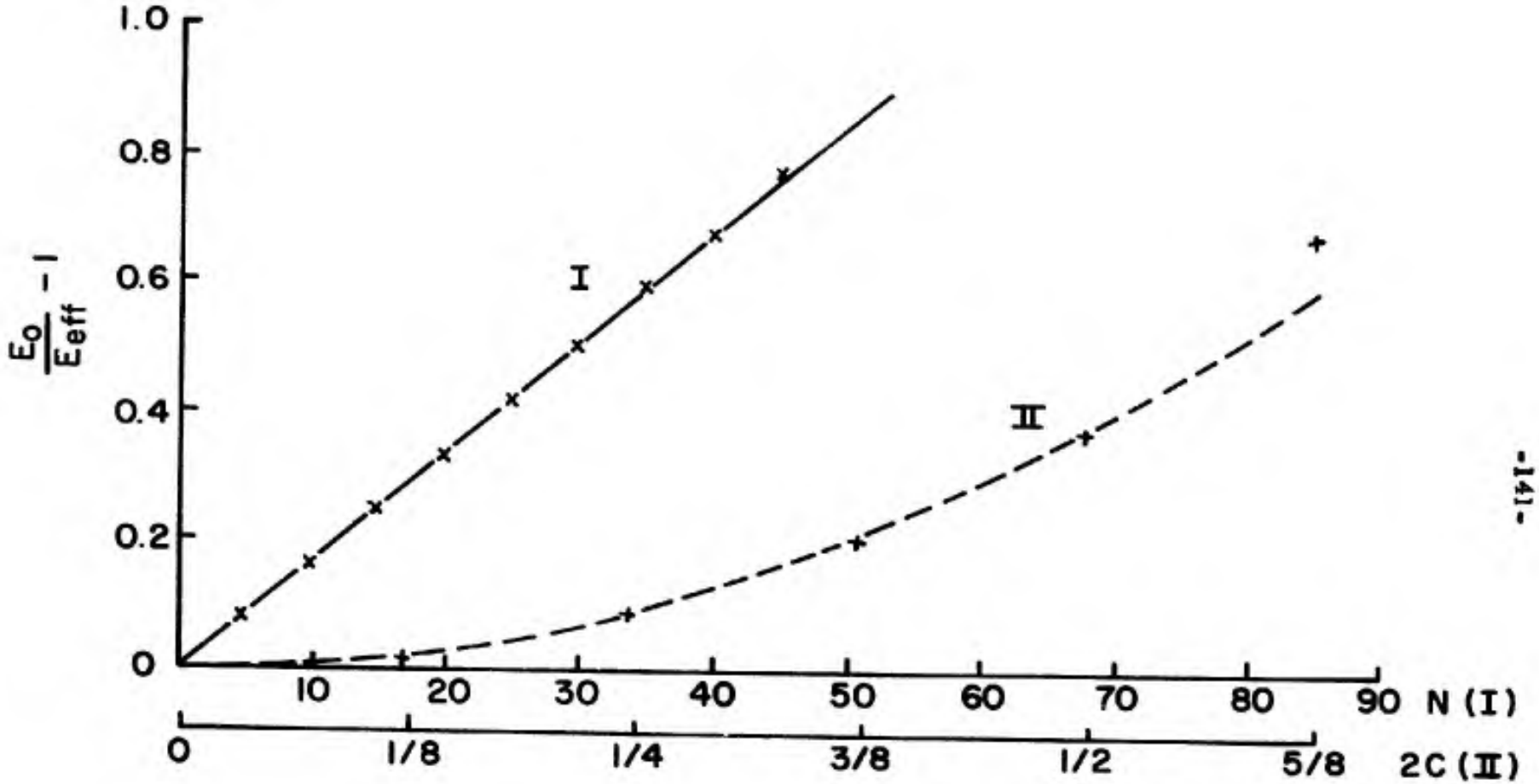

FIG. 42 MODULUS VARIATION WITH CUMULATIVE DAMAGE (CUTS)

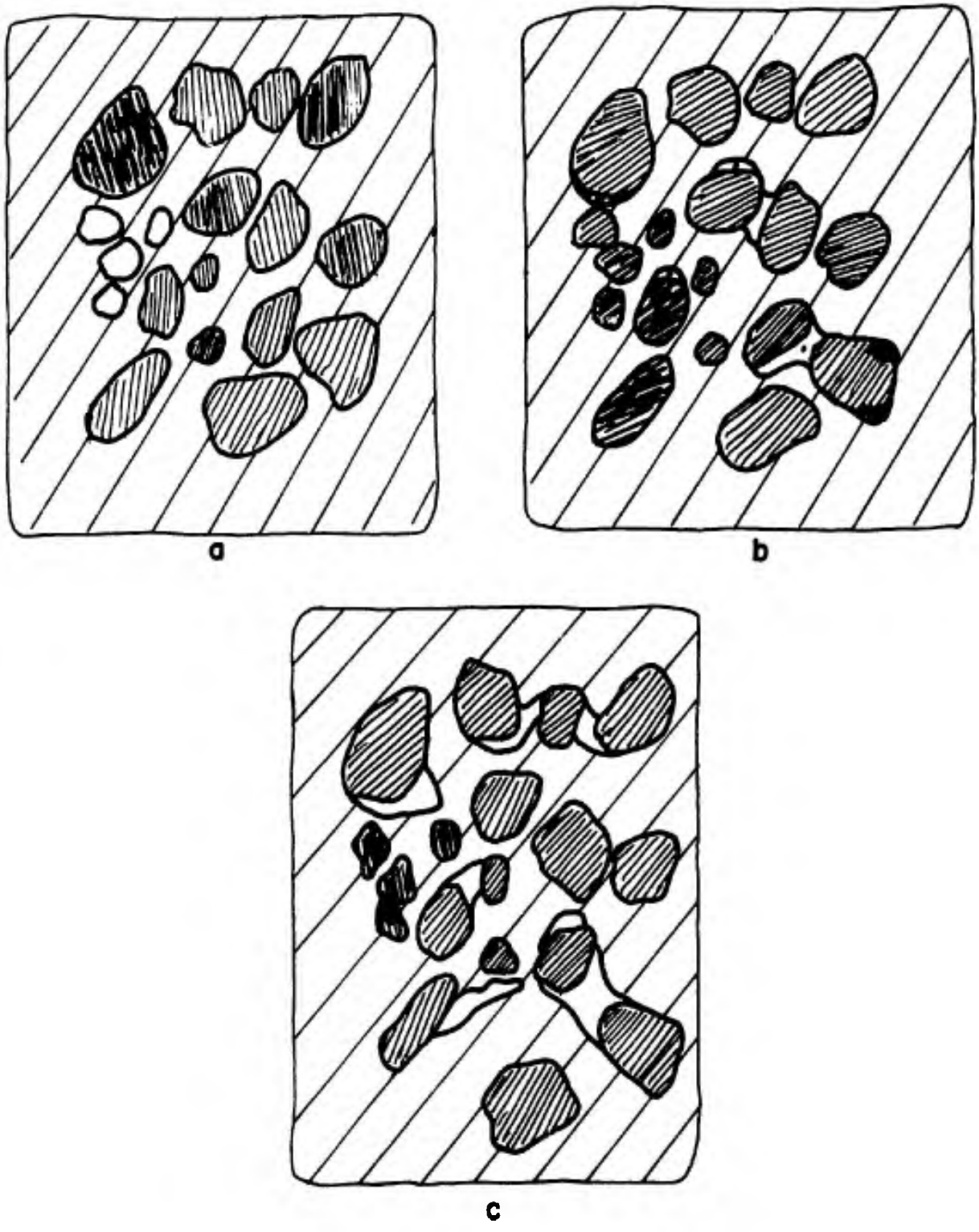

FIG. 43 FLOW GROWTH

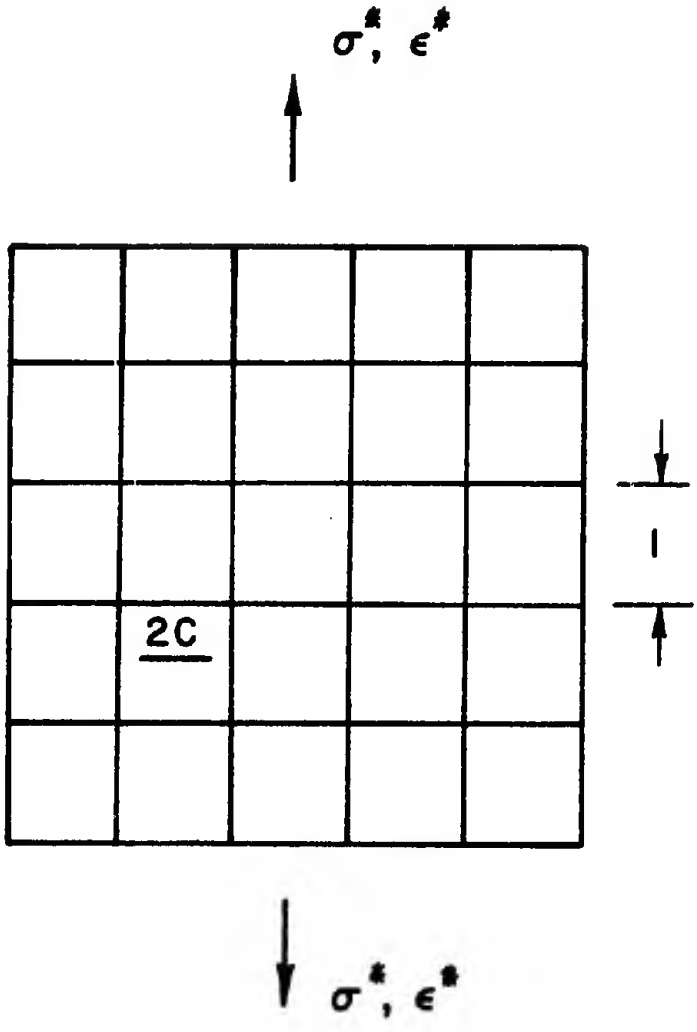

FIG. 44 DIVISION OF THE MICROSCOPIC SOLID INTO SQUARE UNIT CELLS

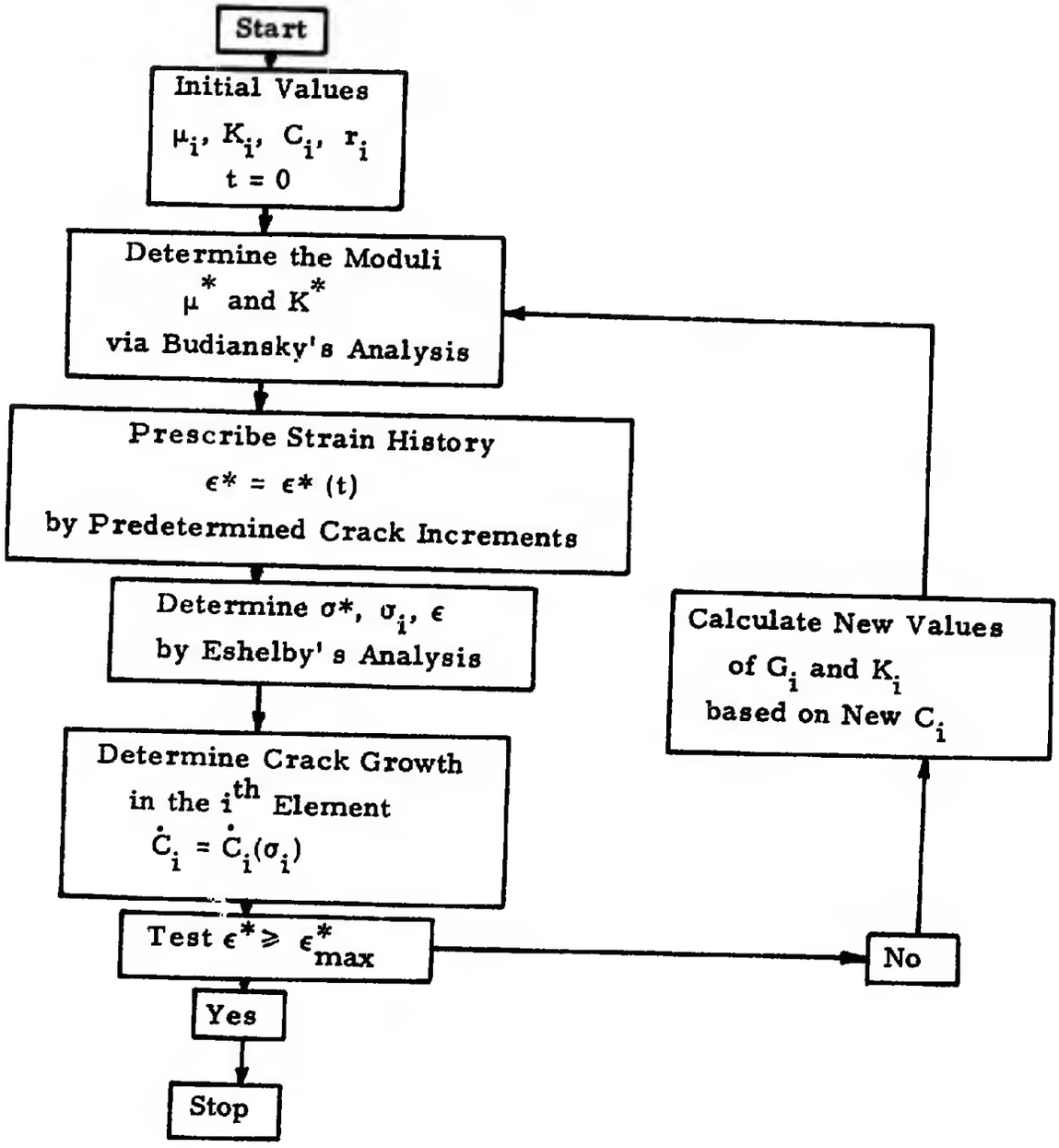

Fig. 45. Computer Program Flow Chart

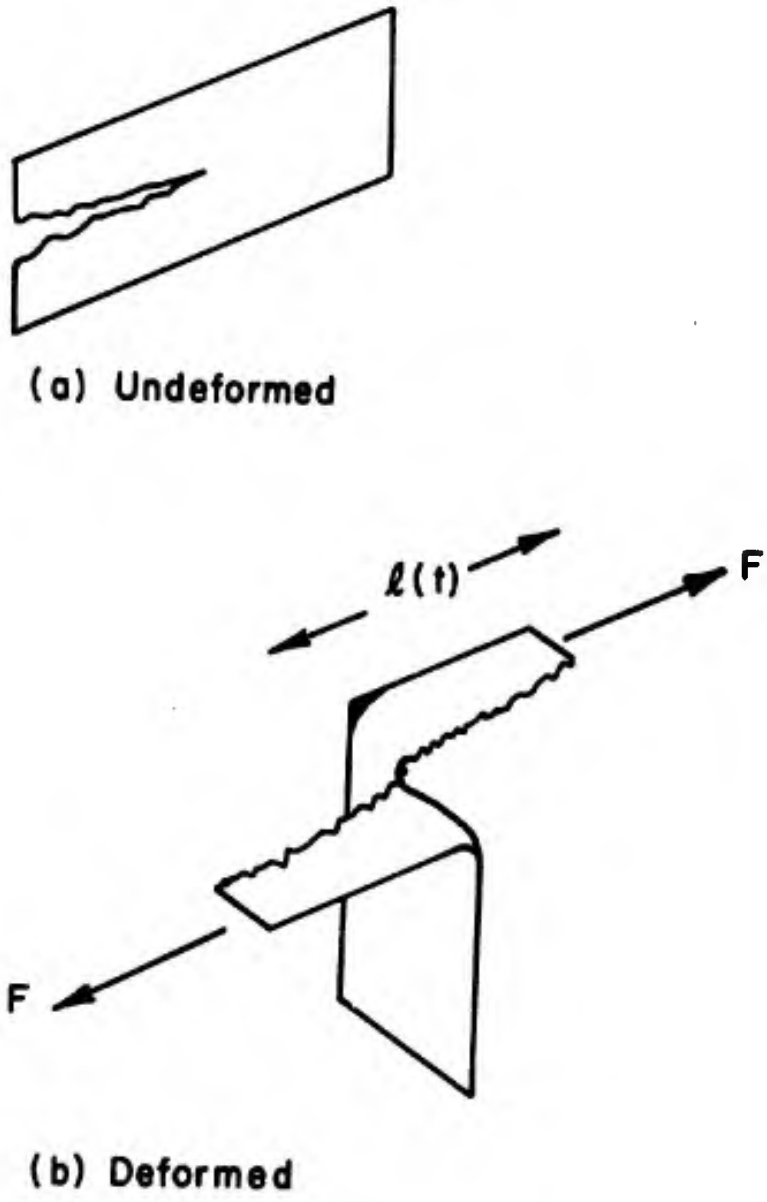

FIG. 46 MODEL OF A TEAR ELEMENT

m = Power Of Crack Rate Law
m_t = Power Of Tear Rate Law

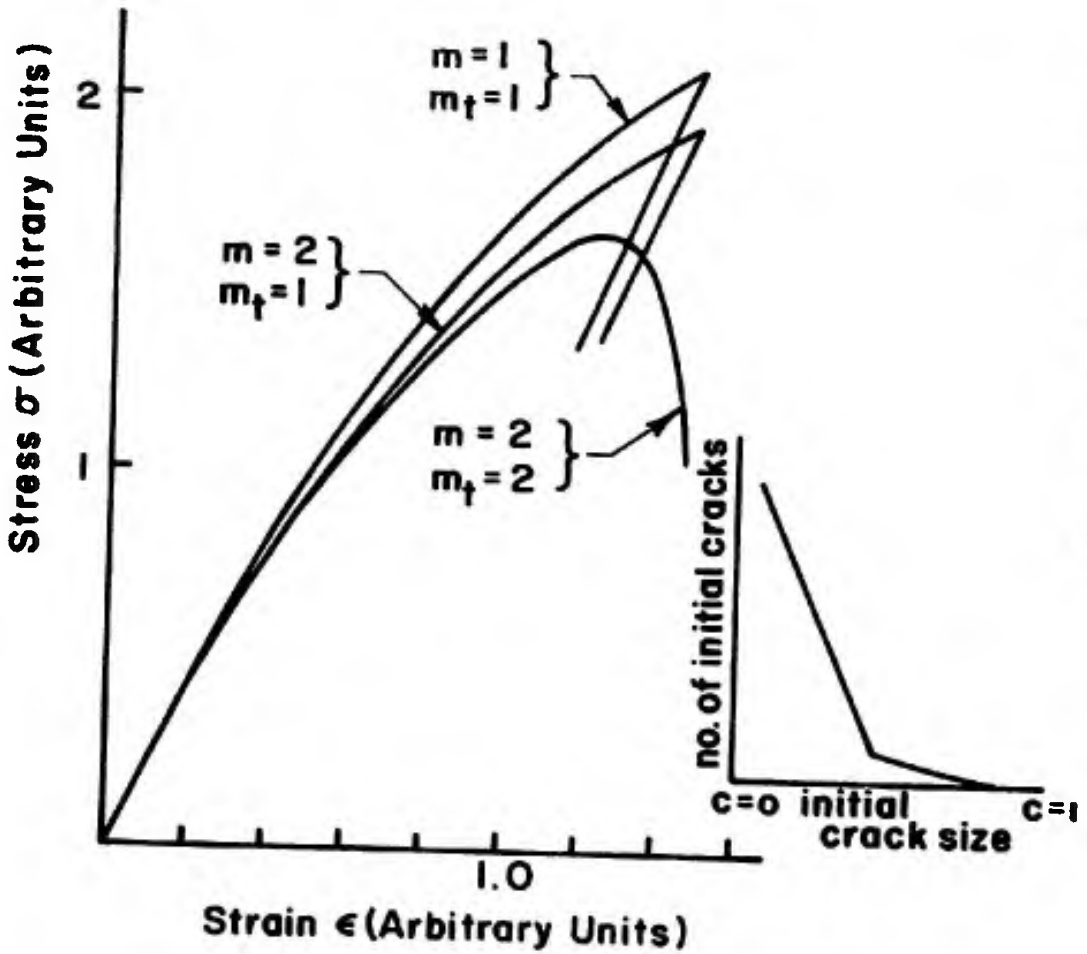

FIG. 47 EFFECT OF CHANGING THE POWER COEFFICIENTS OF THE RATE LAWS

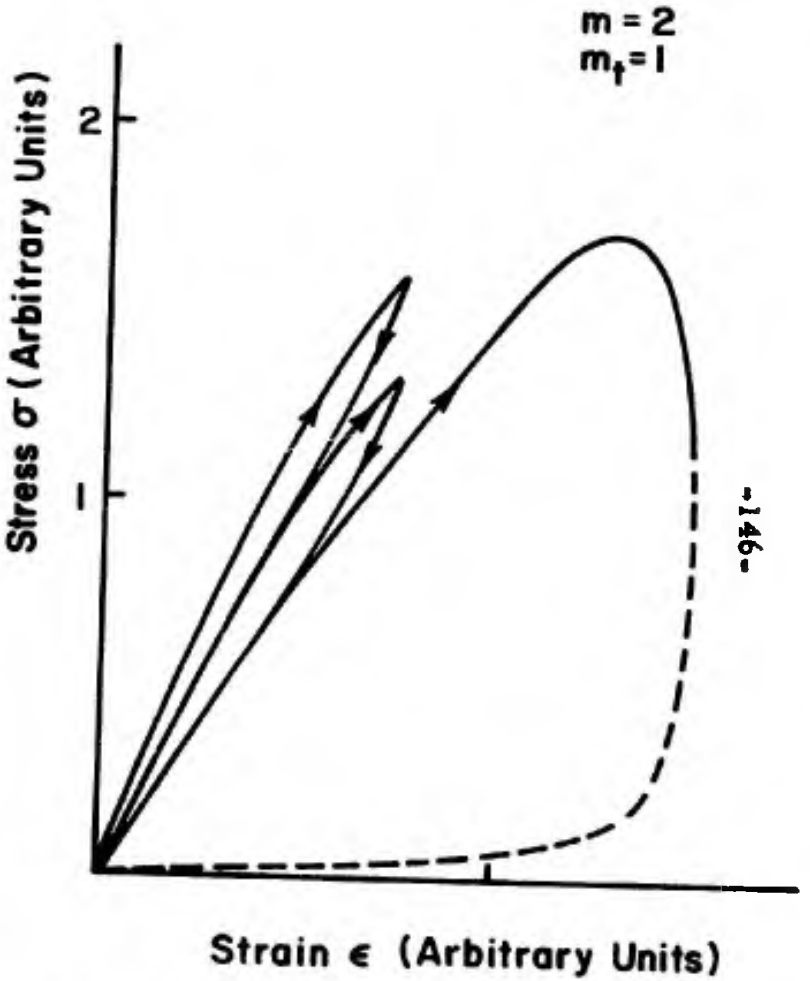

FIG. 48 EFFECT OF DEFORMATION HISTORY

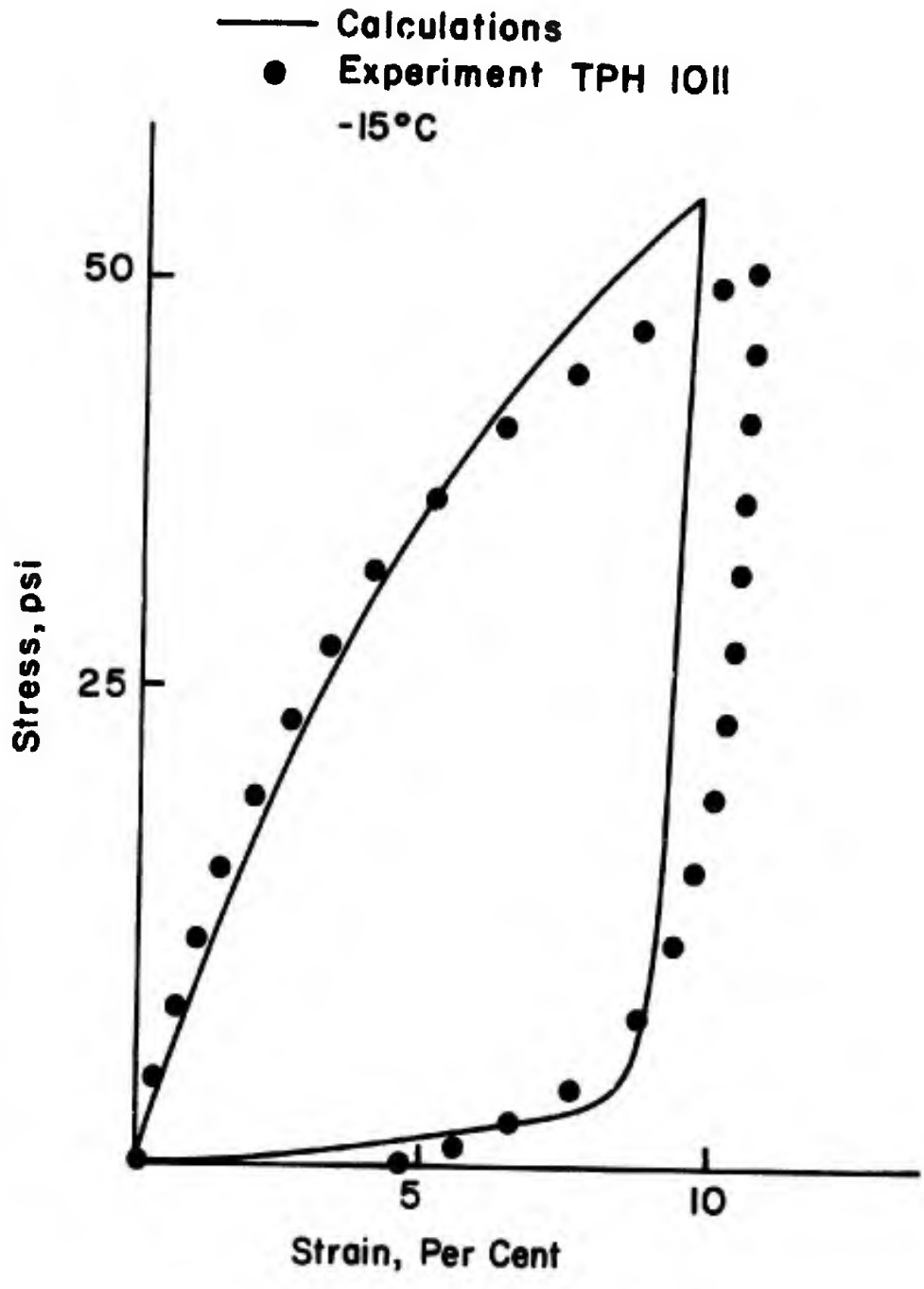

FIG. 49 COMPARISON OF COMPUTATIONS WITH PROPELLANT BEHAVIOR

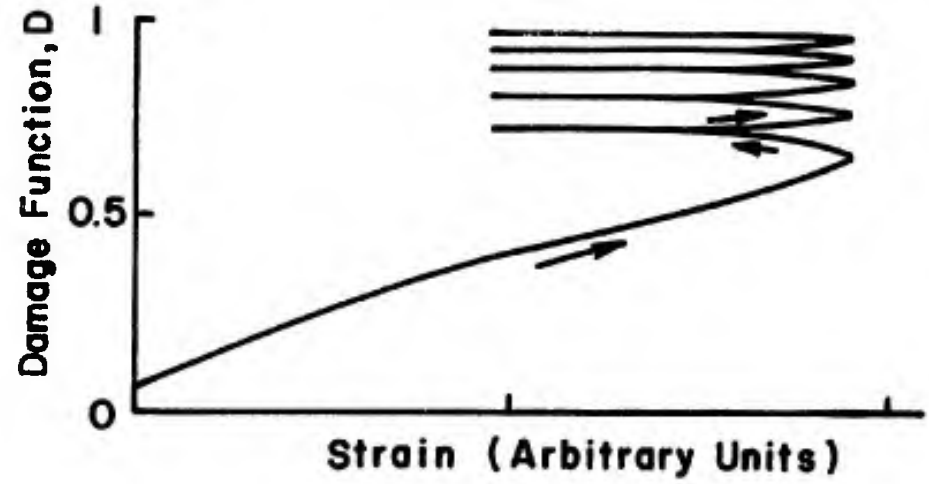

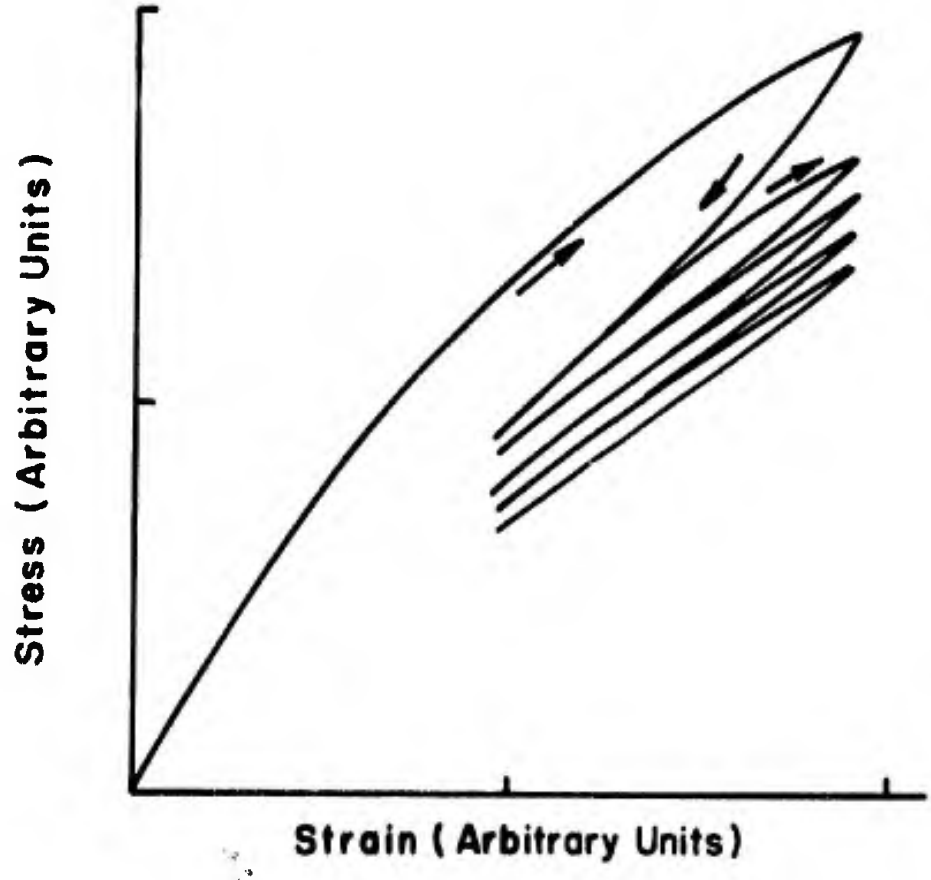

FIG. 50 DAMAGE ACCUMULATION IN STRAIN CYCLING HISTORY
$m = 5$, $m_1 = 5$, $k_0 = 0.44$

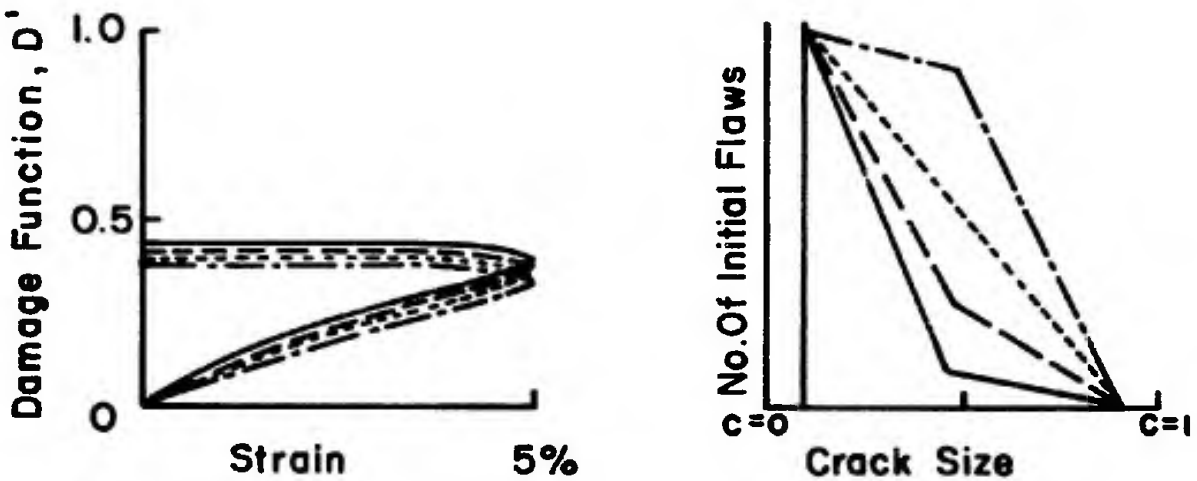

FIG. 51 EFFECT OF INITIAL FLAW DISTRIBUTION ON DAMAGE ACCUMULATION IN SINGLE CYCLE

$m = 5$, $m_t = 5$

(D' = D − Initial Damage)

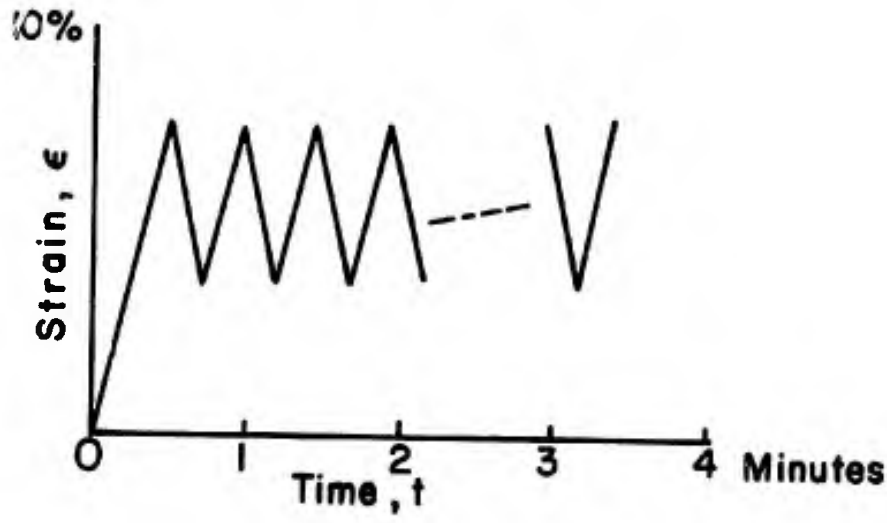

FIG. 52 CYCLIC STRAIN HISTORY

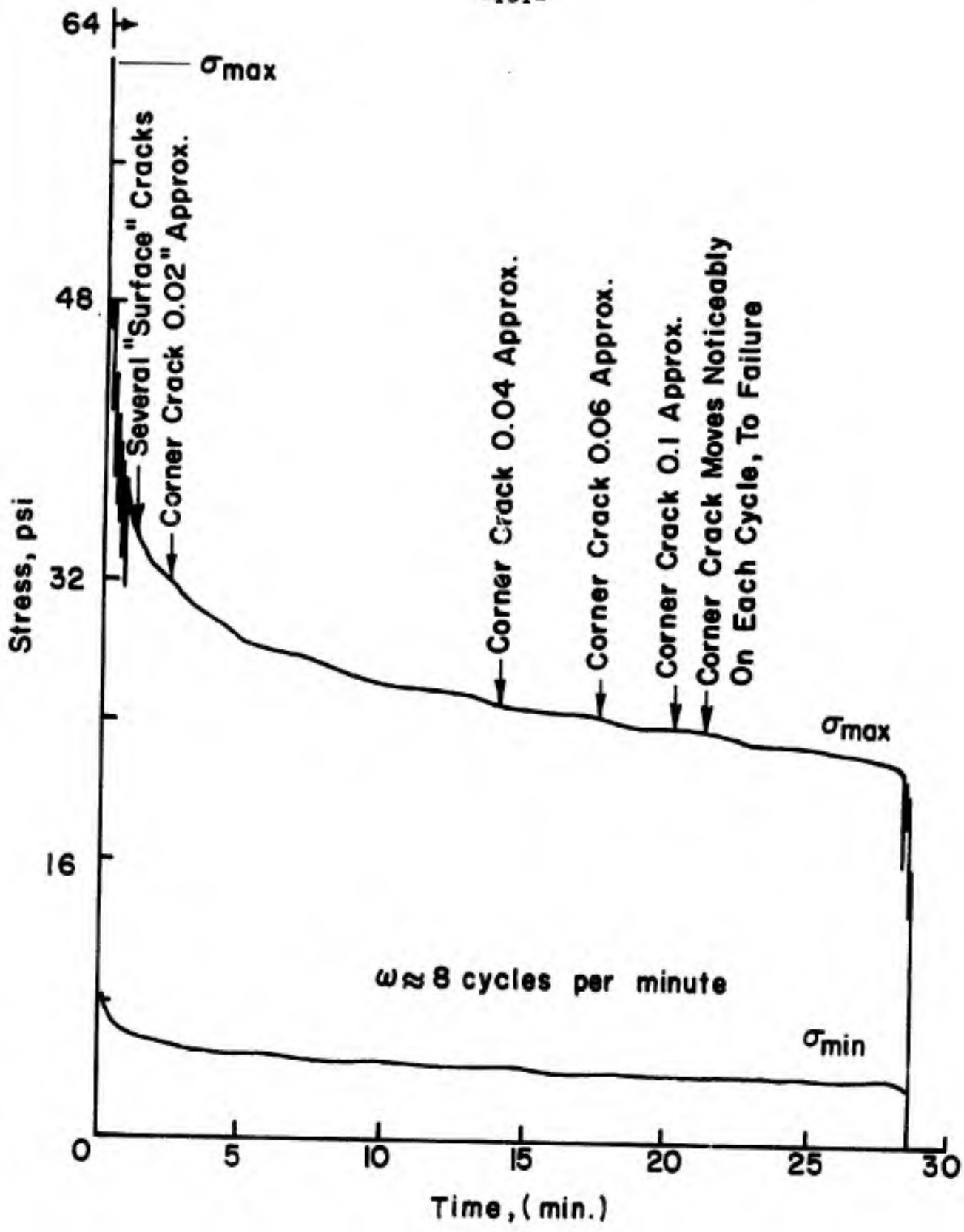

FIG. 53 HISTORY OF MAXIMUM AND MINIMUM STRESS IN STRAIN CYCLING EXPERIMENT TPH 1011

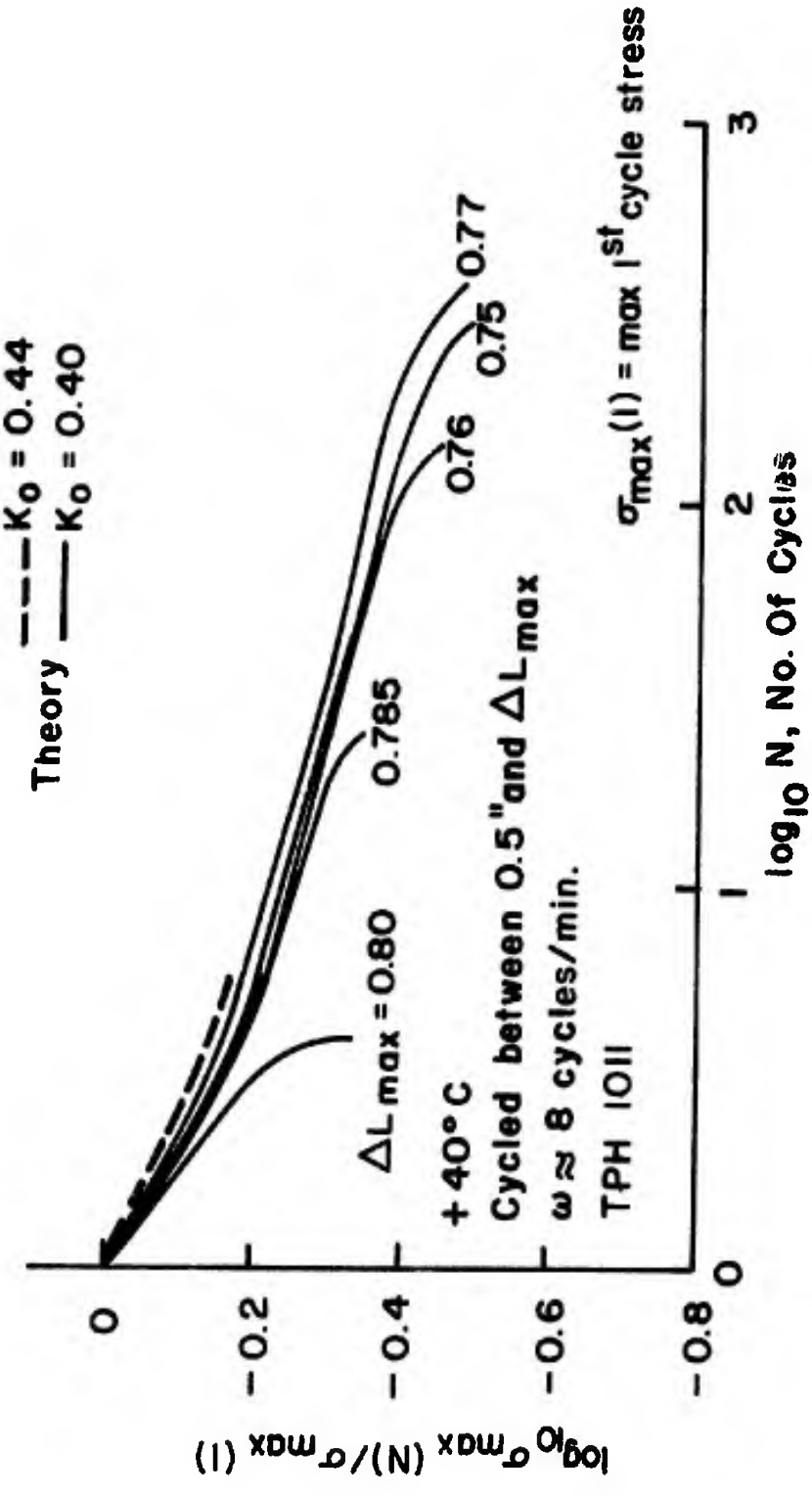

FIG. 54 DECREASE OF MAXIMUM STRESS WITH NUMBER OF CYCLES (EXPERIMENT AND THEORY)

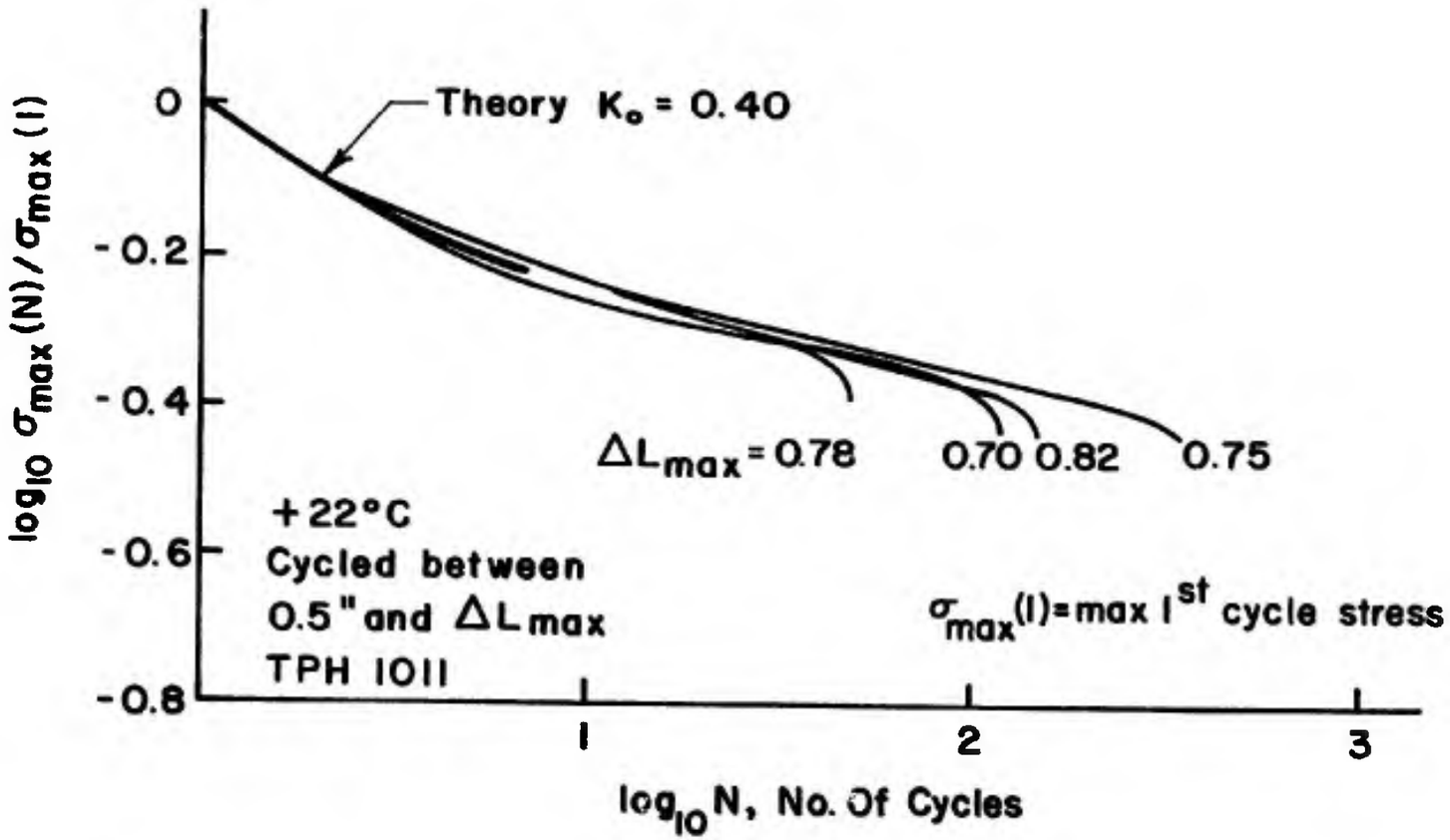

FIG. 55 DECREASE OF MAXIMUM STRESS WITH NUMBER OF CYCLES

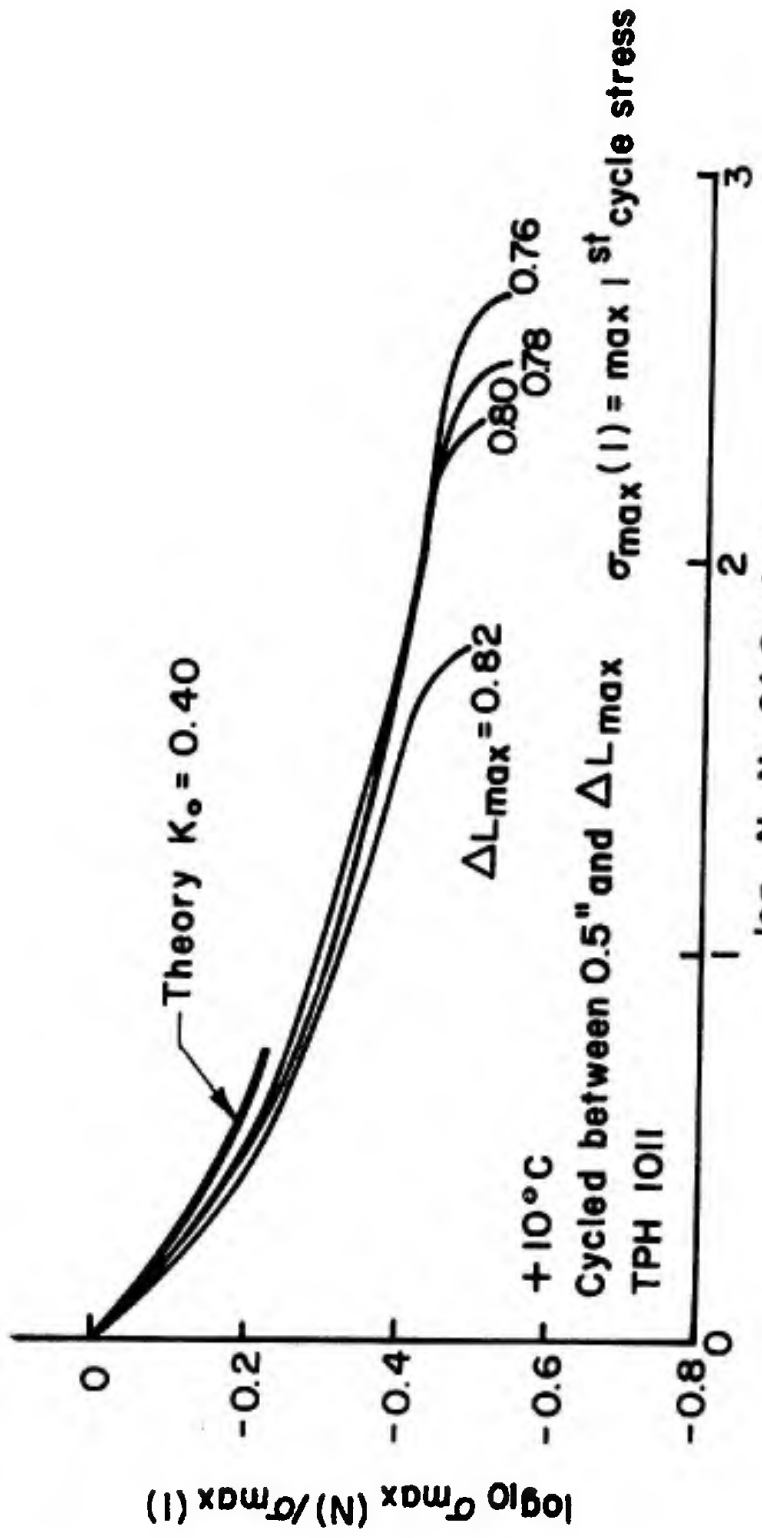

FIG. 56 DECREASE OF MAXIMUM STRESS WITH NUMBER OF CYCLES

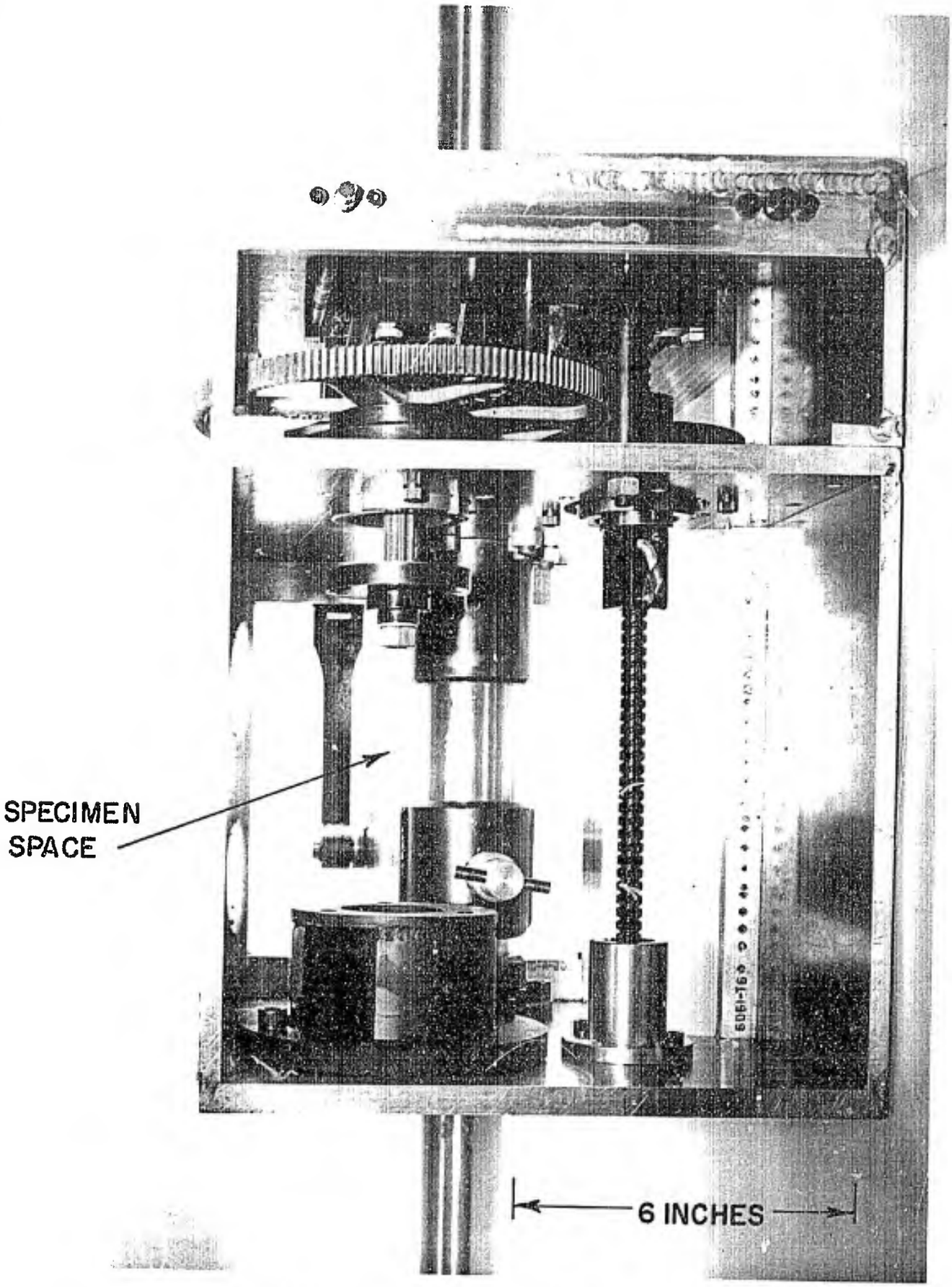

FIG. 57 BIAXIAL LOADING FIXTURE (FRONT VIEW)

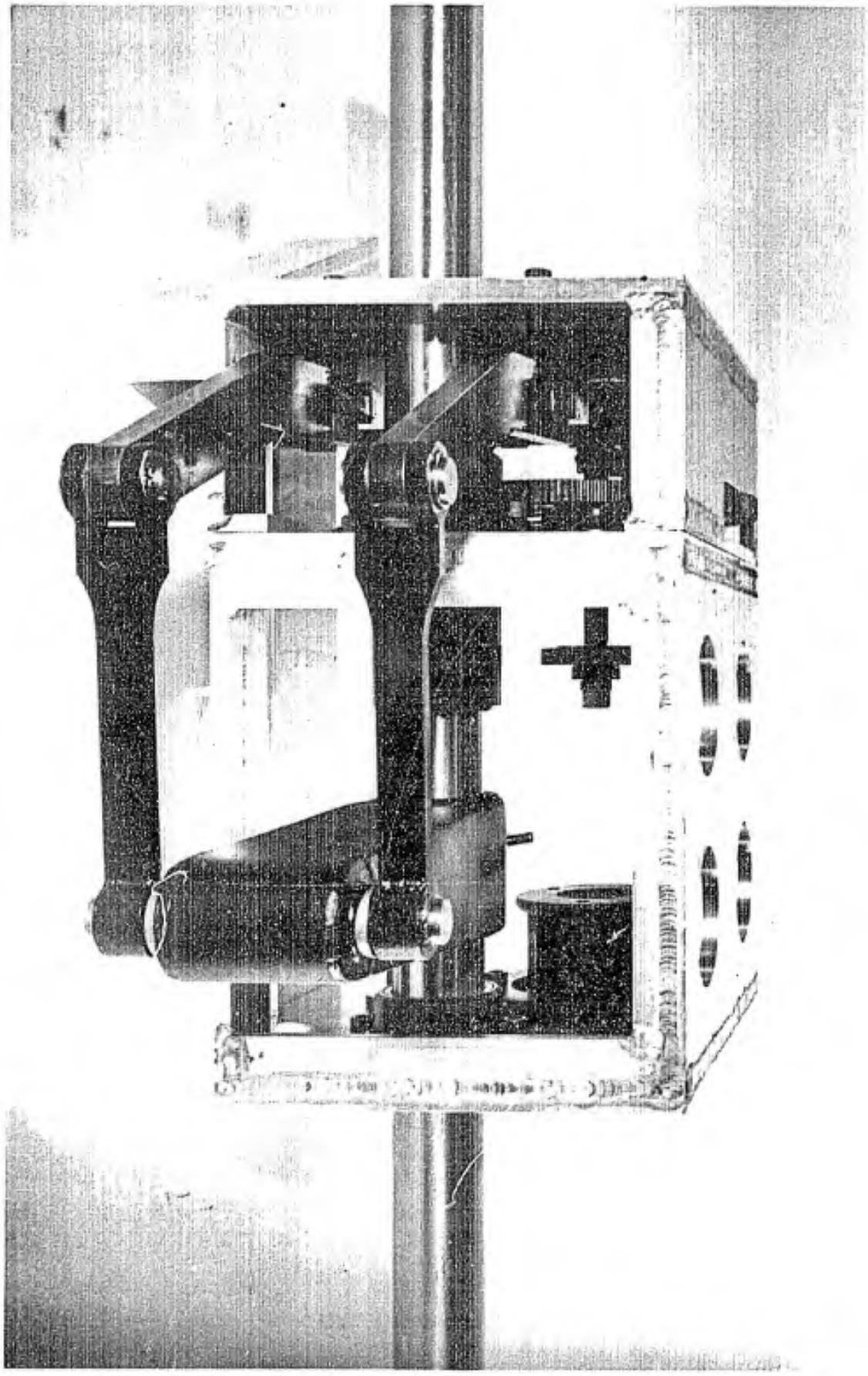

FIG. 58 BIAXIAL LOADING FIXTURE (REAR VIEW)

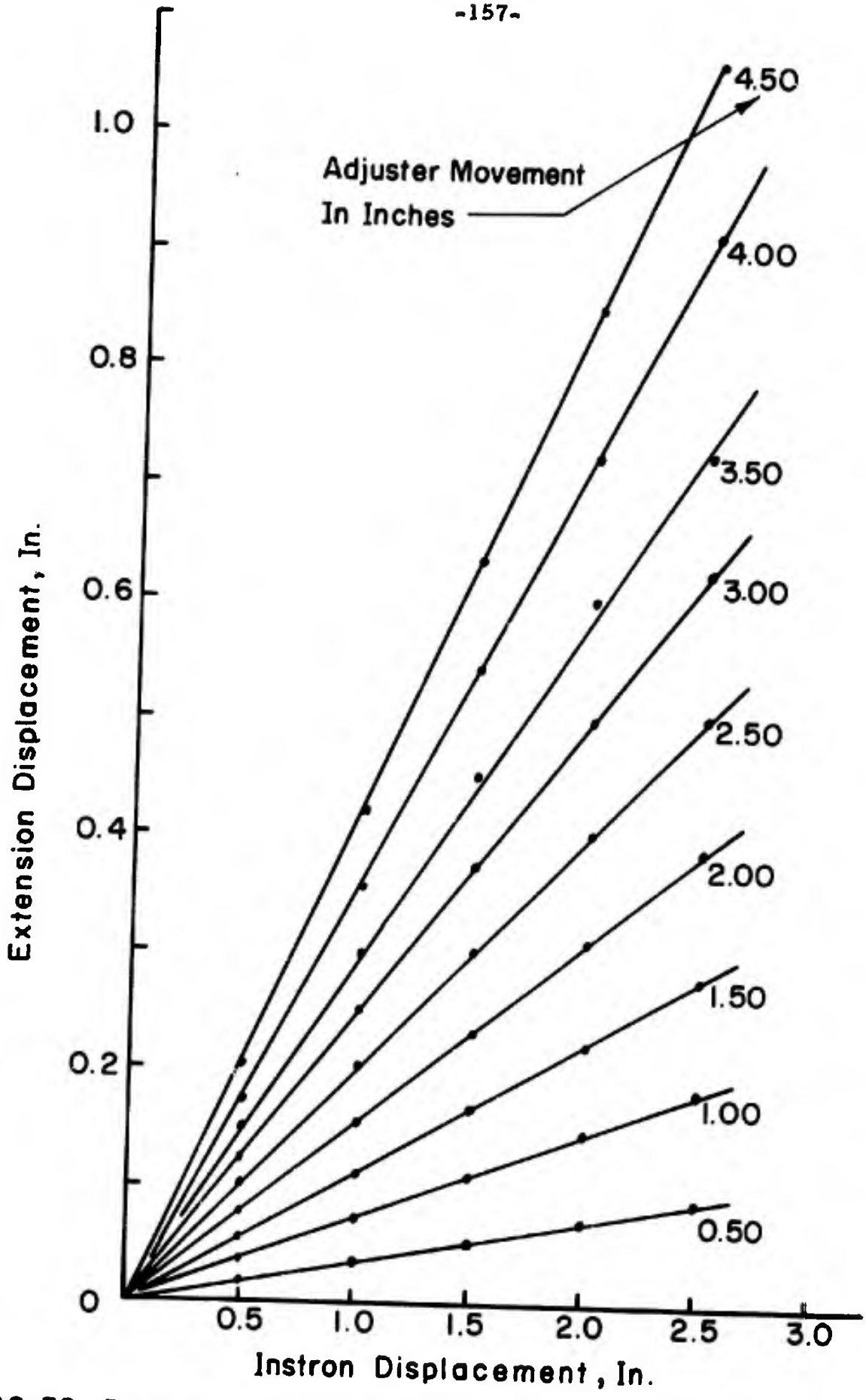

FIG. 59 BIAXIAL LOADING FIXTURE EXTENSIONAL CHARACTERIZATION

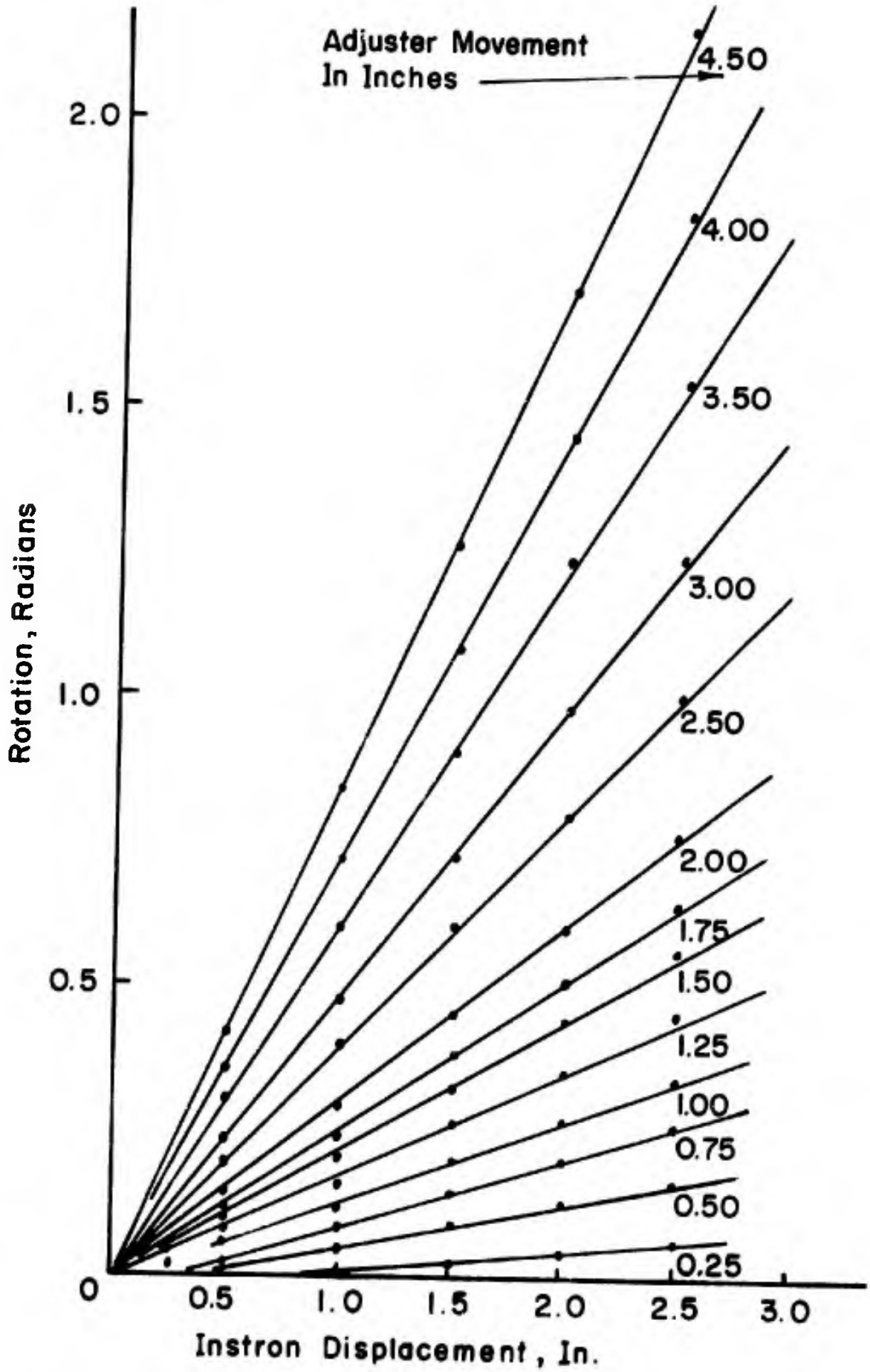

FIG. 60 BIAXIAL LOADING FIXTURE ROTATIONAL CHARACTERIZATION

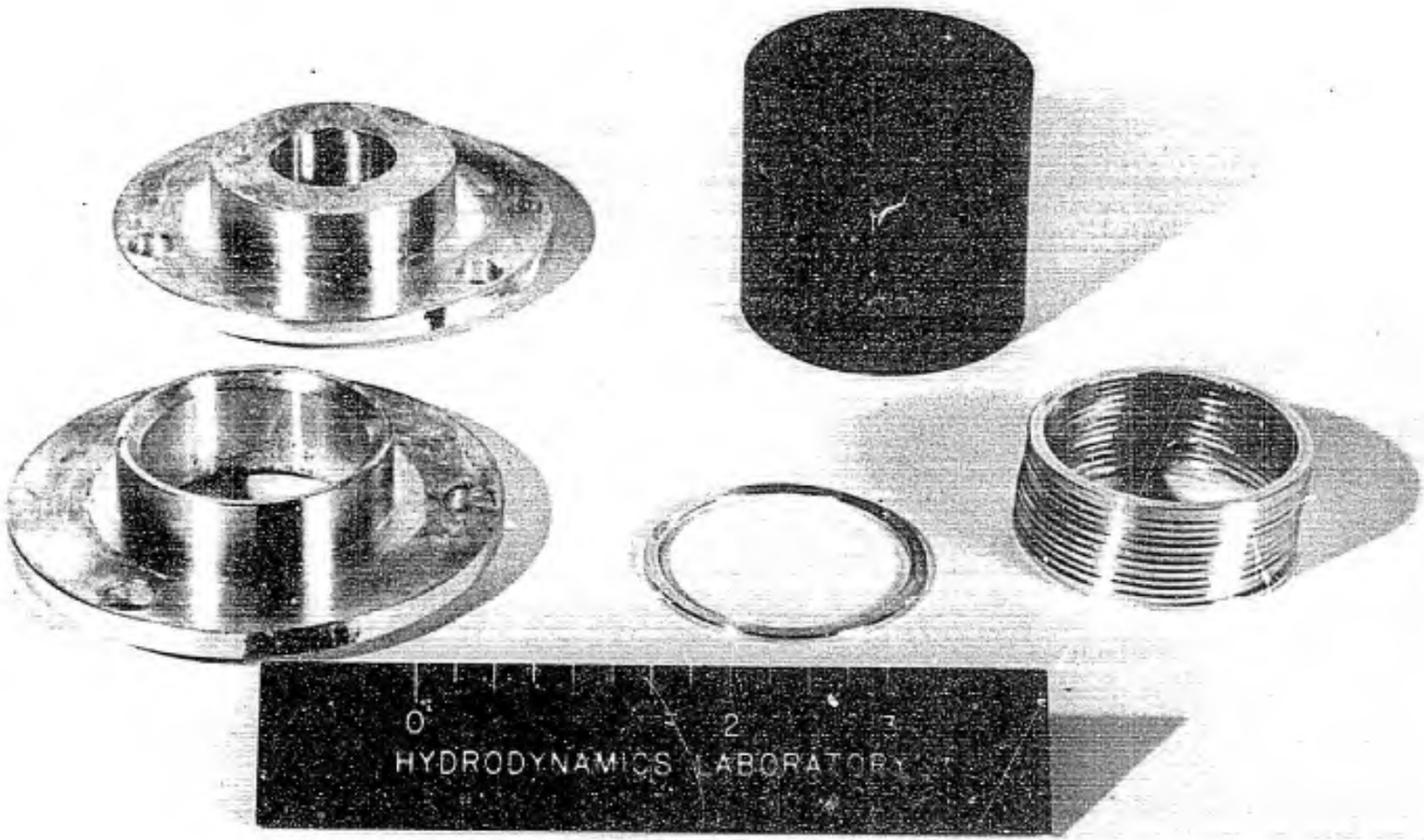

FIG. 61 BIAXIAL TEST SPECIMEN COMPONENTS

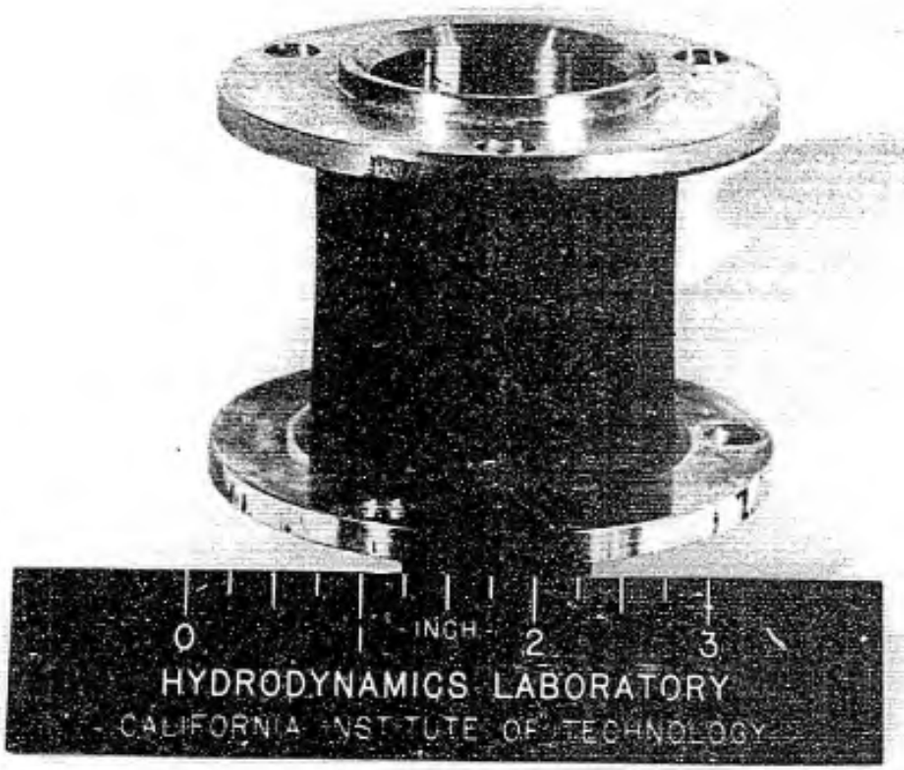

FIG. 62 ASSEMBLED BIAXIAL TEST SPECIMEN

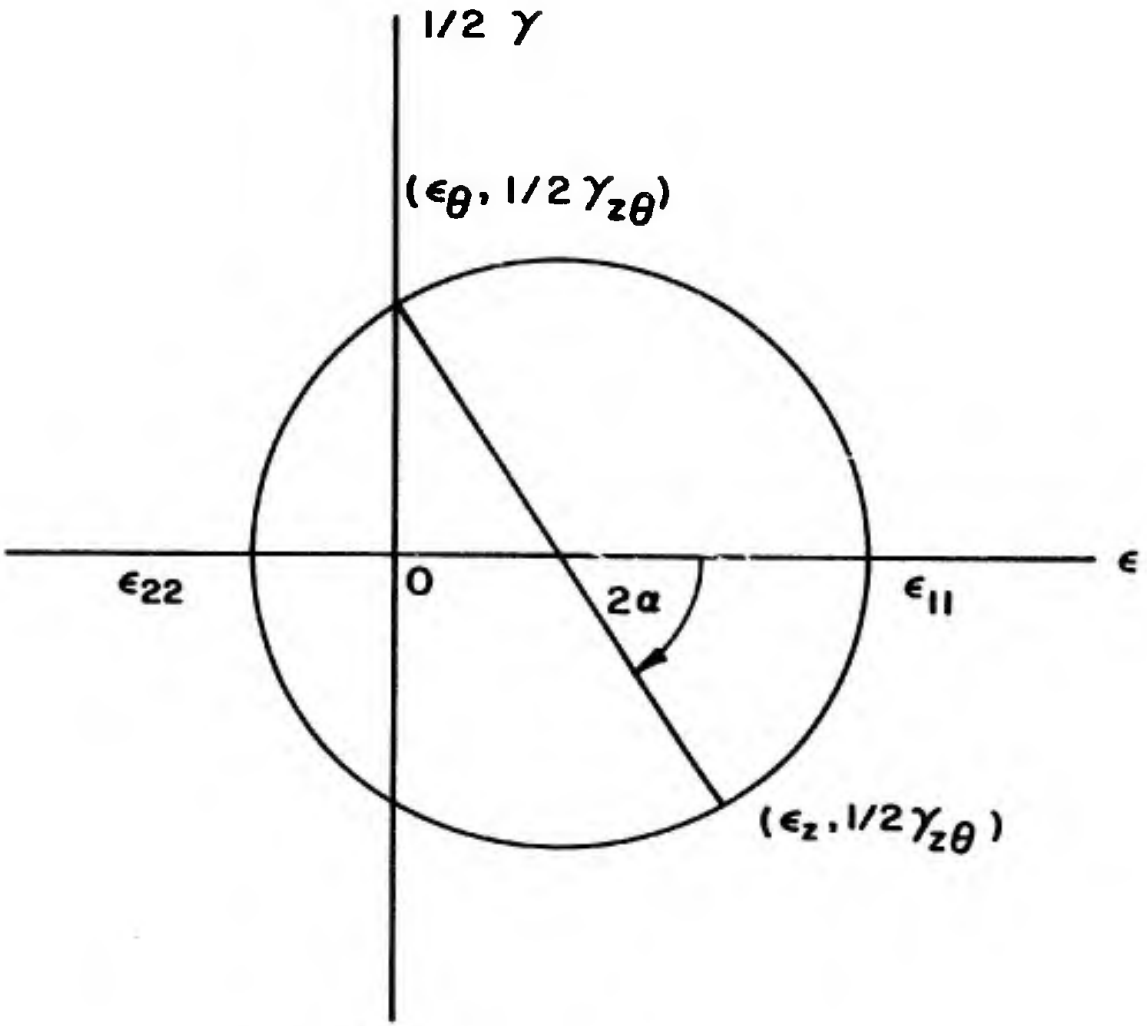

FIG. 63 MOHR'S CIRCLE

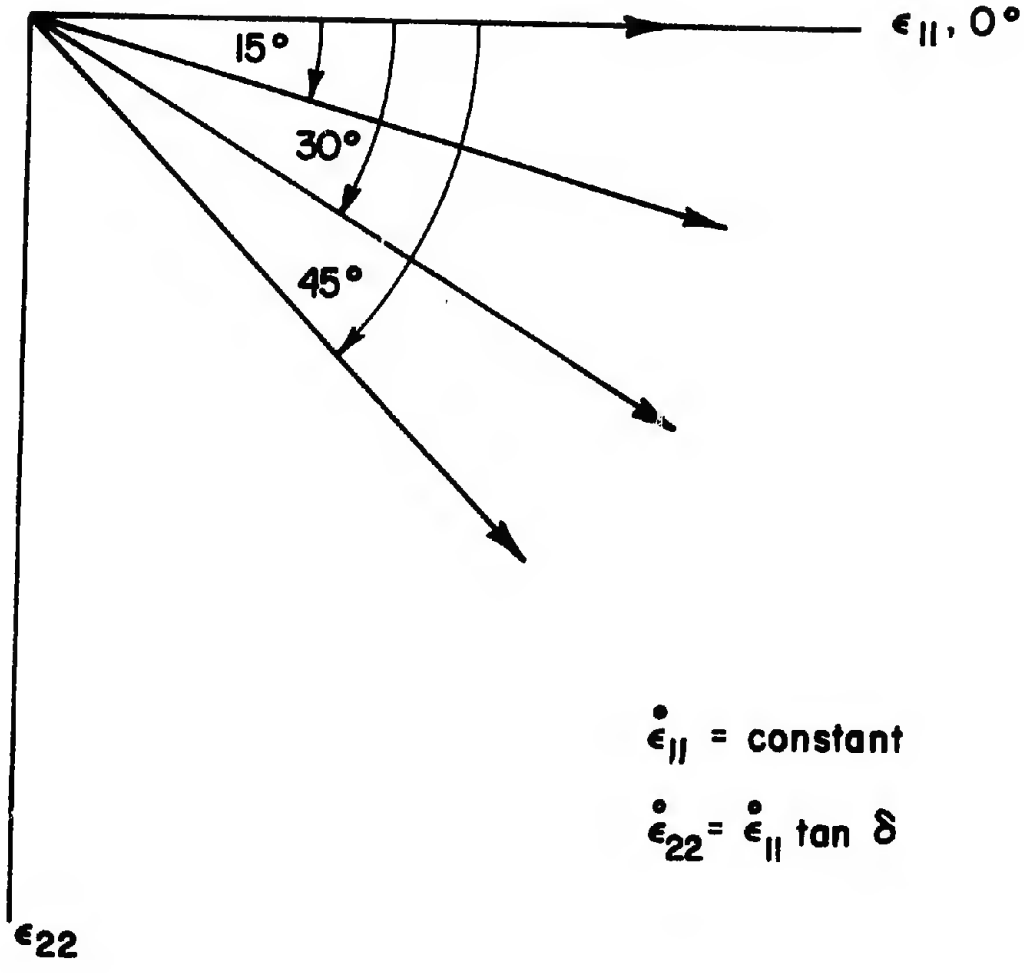

FIG. 64 BIAXIAL LOAD PATHS

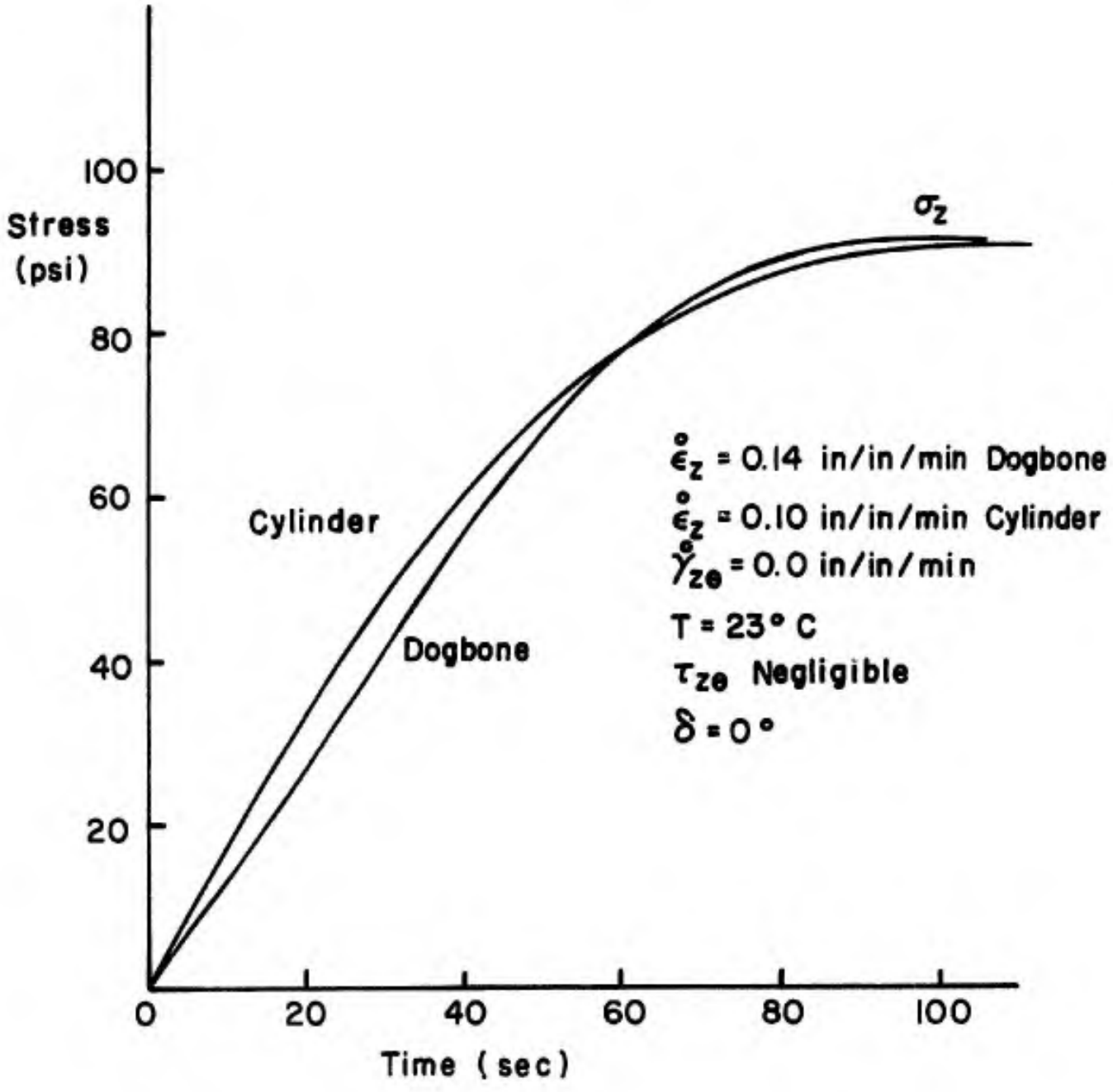

FIG. 65 BIAXIAL TEST # 1

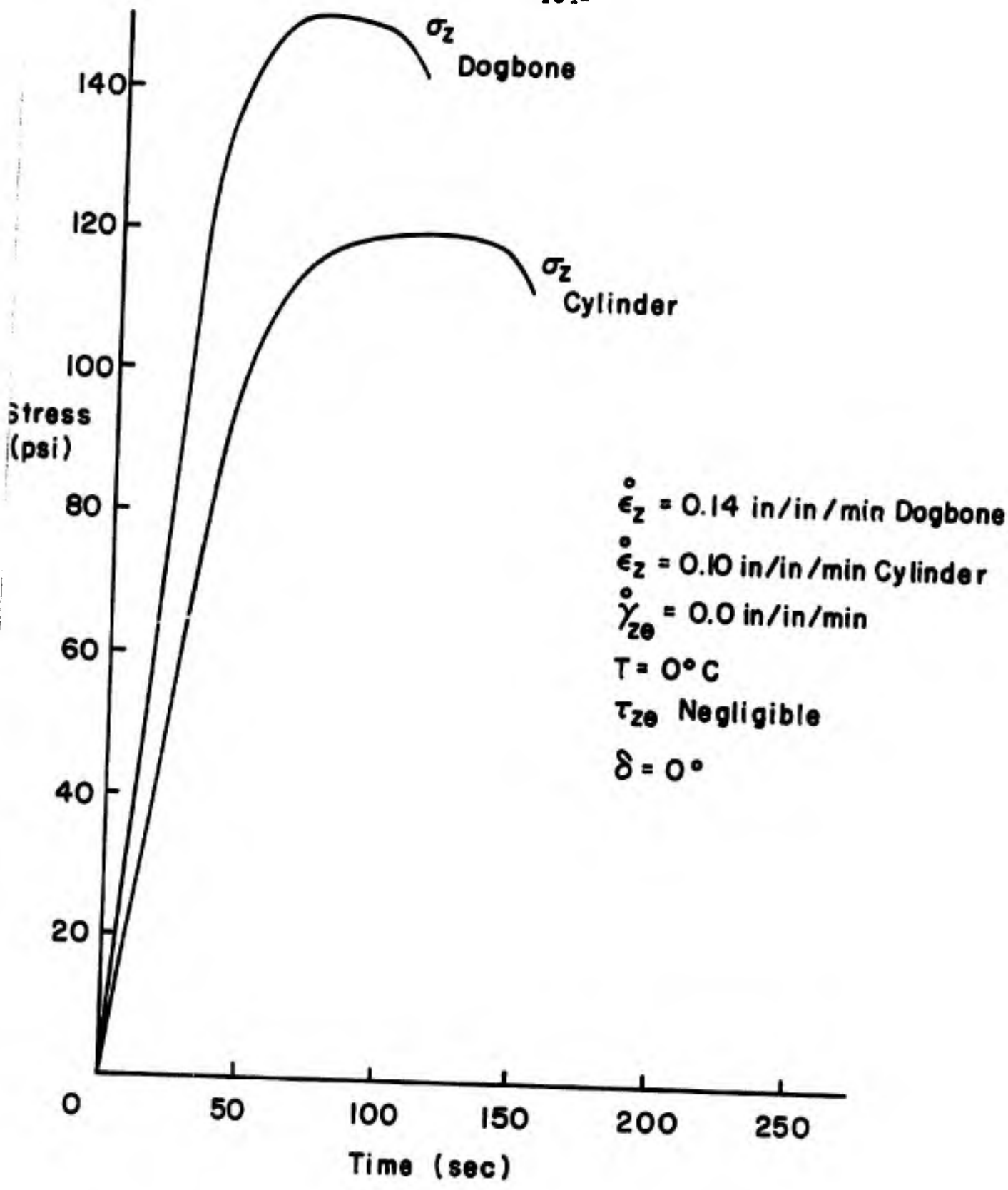

FIG. 66 BIAXIAL TEST # 2

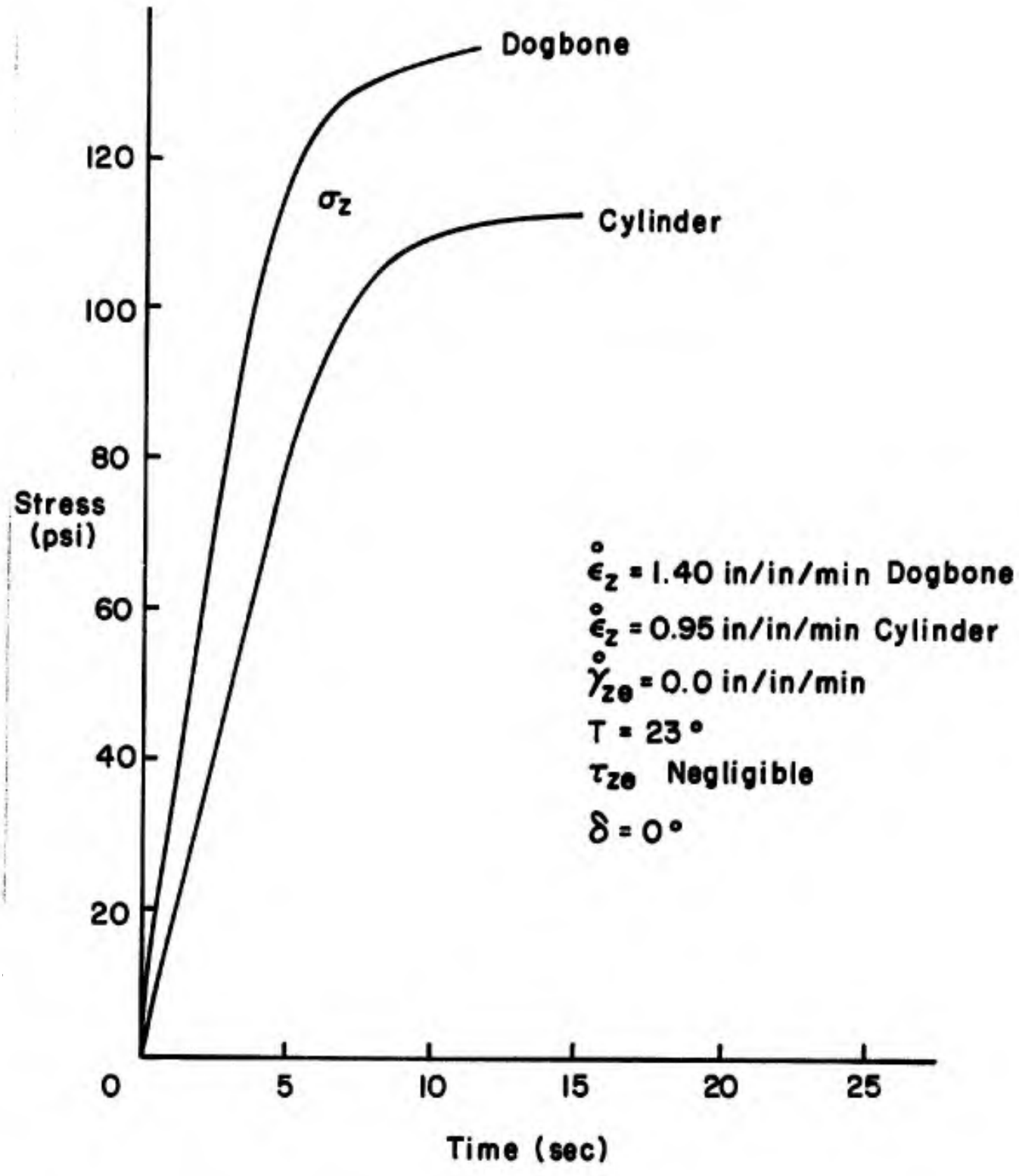

FIG. 67 BIAXIAL TEST # 7

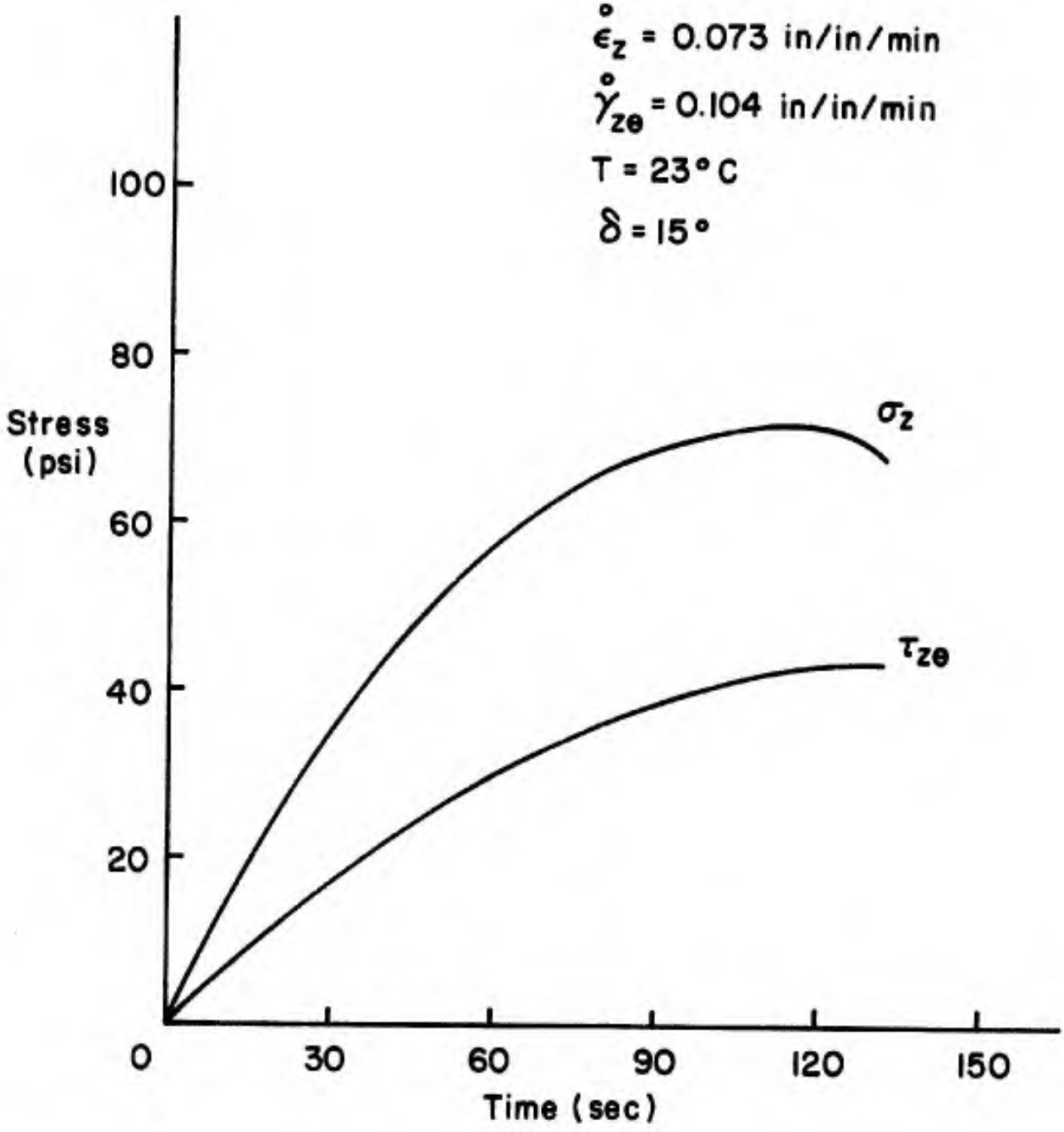

FIG. 68 BIAXIAL TEST # 3

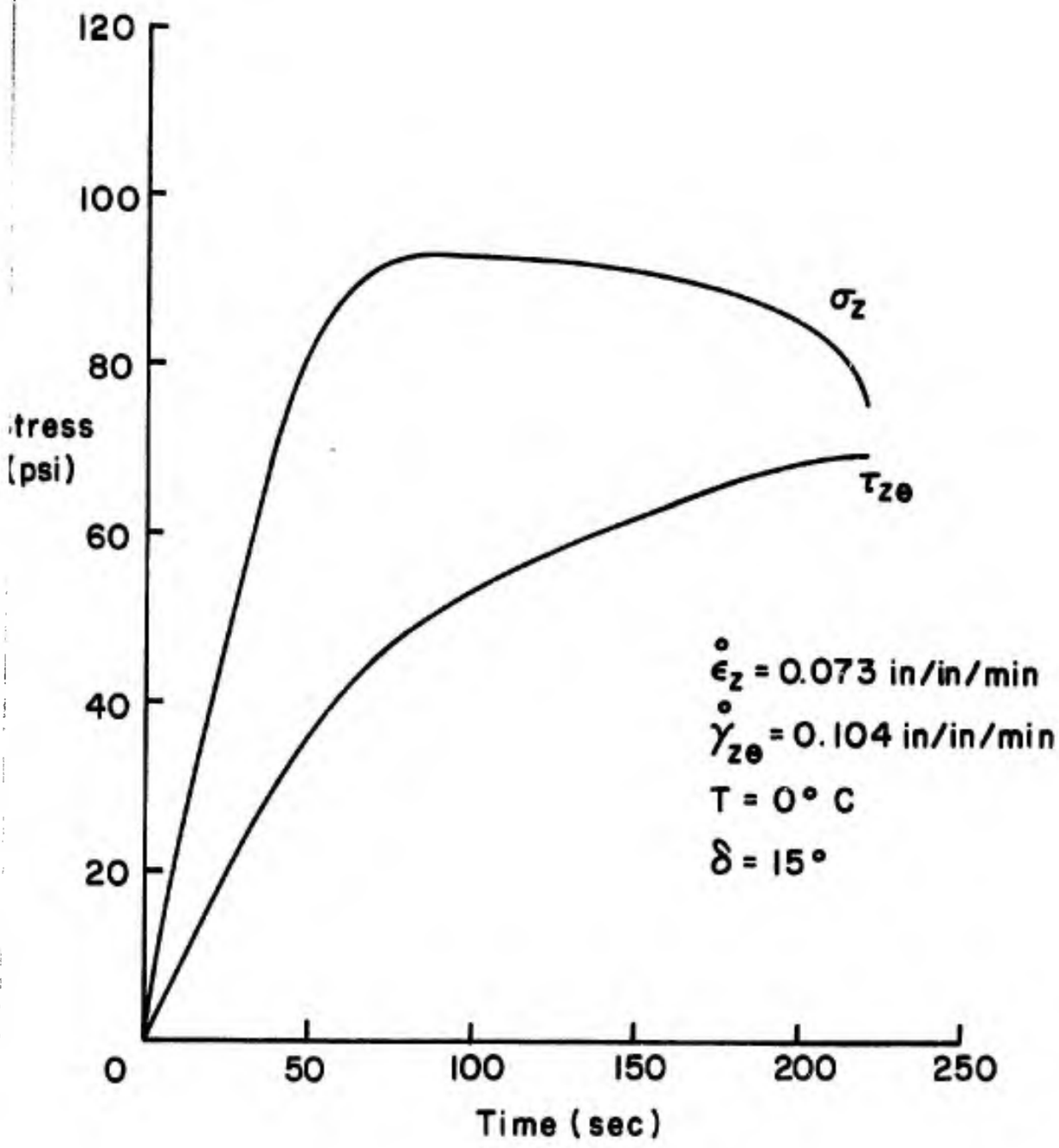

FIG. 69 BIAXIAL TEST # 11

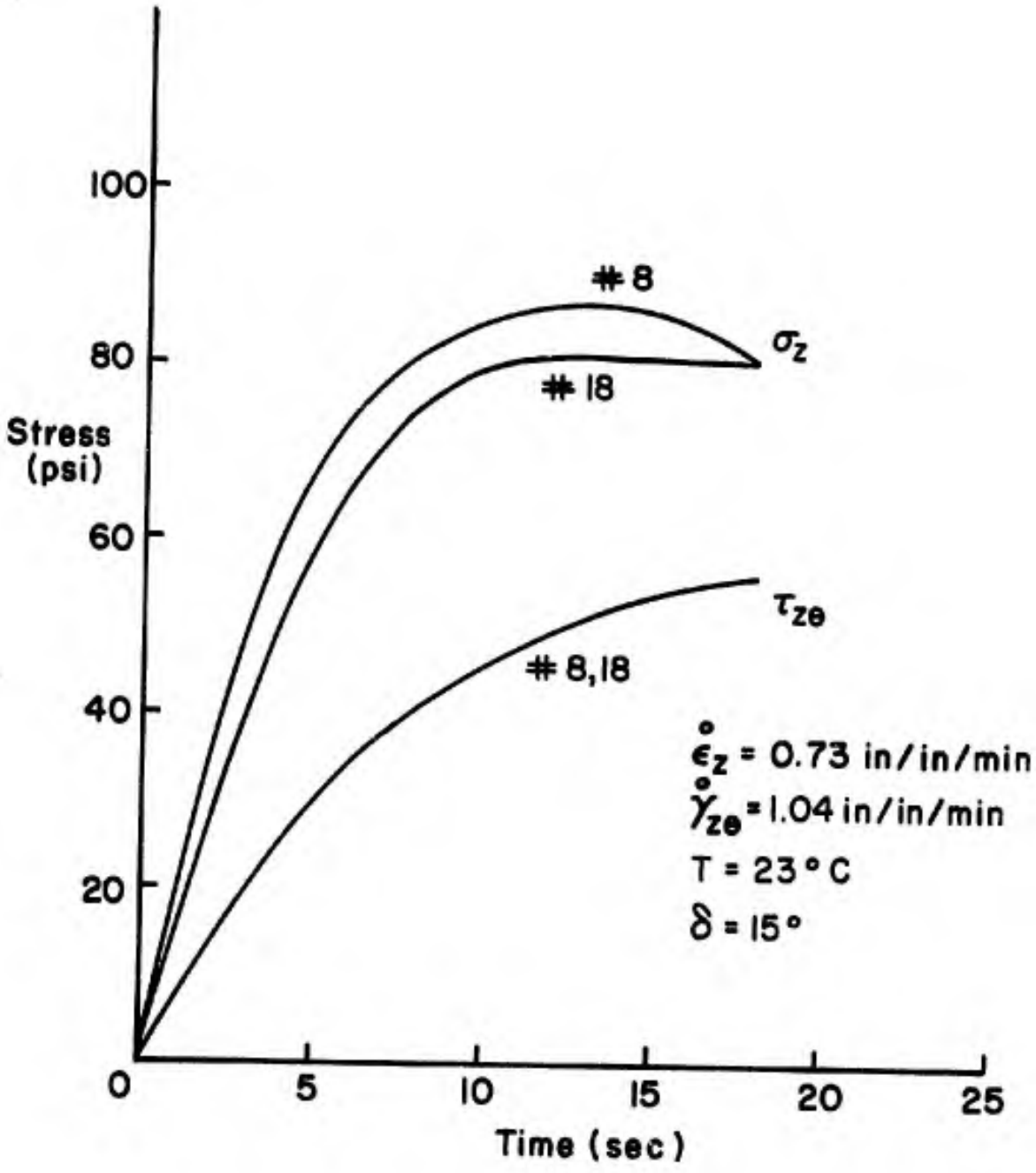

FIG. 70 BIAXIAL TESTS # 8 AND # 18

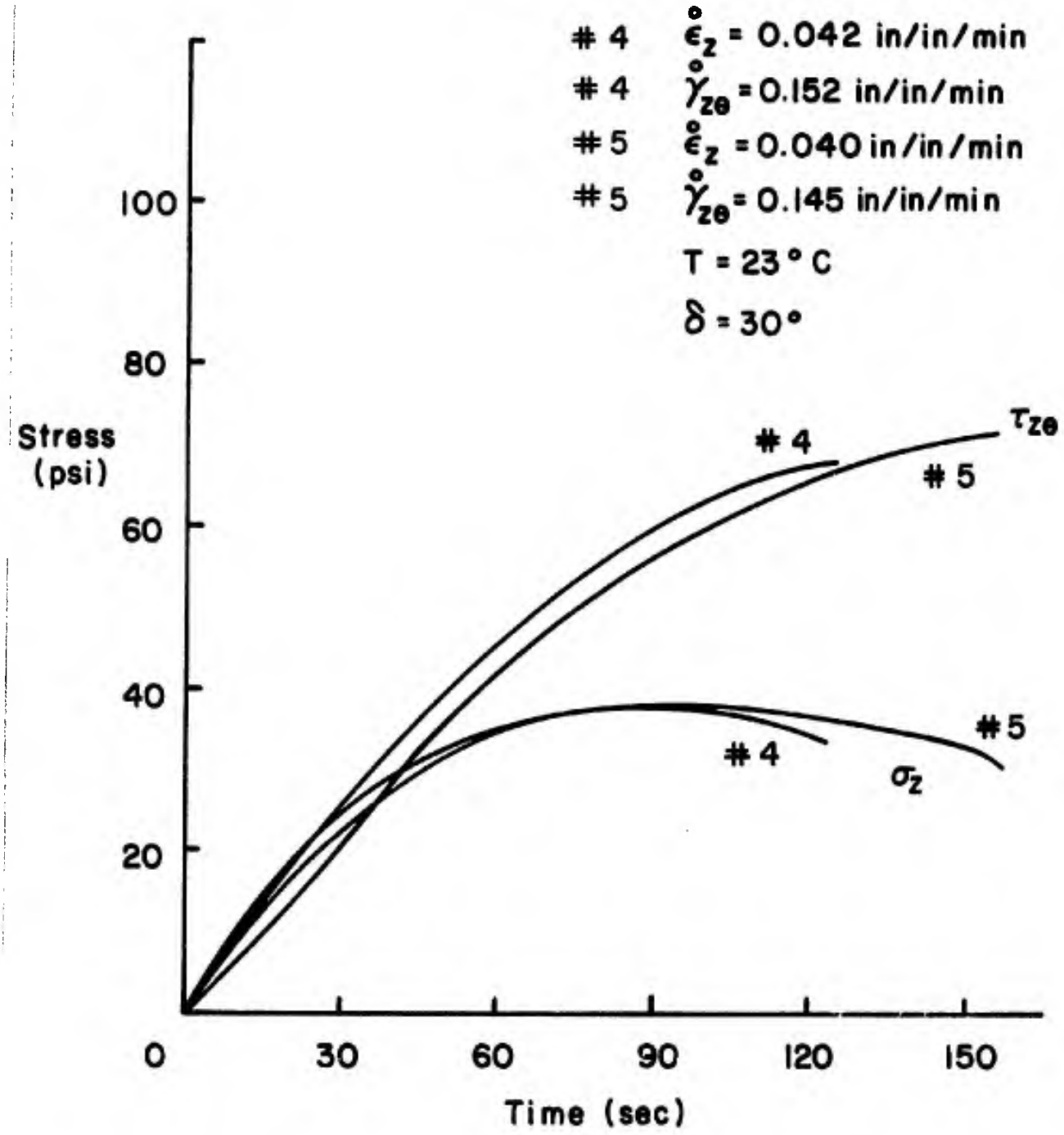

FIG. 71 BIAXIAL TESTS # 4 AND # 5

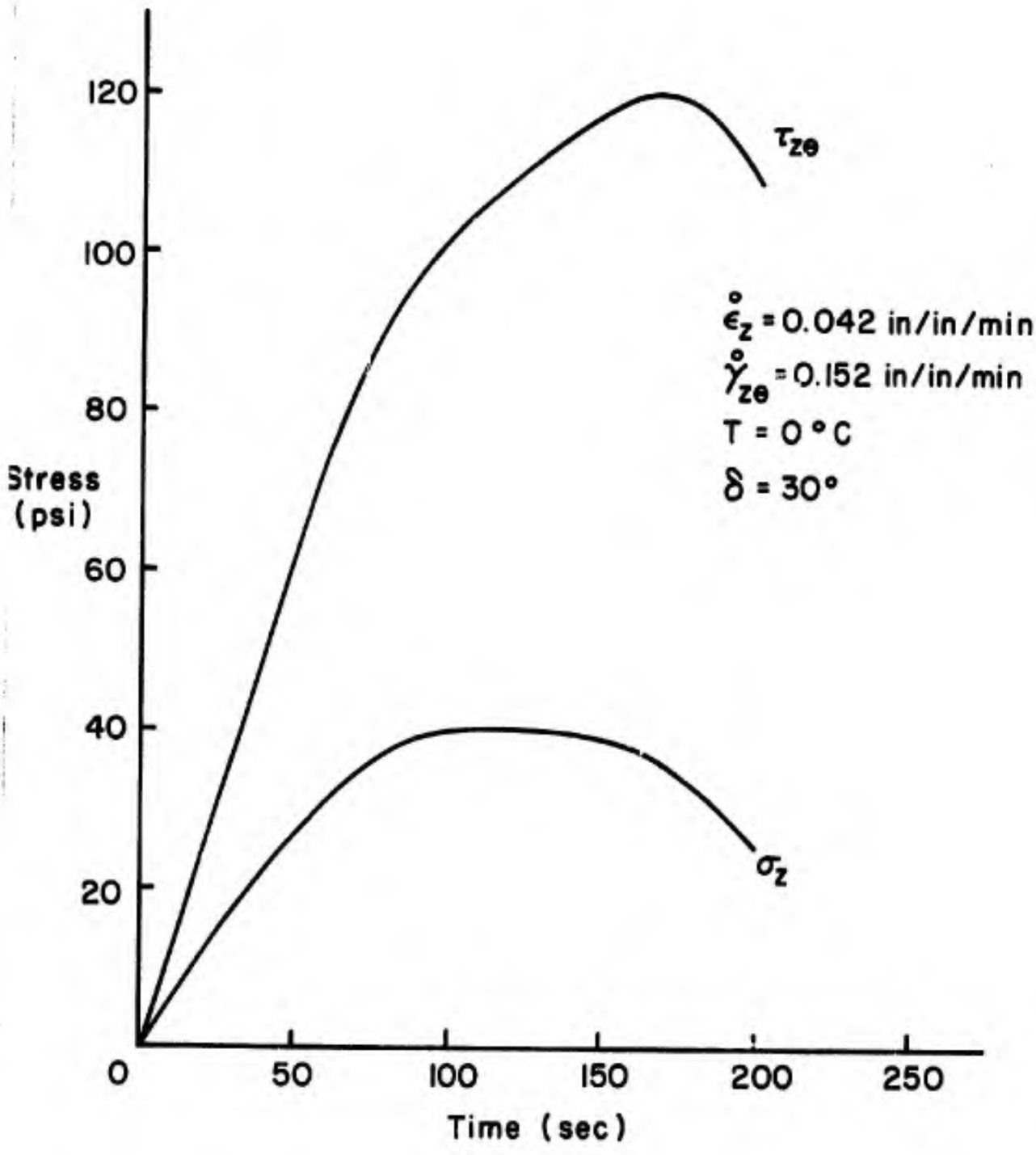

FIG. 72 BIAXIAL TEST # 13

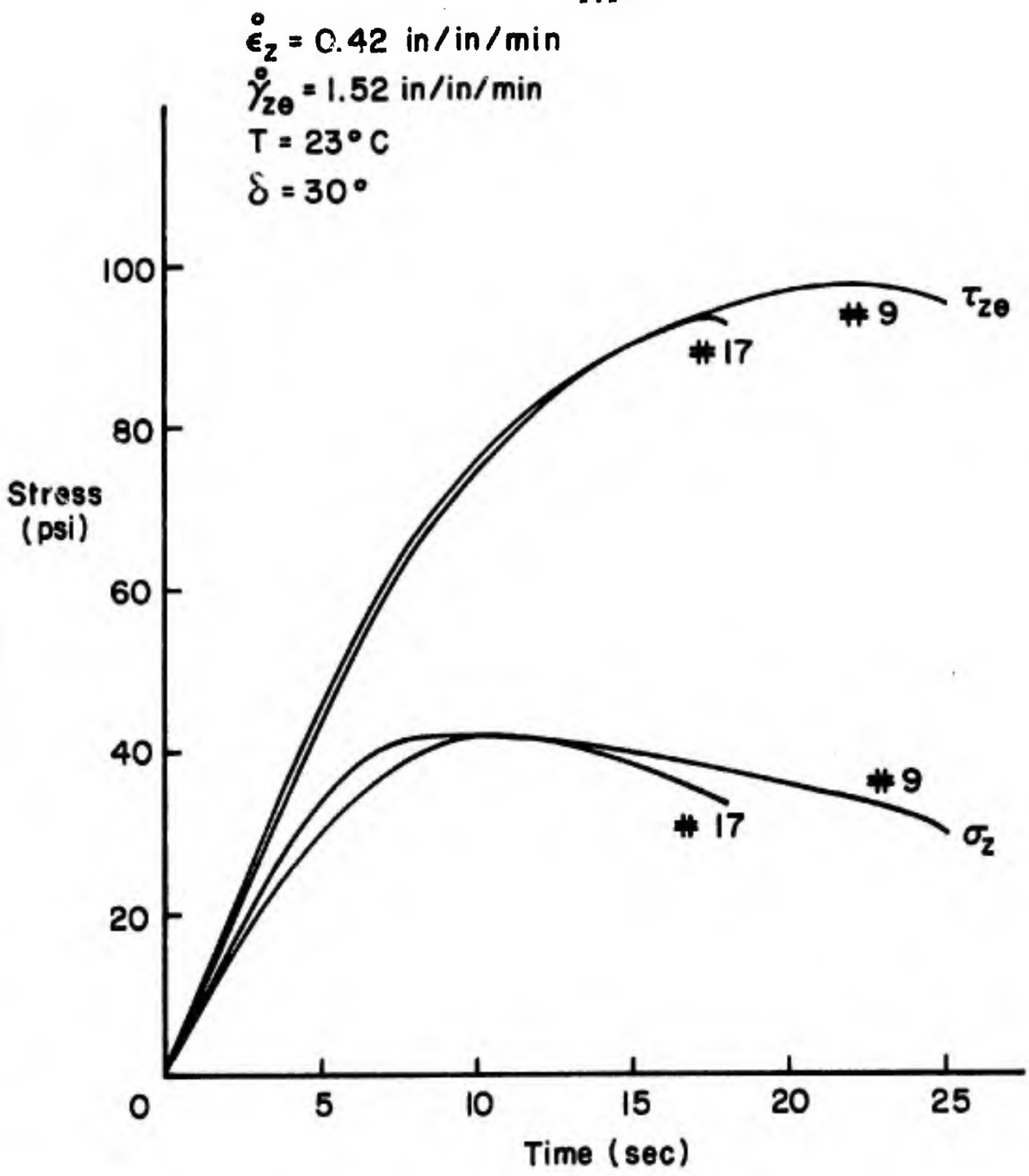

FIG. 73 BIAXIAL TESTS # 9 AND # 17

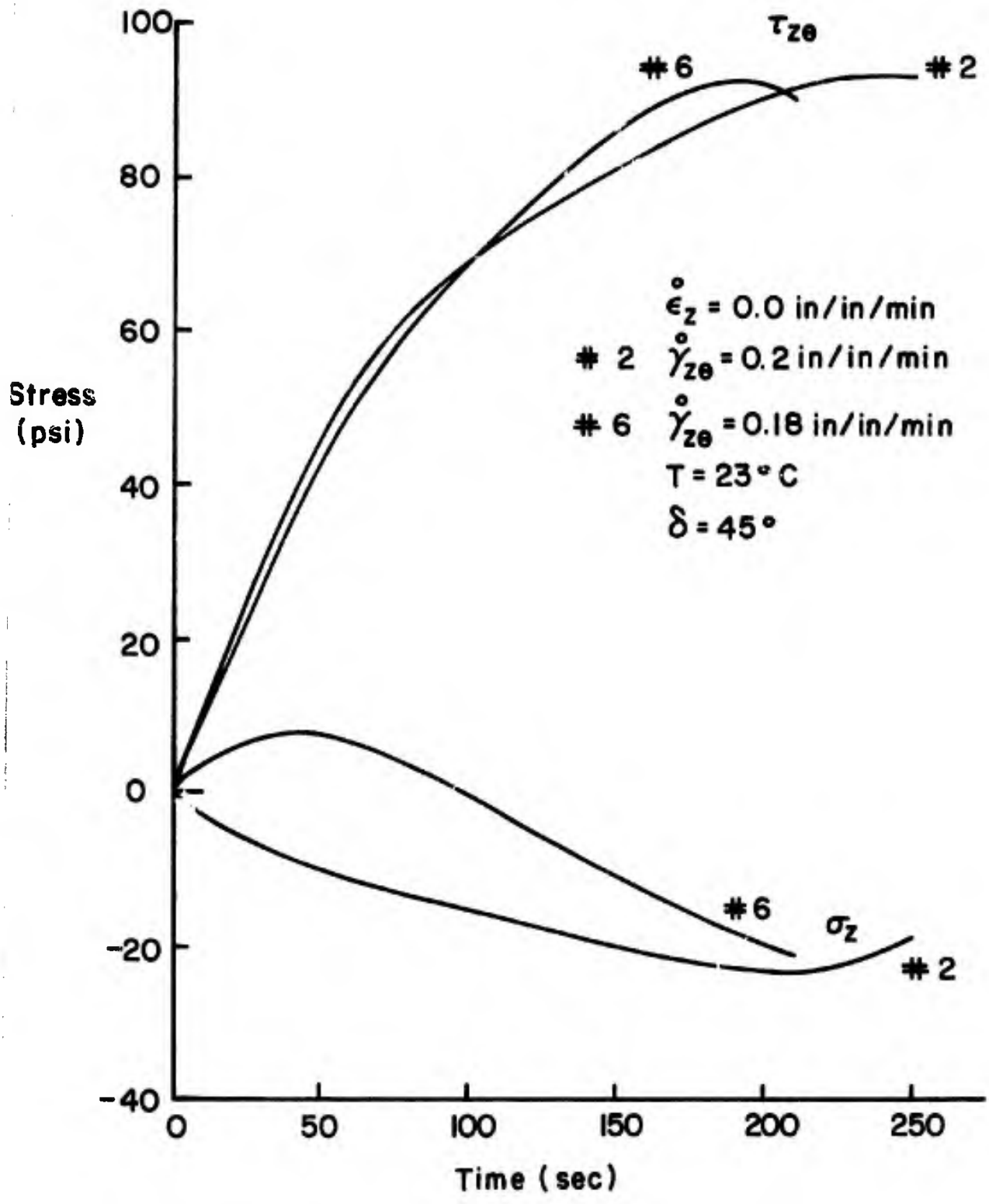

FIG. 74 BIAXIAL TESTS # 2 AND # 6

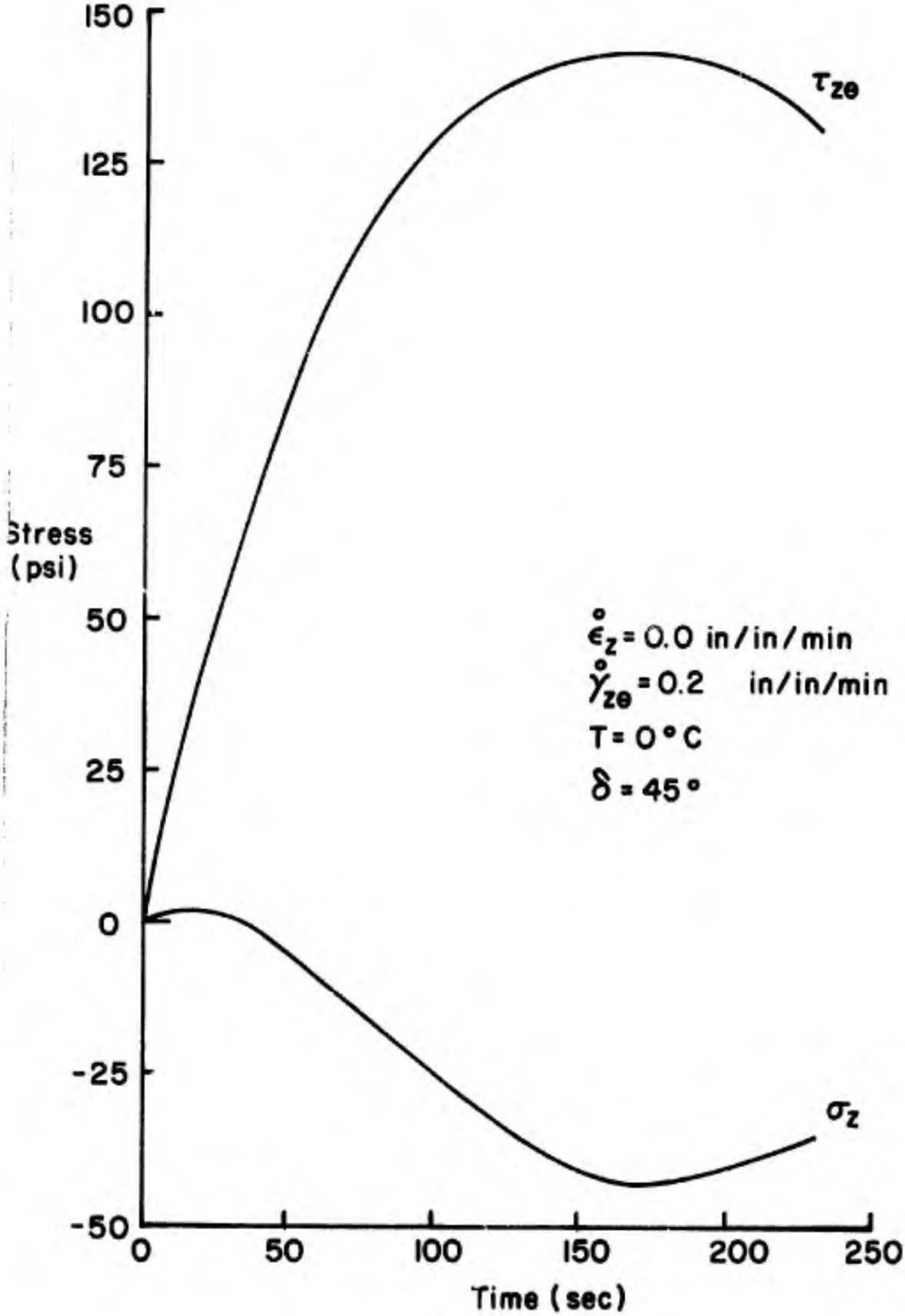

FIG. 75 BIAXIAL TEST # 15

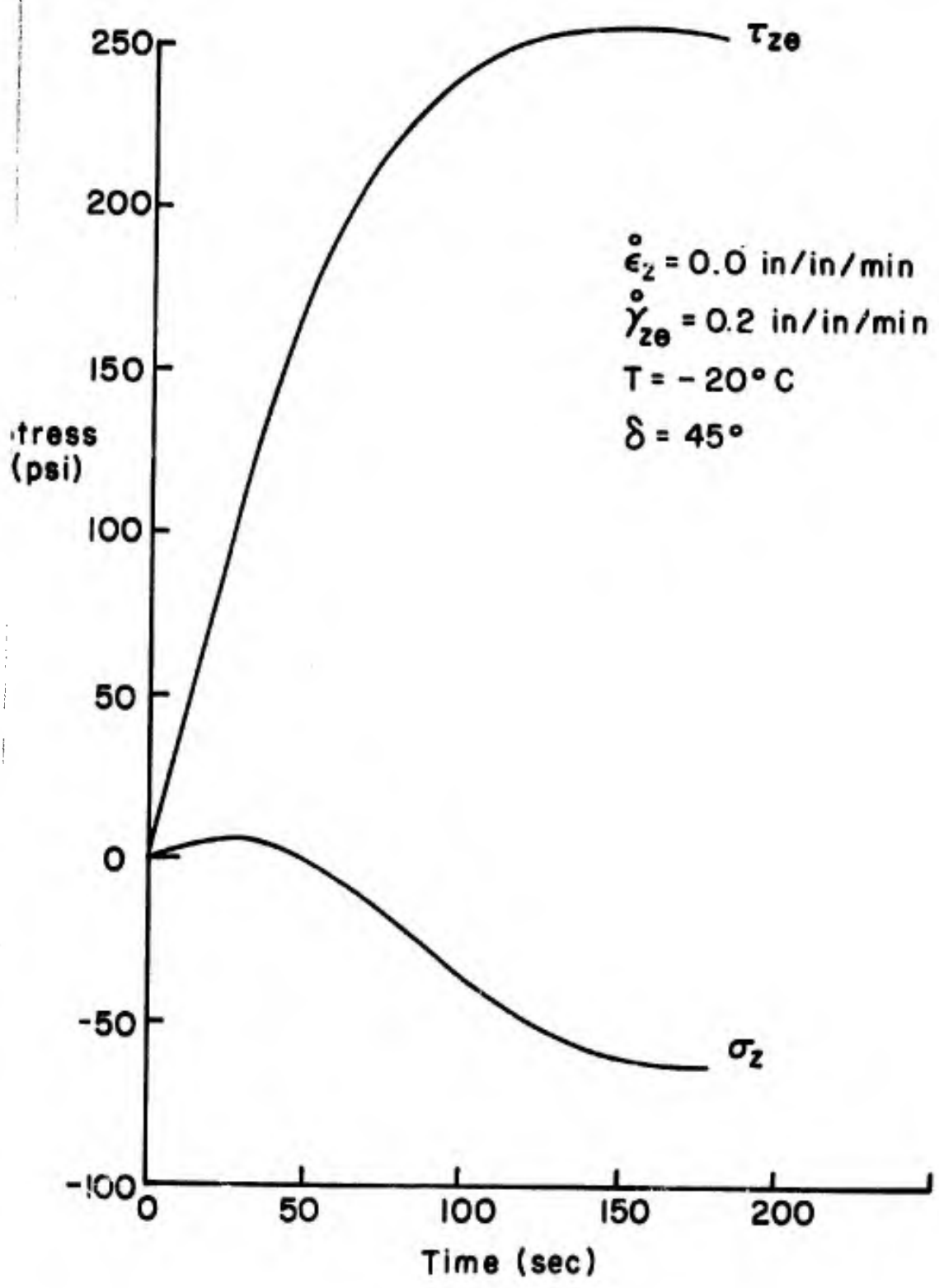

FIG. 76 BIAXIAL TEST # 14

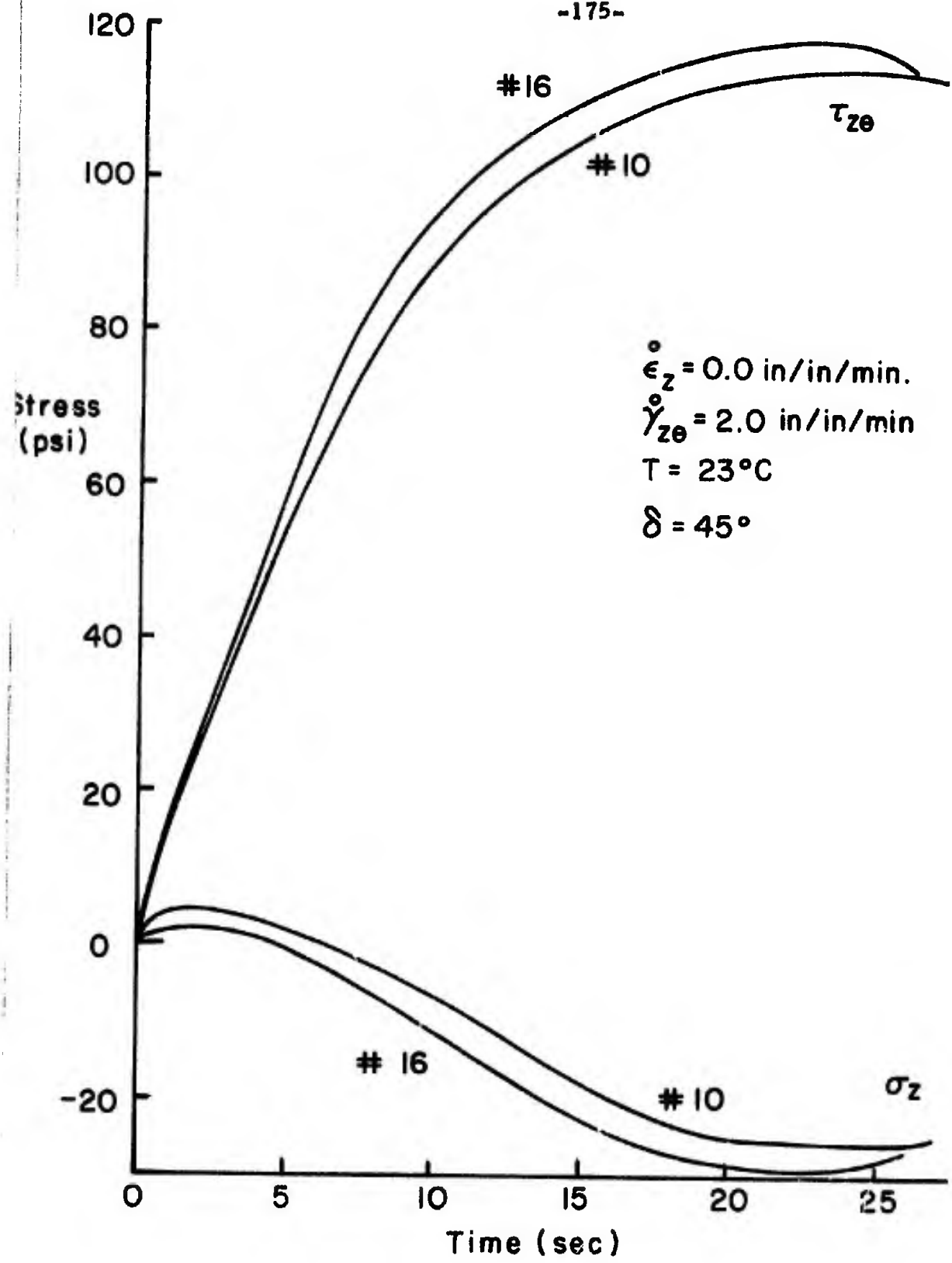

FIG. 77 BIAXIAL TESTS #10 AND #16

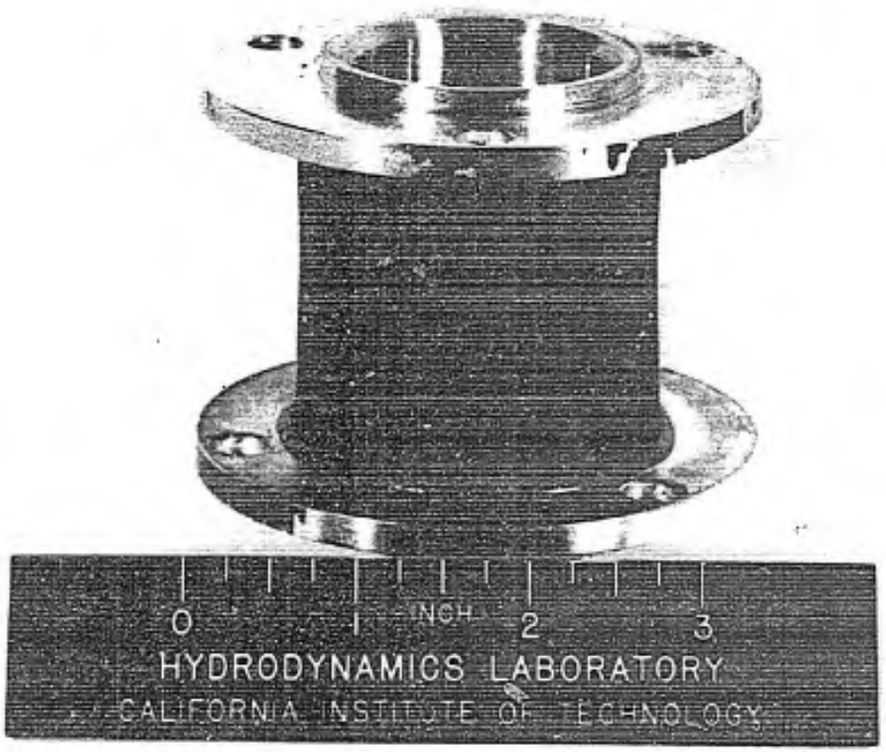

FIG. 78 SPECIMEN FAILURE (SHEAR TEST)

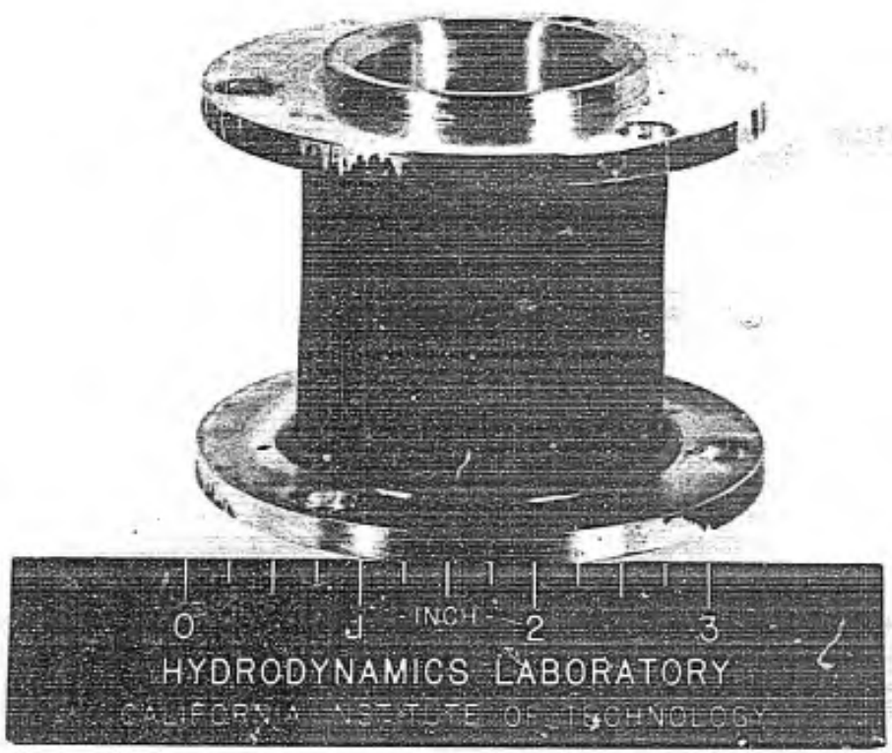

FIG. 79 FRACTURE ALIGNING WITH END FITTING

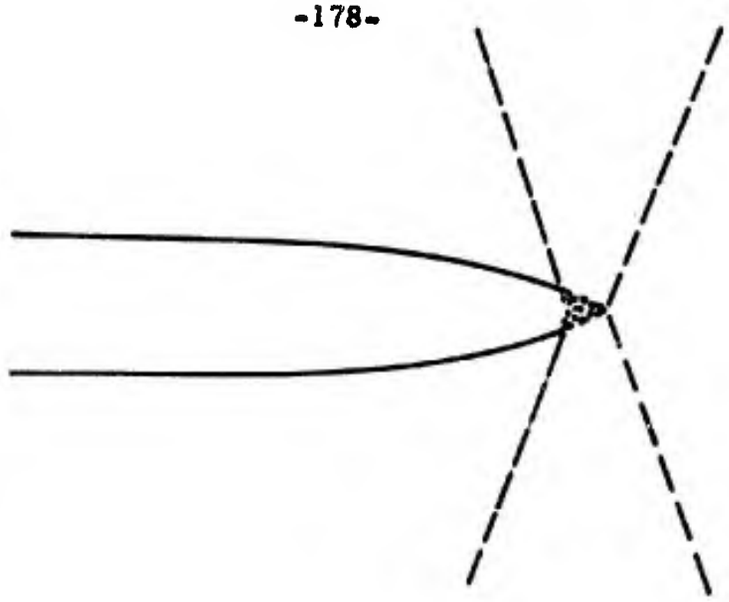

a) MATERIAL AT CRACK TIP REGION

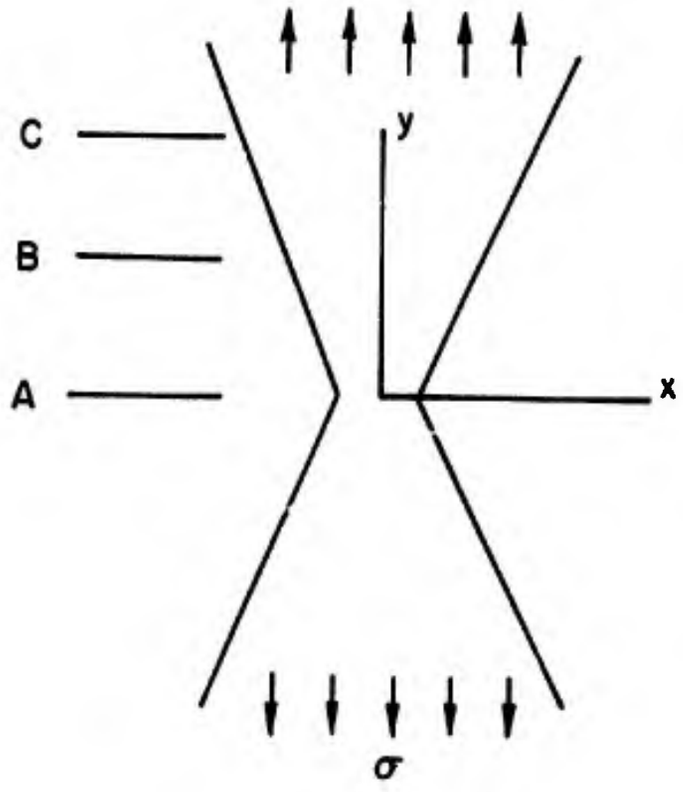

FIG. 80 b) TWO DIMENSIONAL CRACK SIMULATION

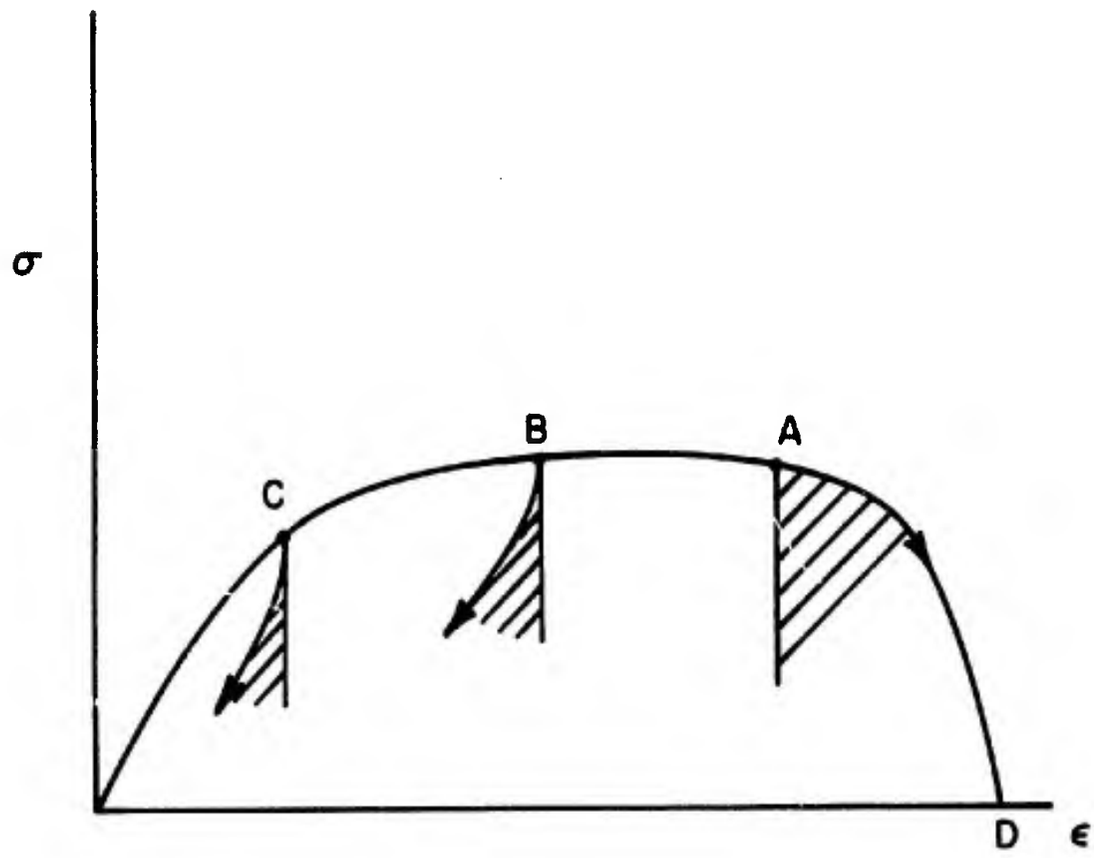

FIG. 81 QUALITATIVE STRESS-STRAIN CHARACTERISTIC USED IN CRACK PROPAGATION CONSIDERATION